PROTEIN STABILITY AND FIBRILLATION IN IONIC LIQUIDS: A SPECIAL REFERENCE TO HYDROPHOBIC INTERACTIONS

A thesis submitted
for the degree of

Doctor of Philosophy

by

PRATIBHA KUSHWAHA

Department of Biotechnology and Bioinformatics
School of Life Sciences
University of Hyderabad
PO Central University, Gachibowli
Hyderabad – 500046, India

December 2022

UNIVERSITY OF HYDERABAD
(A central university established in 1974 by an act of Parliament)
Department of Biotechnology and Bioinformatics
School of Life Sciences
University of Hyderabad, Hyderabad 500 046, India

STATEMENT

I, Pratibha Kushwaha, hereby declare that the work presented in this thesis, entitled as **"Protein Stability and Fibrillation in Ionic Liquids: A Special Reference to Hydrophobic Interactions"** has been carried out by me under the supervision of ***Dr. N. Prakash Prabhu*** at Department of Biotechnology and Bioinformatics. To the best of my knowledge, this work has not been submitted for the award of any degree or diploma at any other university or institution. A report on plagiarism statistics from the University Librarian is enclosed.

Place: Hyderabad

Date: 30/12/2022.

Pratibha Kushwaha

15LTPH06

Supervisor
Dr. N. Prakash Prabhu

N. PRAKASH PRABHU PhD
Associate Professor,
Dept. Biotechnology & Bioinformatics
School of Life Sciences
University of Hyderabad
Hyderabad-500 046

UNIVERSITY OF HYDERABAD
(A central university established in 1974 by an act of Parliament)
Department of Biotechnology and Bioinformatics
School of Life Sciences
University of Hyderabad, Hyderabad 500 046, India

CERTIFICATE

This is to certify that the thesis entitled **"Protein Stability and Fibrillation in Ionic Liquids: A Special Reference to Hydrophobic Interactions"** submitted by *Ms. Pratibha Kushwaha* bearing registration number 15LTPH06 in partial fulfilment of the requirements for award of **Doctor of Philosophy** in the Department of Biotechnology and Bioinformatics, School of Life Sciences is a bonafide work carried out by her under my supervision and guidance.

This thesis is free from plagiarism and has not been submitted previously in part or in full to this or any other university or institution for award of any degree or diploma.

Further, the student has the following publication before submission of the thesis for adjudication and has produced evidence for the same in the form of acceptance letter or the reprint in the relevant area of her research.

1. Imidazolium-based ionic liquids with increasing alkyl chain length of cations decrease the stability and fibrillation propensity of lysozyme. Kushwaha, P.; Prabhu, N. P., New J. Chem., 2022, 46, 11082-11094. https://doi.org/10.1039/D2NJ00559J. (ISSN Number: 1369-9261).

This publication appears in chapter number 2 of this dissertation.

And has made presentations in the following conferences:

1. As a poster in "43rd Indian Biophysical Society Meeting (Molecules to Systems)" held at Indian Institute of Science Education and Research, Kolkata on 15-17, Mar-2019. (International)

2. As a poster in "90th Annual Meeting of the Society of the Biological Chemists, India (SBCI, 2021) Metabolism to Drug Discovery: Where Chemistry and Biology Unite" held at Amity University, Haryana on 16-19, Dec-2021. (National)

Further, the student has passed the following courses towards the fulfillment of the course work requirement for Ph.D.

S.No	Course code	Name	Credits	Pass/Fail
1	BT801	Seminar I	1	Pass
2	BT802	Research Ethics & Management	2	Pass
3	BT803	Biostatistics	2	Pass
4	BT804	Analytical Techniques	3	Pass
5	BT805	Lab Work	4	Pass

30/12/2022

Supervisor

N. PRAKASH PRABHU PhD
Associate Professor,
Dept. Biotechnology & Bioinformatics
School of Life Sciences
University of Hyderabad
Hyderabad-500 046

Head of Department of Biotechnology and Bioinformatics

HEAD
Dept. of Biotechnology & Bioinformatics
University of Hyderabad
Hyderabad.

30/12/22

Dean of School of Life Sciences

DEAN
School of Life Sciences
University of Hyderabad
Hyderabad-500 046.

To my lifelines, loving **MAA** and **DIDI,** who always poured infinite love and support, and always encouraged me to keep going.

Your words, “give it a try before you quit or give up” drove me this far Maa.

To my supervisor, **Dr. N. Prakash Prabhu** who believed in me and helped me at every stage of my Ph.D. journey.

ACKNOWLEDGEMENT

My Ph.D. was an insightful journey. I can compare myself to a nascent polypeptide, synthesized through 2 years of M.Sc. course in Hyderabad University. I joined the pool of research arena to pick up the intricate details of learning how well-sounding research is carried out. It was not a solitary walk and neither a tunnel. Rather, I describe it as a "rugged funnel." I met new people, a few friends for life and hold gratitude towards so many people. It brings me a lot of delight to acknowledge the significant elements of this rugged funnel, the way to reach a global minima of my education landscape, the Ph.D. degree.

I hold the deepest gratitude towards my supervisor, ***Dr. N. Prakash Prabhu****, who constantly guided me to achieve the step-by-step targets of my thesis and overcome the puzzles of achieving it quickly and the question how? His support, patience, motivation, enthusiasm, and vivid ideas were the driving force for my Ph.D. Also, his support in many ups and downs of my life, helped me accelerate my progress. I will always be indebted.*

Further, I would like to thank my doctoral committee members, Dr. M. Venkatramana, Dr. Nooruddin Khan and Prof. KPMSV Padmasree, for their valuable suggestions throughout my research work. I would like to thank the present and former Heads of the Department of Biotechnology and Bioinformatics, and present and former Deans of the School of Life sciences for allowing me to use the Departmental and School facilities. I am thankful to all non-teaching staff from the Department and the School for their help in doing all the official works throughout this period.

I would like to thank the University for providing me with fellowship, and SERB, IoE and CSIR for funding our lab. I would also like to thank UGC-SAP and DST-FIST for their support to the Department. I would like to acknowledge the common facilities of our School and the Department. A sincere thanks to School of Chemistry, UoH, CCMB and NIAB for TEM facility and CMSD, UoH for the computational facility.

I would like to acknowledge all the present lab members, Subhasree, Archi, Sanjay, Muzafar, Priyanka, Namrata, Sneha, Saquib, Salik and Chinmay for helping me timely and creating a cheerful environment in the stressful moments. I am thankful to my seniors, especially ***Dr. Bramhini****, who motivated and helped me like an elder sister. I thank the M.Sc. project students of our lab, Abhinav and Mahima for their love and support.*

My heartfelt thanks to my friends, ***Gungun, Rolly, Nikitha,*** *and* ***Dee-cup*** *for making many memories for life and supporting me emotionally in my tuff times. We evolved together from our Master's to our Doctorate, to experience so many sweet and sour tastes. Without you guys, the journey would have been difficult. And, a few School friends,* ***Anjali*** *and the departed dearest souls* ***Dr. Aman and Sonali****, you have always cheered me up saying, "upcoming Dr…."*

My endless gratitude goes to my parents and family members for their cooperation, love, support and inspiration throughout my life. My words fall less to convey my love to these special people in my life, Love you all. Without your support, it would have been a most difficult journey.

A final thanks to the invisible powers surrounding me every moment to keep going constantly.

…Pratibha Kushwaha

ABBREVIATIONS

Lyz	-	Hen-egg lysozyme
IL	-	Ionic liquid
Im-IL	-	1-methylimidazolium ionic liquids
MIC	-	1-methylimidazolium chloride
EMIC	-	1-ethyl-3-methylimidazolium chloride
BMIC	-	1-butyl-3-methylimidazolium chloride
HMIC	-	1-hexyl-3-methylimidazolium chloride
OMIC	-	1-methyl-3-octylimidazolium chloride
BPyroBr	-	1-butyl-1-methylpyrrolidinium bromide
BPipBr	-	1-butyl-1-methylpiperidinium bromide
BPyrdBr	-	1-butyl-4-methylpyridinium bromide
BImBr	-	1-butyl-3-methylimidazolium bromide
ThT	-	thioflavin-T
ANS	-	8-anilinonaphthalene-1-sulphonic acid
DTT	-	Dithiothreitol
NATA	-	*N*-acetyl tryptophanamide
CD	-	Circular dichroism
TEM	-	Transmission electron microscope
MD	-	Molecular dynamics
k_f	-	Rate of fibril elongation
t_{lag}	-	Lag time
τ	-	Elongation time constant
t_o	-	Time required to attain half the maximum fluorescence
t	-	Time
T_{app}	-	Apparent fibrillation time
T_m	-	Temperature of transition midpoint
ΔH_m	-	Enthalpy change at the midpoint transition temperature
ΔC_p	-	Heat capacity change associated with the unfolding transition
R	-	Gas constant
ΔS_m	-	Entropy of unfolding
$\Delta\Delta H_m$	-	Difference between the enthalpy of unfolding in buffer and in IL
$\Delta\Delta S_m$	-	Difference between the entropy of unfolding in buffer and in IL
T	-	Temperature
WLmax	-	Fluorescence emission maximum
RMSD	-	Root mean square deviation
RMSF	-	Root mean square fluctuation
SASA	-	Solvent accessible surface area
R_g	-	Radius of gyration
RDF	-	Radial distribution function
χ_{hyd}	-	Hydration fraction
n_w	-	Number of water molecules around the protein

n_{IL}	-	Number of IL molecules around the protein
N_w	-	Total number of water molecules in the system
N_{IL}	-	Total number of IL molecules in the system
PIC	-	Preferential interaction coefficient
TFE	-	Transfer free energy
$G(r)$	-	Kirkwood-Buff integral
$g(r)$	-	Integrated RDF values
r	-	Distance
$\Gamma_{P\text{-}IL}$	-	Preferential interaction coefficient
ΔF^{t}_{P-IL}	-	Transfer free energy

CONTENTS

Chapter 1
Introduction

Proteins are the second most abundant molecules which contribute to all the functions essential for life. To handle such a sophisticated living system, a large number of different proteins, composed of 20 naturally occurring amino acids are arranged in unique sequences[1,2]. The functional maturity of newly synthesized proteins is attained by folding into a specific three-dimensional conformation. Understanding the packing of vast cellular proteome into a compact intricate machinery with high precision and fidelity has been a tangled mystery for years. The studies on folding mechanisms of ribonuclease protein[3–6] and renaturation of the protein by the reformation of disulphide bonds lead to a generalized concept given by Christian B. Anfinsen, the "thermodynamic hypothesis". It states that the three-dimensional structure of a protein in a physiological milieu is determined by the sequence of amino acids such that the Gibbs free energy of the whole system is lowest and governed by the interatomic interactions[7]. Later, Cyrus Levinthal laid critical insights into Anfinsen's hypothesis and questioned whether a nascent polypeptide can attain a meaningful topology among a large number of possible conformations, such that the folding event is very quick. Levinthal's idea of protein folding explained the event as constantly juggling two mutually exclusive goals – reaching the global minima and doing rapidly, could be a result of the specific folding pathway. This paradox explained the folding pathways that can be envisioned as tunnels where unfolded conformation on the top of the tunnel reaches native structure at the bottom[8,9] through progressively changing dihedral angles.

1.1 Folding funnels

Levinthal's paradox was a solution to the question of how to search the way to native conformation, but the existence of on- and off-pathways in the folding pathway and locating the available intermediates on the energy landscape made it challenging to be accepted. Perhaps the existence of various unfolded ensembles led to transform the tunnels into funnels, as the folding pathway could begin from many starting conformations[9]. A denatured protein can be found in various local minima before falling down to the base of the folding funnel, the native conformation, characterising the rugged feature rather than a smooth funnel. The entropy of unfolded or denatured protein is overcome by the forces required for its correct folding in an appropriate magnitude[10]. These denatured ensembles are sometimes kinetically trapped in these bumps, misfolded, and tend to fall slowly down the global minima. In such cases, folding is not a two-state process, but a multistep kinetics which is governed by the rate-limiting step known

as the transition state. Moreover, the funnels can be shallow if the conditions for protein folding are not favourable. On the other hand, funnels are steep and folding is faster when favourable conditions are available[9].

1.2 Hydrophobic interactions: keystones in the native structure of proteins

Interactions responsible for maintaining the structural integrity of a native protein can be as strong as disulphide bonds (covalent interactions) or weak interactions, including inter- and intrachain hydrogen bonds, ionic interactions and/or apolar interactions (non-covalent interactions)[11]. Kauzmann[12] explained the significance of apolar interactions in protein folding and stated that it is solely due to the packing of residues having non-polar side chains to the core region of the protein to avoid meeting water molecules. These interactions were the same as the one between water and oil, not letting two to mix, termed as "Hydrophobic interactions"[13,14]. The success rate of forming correct interactions between residues lies in the fact that native-like interactions are more stable as compared to non-native ones[2]. Moreover, how the non-polar and polar residues behave with the surrounding water molecules in a cellular milieu is another reason that imparts structure and functional stability to the protein. In the nutshell, the folding of a nascent polypeptide in the conformational space is contributed by the biases towards different types of secondary structure in different regions of the chain which is accompanied by free energy preferences related to hydrophobic collapse, i.e., the burial of non-polar residues and exposure of hydrophilic residues to the solvent molecules[15]. Native conformations are reached when "on-pathways" of protein folding operate in the presence of appropriate physicochemical conditions (Fig 1.1). Such conformations often require establishing intramolecular interactions between the residues of the same chain[16].

1.3 Stable non-native interactions: fibril formation

Unlike folding of native proteins, which depends on the sequence of amino acids, fibril formation arises from certain sequences often unrelated[17]. Various neurodegenerative disorders such as Huntingtun's disease, Kennedy disease, spino cerebellar ataxia type 1 (SCA1) and dentatorubral pallidoluysianatrophy (DRPLA) are identified related to polar residue repeats. Sheets or barrels are formed by associating β-strands through the networks of hydrogen bonds between the amide groups of main chain and side chains of glutamine repeats[18,19]. In a few cases, combination of alternative polar and non-polar residues is capable of forming fibrils[20]. Therefore, the partial unfolding of a protein plays a pivotal role in initiating fibril formation as it exposes the side chains of residues crucial for amyloid formation, which are otherwise buried to the core of native conformations[21]. Irrespective of native conformation such non-native species are stabilized by strong intermolecular interactions. These altered conformations may interact to form amorphous aggregates with poorly defined shapes or highly ordered assemblies to form fibrils having high β-sheet content[16,22,23]. Such mechanisms are termed "off-pathways" of protein folding (Fig. 1.1).

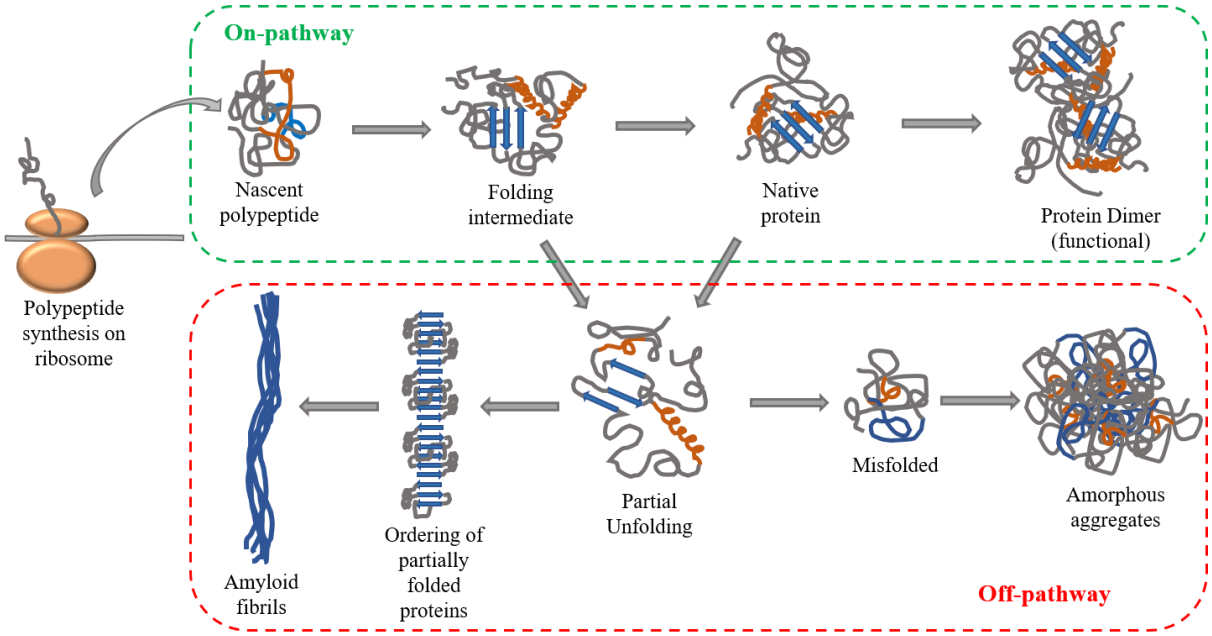

Fig. 1.1 Schematic diagram showing on- and off- pathways of protein folding leading to native conformation and aggregate and/or fibril formation, respectively.

Generally, fibrillar assemblies are formed as a consequence of aberrative intrinsic properties such as mutations and/or truncations or altered physicochemical parameters surrounding the proteins[24]. In the presence of such non-native conditions, thermodynamic

equilibrium between folded and unfolded ensembles is altered[25]. Studies have compelled one to believe that the native conformations and fibrillar assemblies arise from the same precursor folding intermediate which is in a dynamic equilibrium with the folded state. When physicochemical properties of the surrounding medium such as temperature, pH, ionic strength, pressure, etc., are perturbed or there is an addition of cosolvents to the reaction milieu, the native interactions in a protein might be disrupted. All these facts indicate that fibrillation is a generic property of every protein guided by non-native physicochemical conditions[26].

1.4 Energy landscape of protein conformations

In a funnel-shaped energy landscape, conformations involved in on-pathway often have a target of the global minima to reach and to stay as stable molecules in the system. Conformations formed as a result of off-pathways also form funnel shapes with more ruggedness which is attributed to the competitiveness between intermolecular interactions (non-native structures) and intramolecular interactions (native structures). It is now well established that the products of off-pathways are the most stable species in any system such that they occupy the lowest energy minima (Fig. 1.2).

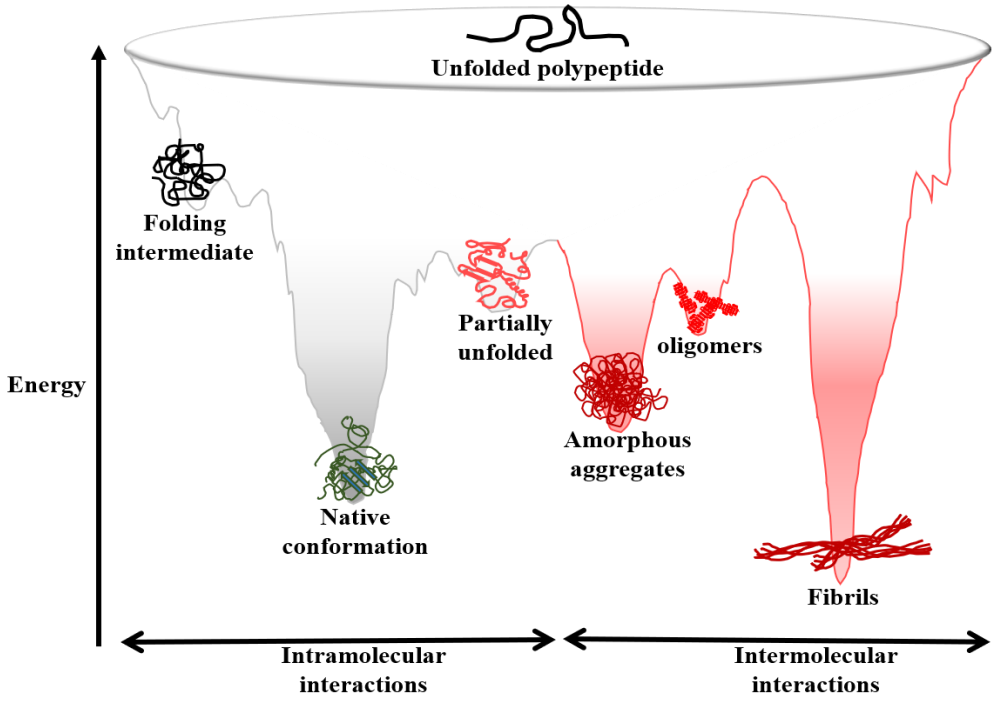

Fig. 1.2 Protein folding funnel depicting the regions for the native folding pathway (shaded in grey) of a nascent polypeptide and the aggregate or fibril formation pathway (shaded in red).

These conformations form multiple peaks in the funnels as fibrillar structures assemble with different morphological features[16,27–29] Though the native conformation is more stable as compared to its respective initial unfolded chain, it remains only metastable with respect to fibrillar states, because of high kinetic barriers linked with the self-assembled polypeptide chains. Apart from higher stability, these conformations are insoluble and acquire toxic functions, thus posing deleterious effects on many biochemical pathways in the cell[30]. To combat the off-pathways in the cellular milieu, regulatory mechanisms take over and prevent any such events leading to aggregation or fibrillar assembly[21,31,32]. As a protective measure, the intrinsic kinetic barriers are increased for the aggregates. But in certain circumstances, such as mutations, stress and ageing, aggregation of proteins leads the debilitating consequences and thus pathogenic conditions[33].

1.5 Structural features of fibrils

All the fibrils regardless of the amino acid composition and morphology, have a dominating structural feature, i.e., the presence of cross-β-structures. X-ray crystal structures have revealed that β-sheets are arranged parallelly to the axis of fibril growth whereas β-strands in the individual sheets acquire a perpendicular orientation. The β-stands constituting the sheets remain separated by a distance of 4.7- 4.8 Å and β-sheets have a gap of 10-12 Å[34–36]. In general, amyloid fibrils contain 2 to 6 protofilaments forming the fibril with diameter of 2-5 nm. Various imaging techniques show that the protofilaments are either linked to each other by arranging them adjacent or twisting along each other. Matured fibrils possess a girth of a few nanometres and length in micrometres scale[37].

1.6 Mechanisms of fibril formation

An understanding on fibril formation mechanisms involves distinguishing all the conformational states and the small assemblies formed by partially unfolded structures of a polypeptide chain and evaluating how each conformation is differing on the thermodynamic and kinetic parameters[33]. On a broader perspective, fibrils can be formed by either of two mechanisms: (i) nucleation-dependent, and (ii) nucleation-independent (Fig. 1.3). Fibrillation mechanism highly depend on the solvent conditions such as pH[38] and the concentration of added cosolvents, if any[39].

(i) Nucleation-dependent mechanism

Nucleation-dependent pathway occur in a three-step process, conversion of native protein into a partially unfolded conformation, association of monomer species formed in step one into oligomers, known as nuclei, and the addition of more monomeric species on either end of the nuclei to form a mature fibril[40]. Progression of assembly steps needs to be battled out by forming intermolecular bonds which are often retarded due to unfavourable events such as rotational and translational entropy of the monomer. Once this entropy barrier is crossed, protofibrilar species are formed as the result of monomer association. Thus, nucleus formation plays a pivotal role between the monomers entropy to be lost (retards assembly process) and the bond energy that would stabilize the protofibril formation. Also, it explains that on the kinetic parameters, the rate of addition of monomers further to the initial nuclei would be more than the rate of monomer loss once the critical size or nucleus is reached[41]. A few other studies suggests that aggregates of partially folded monomers can assemble to form a nucleus, elongate to a certain length by the further addition of monomers on either end, fragment into smaller assemblies to form templates to again undergo elongation process by monomer addition and so on. Such secondary nucleation mechanisms have faster rates of assembly as compared to the initial nucleus formation from the monomers[42].

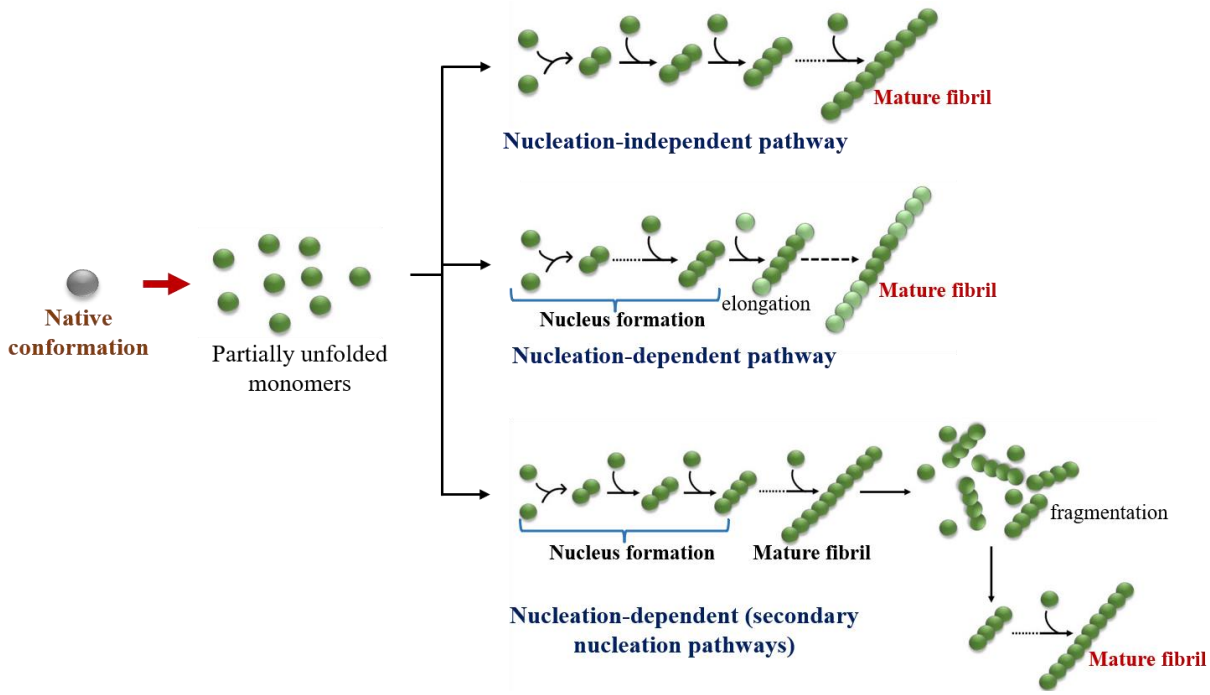

Fig. 1.3 A schematic representation of different mechanisms of fibril formation.

(ii) Nucleation-independent mechanism

There are pathways in which nucleation phase is completely by-passed. Also known as isodesmic mechanisms, fibril growth follows a monotonic pattern. Fibril grows linearly with the gradual addition of monomer at each step. Barshop et al., described earlier a numerical integration program, KINSIM, which could simulate the isodesmic polymerization[43]. Since there is no nucleation phase, polymerization reaction can begin with any monomeric unit. At each step of the fibril growth, bonds are identical indicating that the rate constants do not depend on the size of the fibril. Therefore, nucleation-independent assemblies possess close resemblance to the elongation phase of nucleation-dependent fibrillation. The kinetic rates are fastest at beginning of polymerization reaction which highly depends on the monomer concentration. Further as the reaction proceeds, monomer's concentration decreases and slowly the equilibrium condition is reached. Overall, there is no concentration barrier to be crossed to enter the elongation phase[44].

1.7 Lysozyme: a model protein

Partially unfolded conformations of proteins harbour plethora of pathological conditions, thus it is necessary to understand the structure and dynamics of these non-native states of proteins[45]. It is known that the fragments of large protein precursors deposit in the form of amyloids within the tissues which are detrimental for various biochemical pathways. Fibrils formed in an individual suffering with Alzheimer's disease is one such example. Secretase enzyme performs limited proteolysis of amyloid precursor protein (APP) which assembles to form fibrils. A few other examples, such as serum amyloid A protein, gelsolin, apolipoprotein A1, prolactin, calcitonin, transerythrin, etc., also undergo limited proteolysis to form fragments that are prone to form amyloids. A common feature among all these polypeptides is the loss of long-range interactions that are necessary to form the native conformation of functional protein.

Point mutations in human lysozyme are known to be responsible for non-neuropathic systemic amyloidosis. Individuals are heterozygous for the mutations of lysozyme gene and the translated product of such genes deposit in different tissues. However, the deposition of amyloids is a very slow process and shows its fatality in the fifth decade from the onset of amyloid deposition[46]. From the detailed study on two lysozyme mutants, I56T and D67H with

amyloidogenic properties, it is noted that these mutants have less structural stability and altered folding kinetics as compared to wild type[47–49]. Further studies show that the mutant D67H of human lysozyme has notable destabilization in β-domain (residues 40-82) and C-helix (residues 89-100), also the regions significantly participating in amyloid formation[50–53]. Therefore, it is proposed that any protein undergoing aggregation should have lower thermodynamic stability and have structural cooperativity prone to adopt partially unfolded states.

Studies have unravelled that the mutants and the native protein do not vary structurally, and the morphologies of fibrils formed by the native protein at different conditions are similar to the fibrils formed by mutant proteins[52]. Thus, fibrillation mechanisms can be studied using lysozyme as the model protein for structural and fibrillar characterization. Hen egg white lysozyme has ~60% sequence identity with human lysozyme and shares a similar structural topology (CATH domain: 1.10.530.10). Thus, hen egg white lysozyme could also serve as an appropriate model to study the self-assembly and stability.

Hen egg white lysozyme (Lyz) is a globular protein with 129 amino acid residues and has two structural domains, α-domain (sequence 1-35 and 85-129) and β-domain (residues 36-84) as shown in Fig 1.4 (A)[54,55]. Lyz retains some of its residual structure when treated under strong denaturing conditions such as 8 M urea[56–59]. These residual structure is mainly composed of six hydrophobic clusters[60,61], having Trp or His residues surrounded by the other hydrophobic residues. Stabilization of hydrophobic clusters is due to long-range interactions which in turn assist the protein folding[62–64]. Studies have shown that these clusters are present at discrete

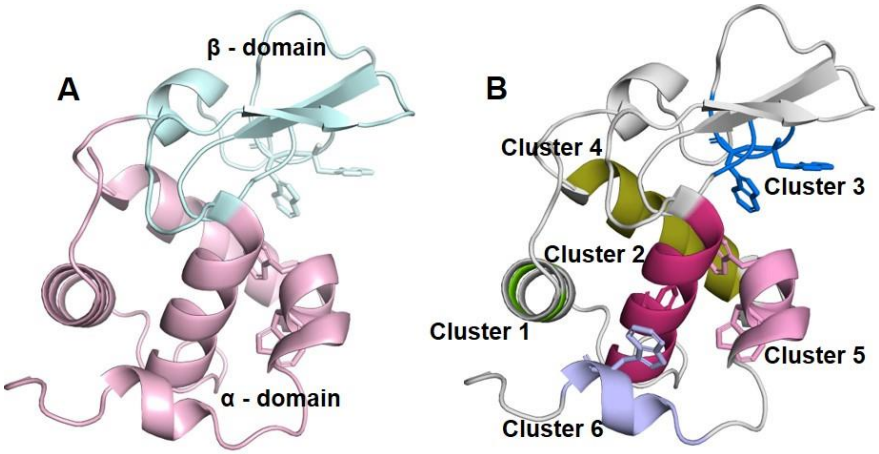

Fig. 1.4 Crystal structure of Lyz (PDB ID: 5K2P) showing (A) α- and β- domains in light pink and light cyan colors, respectively, (B) hydrophobic clusters in light green (cluster 1), dark pink (cluster 2), dark blue (cluster 3), dark green (cluster 4), light pink (cluster 5) and light blue (cluster 6).

locations in a sequential manner (Fig 1.4 B) and six Trp residues are found in four of the six hydrophobic clusters such that Trp-28 in cluster 2, Trp-62 and Trp-63 in cluster 3, Trp-108 and Trp-111 in cluster 5 and Trp-123 in cluster 6[45]. Hydrophobic clusters 3 and 5 which include the inter-domain loop region and helix-D are involved in fibril formation by establishing long-range interactions[46,65].

Studies have revealed the effects of surfactants[66–69], osmolytes[69] and naturally occurring polyphenols[70,71] on Lyz fibrillation and it is known that the fibril assembly begins by establishing hydrophobic interactions at early stages. Fibrillation of Lyz has been observed under various solution conditions. Studies at acidic conditions[52,72,73], neutral pH and high temperature[73], alkaline conditions[74,75] and with the addition of denaturants, demonstrate that in all these conditions partial unfolding of Lyz is the initiation step in the fibril formation. In a few studies, Lyz-surfactant complexes are analysed to probe the charge and hydrophobic interactions existing between the protein and surfactants. Lyz is a positively charged protein (+8) at neutral pH[76]. Thus, the stability of Lyz has been studied by charge neutralization upon addition of sodium dodecyl sulfate (SDS) which showed turbidity at lower concentrations of SDS. With further addition of SDS more precipitate is formed, but when SDS concentration reaches saturation redissolution begins[77].

To study the role of hydrophobic interactions on the stability and fibrillation of Lyz, cosolvents with different functional groups having varying hydrophobicity and yet soluble in water could be a suitable option. Addition of such solvents could perturb the hydrophobic interactions in the protein. Ionic liquids can be one such cosolvent molecules, as they possess all these properties[78,79].

1.8 Ionic liquids

Ionic liquids (ILs), also known as “green solvents,” are the organic salts which possess low melting points, usually below 100 °C. These are compounds of cations such as imidazolium, pyridinium, quaternary ammonium and quaternary phosphonium, and anions such as halogens, triflate, tetrafluoroborate and hexafluorophosphate, which exist in the liquid state. Wilkes and Zaworotko, first time in 1992, reported that the air- and moisture-stable ionic liquids are feasible at room temperature[80]. Since then, the use of ionic liquids was revolutionised in various areas of chemistry and biochemistry. Though ILs were designed as non-flammable

alternatives to common organic solvents, there are enormous applications in many fields. Ionic liquids are efficiently used for chemical synthesis and catalysis[81,82], electrochemistry, biomass conversion, fuel production and processing liquid crystal development, biotechnology and many more[83]. Ionic liquids are versatile chemical species and generally can be used as cosolvents, emulsifiers, copolymers and solvents or antisolvents (design of crystalline substances). ILs can also be used in micellization, electrochemistry and spectroscopy. In addition to the multitude of uses in the pharmaceutical field, these green chemicals are also useful as adjuvant components in crystallization[84,85].

ILs have proved to be of great importance in the field of drug synthesis and delivery systems. ILs possess good solvent characteristics, thus extensively used as reaction media and catalysts as they possess excellent capability of forming intense intermolecular interaction with solutes. ILs also called as “chaperones” by many researchers and are used as stabilizing agents for various enzymes, because they have the ability to interact with water as well as protein surface. It has been proved that there are enhanced activity of enzymes[86,87] in the presence of ILs. Moreover, ILs behave as folding/refolding agents of proteins and also reduce protein aggregation[88,89]. Studies have revealed that imidazolium-based cations having short alkyl side chains could better stabilize the protein structure as compared to large proteins with multiple domain[90,91].

Based on the prior knowledge about the stability and fibrillation of various proteins, Lyz was chosen as a model protein. To accomplish a better understanding about how perturbing the hydrophobic factor alters the fibrillation propensity of the protein, nine different ionic liquids with varying degrees of hydrophobicity were chosen and the studies were carried out at neutral pH. The thermodynamic components involved in stabilizing or destabilizing Lyz was studied. Further, the structural changes in the protein and the mechanistic behaviour of fibrillation kinetics were monitored in the presence of these ionic liquids. Microscopic details of fibrils helped to understand the morphology of fibrils formed under varying hydrophobic triggers. Molecular dynamic simulation studies were also performed on Lyz in the presence of all the ionic liquids to understand the molecular level interactions. Moreover, the effects of mixtures of ionic liquids on stability and fibrillation of Lyz was examined to understand the synergistic or counteracting effect of ionic liquids with varying hydrophobicity.

Chapter 2
Alkyl chain-induced hydrophobicity on the stability and fibrillation propensity of lysozyme

2.1 Introduction

Ionic liquids (ILs) have replaced volatile organic compounds as solvents in many chemical and biotechnological applications[92]. The tremendous possibility in the selection of cation and anion combinations enabled them to achieve a wide range of polarity, hydrophobicity, and miscibility in both organic and inorganic solvents. This versatility has extended their applications into electrochemistry, liquid crystal development, biomass conversion, biotransformation, and pharmaceutical industries[93–95].

Since the first report by Summer & Flowers[96] on enhancing the refolding yield of lysozyme, many studies have been carried out to analyze the effect of various ILs on refolding yield and stability of different proteins[97–99]. ILs used as 'neat solvents' or as cosolvents are found to stabilize proteins and increase enzyme activity[100,101], but in many cases, destabilization of proteins by ILs is also observed. For instance, ammonium-based ILs with phosphate or sulfate anions stabilize myoglobin whereas acetate anions destabilize the protein[102]. On the other hand, the same IL might show different effects on different proteins. BMIC stabilizes α-chymotrypsin[103] whereas it destabilizes myoglobin[104]. 1-Butyl-3-methylimidazolium nitrate reduces the aggregation of lysozyme whereas it promotes β-lactoglobulin aggregation[105]. Few ILs show a concentration-dependent effect on the stability that at lower concentrations they stabilize the proteins, whereas at higher concentrations they destabilize [106,107]. Though ILs reduce the stability of some proteins, they might increase the solubility and decrease the aggregation propensity of the proteins [108]. These observations indicate that the IL-induced changes on the stability of proteins depend on various factors such as protein surface charge, polarity of IL, amphiphilicity of IL, and the distribution of water and IL in solution [93,109]. Notably, many studies indicate that ILs do not follow the Hofmeister series in their chaotropic or kosmotropic behavior on proteins [100,103,110] and their effects are different from the effects exerted as individual ions [104].

ILs also influence the amyloid fibril-forming propensity of proteins. Fibrillation propensity of proteins depends on various factors such as conformational flexibility, surface charge, and hydrophobicity [111]. This is also influenced by the presence of small molecules or cosolvents [112,113] as they might alter the conformational state of the proteins. Partially unfolded forms of globular proteins are more prone to adapt to the fibrillation pathway than the native compact states. The partially unfolded protein chains come together to form an initial amorphous oligomeric state known as nucleus. These nuclei are further converted into stable cross β-sheets to form amyloid-like fibrils [114]. Under certain conditions, proteins may directly

form fibril structures without any notable nucleation phase. The former process is known as nucleation-dependent fibrillation and the latter is known as nucleation-independent polymerization. A change in solution condition and the presence of a cosolvent may switch the fibril formation pathway from one to another [115,116]. Also, the cosolvent can alter the kinetic parameters such as lag time and elongation rate. Taurine decreases the fibril elongation rate of lysozyme without any effect on lag time,[117] whereas tetracyclic indole alkaloid increases the lag time and decreases the elongation rate [118].

Lysozyme, a glycosidase enzyme that hydrolyzes the β-1,4-glucosidic linkages of peptidoglycan in the bacterial cell wall, serves as a model protein to study protein stability, folding, misfolding, and fibrillation [119–122]. Lyz forms fibrils under different denaturing conditions such as acidic pH [123], basic pH [119,120] and the addition of denaturants [122]. Further, experiments on the effect of surfactants [119,120,122], osmolytes[124], and naturally occurring polyphenols [125,126] on Lyz emphasize the role of hydrophobic interactions in the early stages of fibril formation. For instance, silybin-B (a flavonoid lignin)[127] and sennoside (a glycoside)[128] interact with the residues in hydrophobic clusters 3 and 5 of Lyz, which increases the nucleation time and reduces the oligomerization of lysozyme[127]. A similar effect on fibrillation is observed in the presence of coralyne (an isoquinoline alkaloid) as well[129]. Surfactants, at their monomeric and micellar states, show different effects on the fibril formation of lysozyme[122,130].

ILs mainly form ionic interactions and hydrogen bonding networks with proteins and solvents, but the role of hydrophobicity in IL-induced effects on proteins cannot be completely ruled out. A recent molecular dynamic simulation study [131] using an amyloidogenic fragment of Lyz suggests that the hydrophobic residues in the long-loop region and helix-C of the protein have larger tendency to form β-strands and might stabilize the intermediate states during oligomer formation. Nevertheless, the effect of change in hydrophobicity of ILs on the fibril formation of proteins is not well understood. In the present study, 1-methylimidazolium based ionic liquids (Im-ILs) with varying alkyl chains (H-, -ethyl, -butyl, -hexyl, and -octyl) and the fibril formation of Lyz reported at pH 7 condition [132] were chosen. Fibril formation of the protein in aqueous solution containing varying concentrations of the ILs was analyzed. Also, the stability and structural changes of the protein with ILs were examined by spectroscopic methods. To obtain mechanistic insights into the effect of (de)stabilization and fibrillation, the atomic-level interactions were analysed by molecular dynamic simulations of Lyz in the absence and presence of Im-ILs. Various global parameters to determine the structural fluctuations and compactness in the protein and residue-level interactions with ILs were

analyzed from the simulation trajectories. The experimental and simulation results indicate that ILs with increasing hydrophobicity tend to interact more with protein and inhibit fibrillation.

2.2. Materials and methods

2.2.1. Materials

Hen egg lysozyme (Lyz), thioflavin-T (ThT), 8-anilinonaphthalene-1-sulphonic acid (ANS), 1-methylimidazolium chloride (MIC, CAS No. 35487-17-3), 1-ethyl-3-methylimidazolium chloride (EMIC, CAS No. 65039-09-0), 1-butyl-3-methylimidazolium chloride (BMIC, CAS No. 79917-90-1), 1-hexyl-3-methylimidazolium chloride (HMIC, CAS No. 171058-17-6) and 1-methyl-3-octylimidazolium chloride (OMIC, CAS No. 64697-40-1) were purchased from Sigma-Aldrich. Dithiothreitol (DTT) and phosphate buffer salts were obtained from SRL, India. All the chemicals were of analytical grade and used without any further purification. Structures of all the Im-ILs chosen for this study are shown in Fig. 2.1.

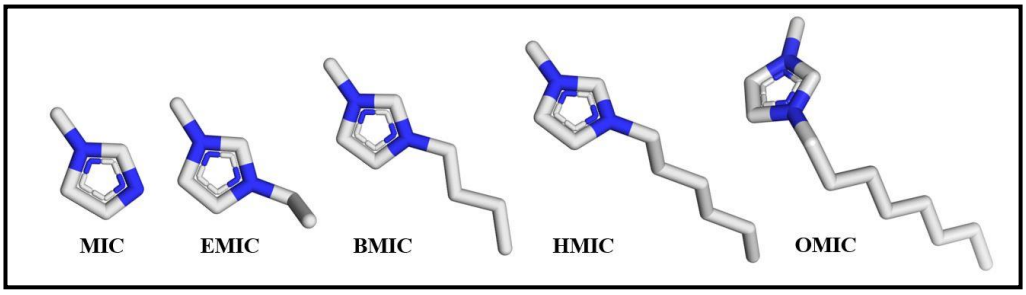

Fig 2.1 Imidazolium-based ionic liquids (Im-ILs) used in the study, 1-methylimidazolium chloride (MIC), 1-ethyl-3-methylimidazolium chloride (EMIC), 1-butyl-3-methylimidazolium chloride (BMIC), 1-hexyl-3-methylimidazolium chloride (HMIC), and 1-methyl-3-octylimidazolium chloride (OMIC). Carbon atoms are in grey and nitrogen atoms are in blue.

2.2.2 Fibrillation Studies

To study the fibril formation of Lyz, 140 μM of the protein was incubated with 14 mM of DTT at 50 ^{o}C in 10 mM phosphate buffer at pH 7.0. Fibril formation was monitored by the change in fluorescence of 50 μM of thioflavin-T added into the reaction mixture. The emission spectra between 460 and 520 nm were collected before and after the incubation at 50 ^{o}C, having been excited the samples at 440 nm. To evaluate the rate of fibrillation, the samples were excited at 440 nm and the emission was followed at 485 nm at different time intervals. The effect of IL on the fibril formation of Lyz was studied by adding varying concentrations of the ILs

ranging between 1 mM to 500 mM. All the spectra were measured in Jasco FP-8500 spectrofluorometer connected to a Peltier. The kinetics at each concentration of IL was measured at least two times.

Lag-independent kinetic data obtained from the experiments were fitted to the following equation,

$$Y = b + a(exp^{-k_f.t}) \quad (2.1)$$

where, *Y* corresponds to change in ThT fluorescence, *b* is exponential maxima, *a* represents the amplitude of fluorescence change, k_f is the rate of fibrillation and *t* is time. Lag-dependent kinetic data were analyzed with the following equation [133,134],

$$Y = (y_i - m_i t) + \frac{(y_f + m_f t)}{1 + (exp^{k_f(t-t_o)})} \quad (2.2)$$

where, *Y* is the change in fluorescence, y_i and m_i, and y_f and m_f are intercepts and slopes of the initial and final phases, respectively. k_f is the rate of fibril elongation, t_o is the time required to attain half of the total fluorescence change and *t* is time.

Lag time was calculated as,

$$t_{lag} = t_o - 2\tau \quad (2.3)$$

where τ is elongation time constant equal to $1/k_f$.

Apparent fibrillation time (T_{app} - the time taken by Lyz to reach the saturation phase of the kinetics) was evaluated by the following relation,

$$T_{app} = \begin{cases} 2.3/k_f & \text{for lag} - \text{independent kinetics} \\ t_{lag} + (2.3/k_f) & \text{for lag} - \text{dependent kinetics} \end{cases} \quad (2.4)$$

2.2.3. Structural studies

The absorbance changes of Lyz in buffer containing varying concentrations of the ILs ranging from 1 mM to 500 mM were measured in Cary 100, Agilent spectrophotometer using a 1 cm pathlength quartz cuvette. For all the measurements, the corresponding concentration of IL was used for baseline correction. The intrinsic fluorescence changes of Lyz were followed from 320 to 400 nm by exciting the protein at 280 nm. Fluorescence of NATA (10 μM) with the studied ILs were performed to confirm the quenching of Trp fluorescence by ILs. The change in fluorescence of ANS, an extrinsic fluorescence probe, was measured between 480 and 650 nm upon excitation at 380 nm. The concentration of ANS was 50 μM in all the samples. Near-UV circular dichroism (CD) spectra of Lyz in the presence of different concentrations of ILs were collected using a 1 cm pathlength quartz cuvette with the protein concentration of 15

μM in 10 mM phosphate buffer at pH 7.0 (± 0.1) in Jasco J-1500 spectropolarimeter. For all the spectra, the corresponding concentration of IL was taken as a baseline. Each spectrum was an average of two acquisitions. Far-UV CD spectra of the protein in the presence of ILs could not be obtained due to high voltage which might arise from the absorption of ILs in the far-UV range [135–137].

2.2.4. Thermal Denaturation

Thermal denaturation of Lyz in buffer containing varying concentrations of ILs was carried out by following the absorbance changes at 301 nm by heating the samples from 20 to 90 ºC with the scan rate of 1 ºC per min using a Peltier attached with the spectrophotometer (Cary 100, Agilent). The thermal denaturation curves following two-state transitions (native ↔ unfolded) were analyzed using the following equation [138],

$$Y = \frac{(y_n + m_n T) + (y_u + m_u T)\, e^{\Delta H_m\left(\frac{T}{T_m} - 1\right) + \frac{\Delta C_p\left(T_m - T + \left(T \ln\frac{T}{T_m}\right)\right)}{RT}}}{1 + e^{\Delta H_m\left(\frac{T}{T_m} - 1\right) + \frac{\Delta C_p\left(T_m - T + \left(T \ln\frac{T}{T_m}\right)\right)}{RT}}} \qquad (2.5)$$

where, Y is normalized values of absorbance, y_n and y_u are the intercepts, and m_n and m_u are the slopes associated with the pre- and post-transition regions, respectively. T_m is temperature at transition midpoint, ΔH_m is enthalpy change at the midpoint transition temperature, and ΔC_p is heat capacity change associated with the unfolding transition. T is temperature in kelvin and R is the gas constant.

2.2.5. Microscopic images

The 200-mesh carbon-coated transmission electron microscopy (TEM) grids (purchased from Ted Pella) were mounted on the top of 5 μl Lyz fibrils, formed in the absence and the presence of different ILs for 5 minutes. Excess sample was removed by wicking method, using the ashless filter paper at the edge of TEM grid and air dried at room temperature for 5 minutes. Immediately after drying, grid was stained with 2% uranyl acetate prepared in distilled water. After 5 seconds, excessive stain was removed by the wicking method and grid was washed with MilliQ water twice to remove stain particles in the regions other than fibril. Stained and washed grids were left overnight to completely air dry in TEM grid carrier case and examined the

following day using JEOL transmission electron microscope (TEM) at an accelerating voltage of 200 kV. The fibril morphology was analyzed using FIJI software.

2.2.6. Molecular dynamic (MD) simulations

GROMACS package 5.1.4. with OPLS AA/L forcefield and TIP3P water model were used to carry out all the simulations at 300 K. The crystal structure of Lysozyme (lyz) (PDB ID: 5K2P) was obtained from the Protein Data Bank (www.rcsb.org). Co-crystallized ligands and water molecules were removed prior to the simulations. The parameters for ionic liquids were obtained from LigParGen, OPLS/CM1A Parameter Generator for organic ligands (http://zarbi.chem.yale.edu/ligpargen)[139–141]. Lyz molecule was placed in a cubic box extended by 1.3 nm from its surface with the volume of 448.47 nm^3. Simulations of the protein in the absence and presence of 50 mM and 200 mM ILs were carried out. Number of water and IL molecules used in each simulation are presented in Table 2.1. Bulk system properties were mimicked by applying the periodic boundary conditions. All the simulation systems were energy minimised using 10,000 steps of steepest descent algorithm. Pressure was kept constant at 1 atm for 1 ns by using Parrinello-Rahman barostat and temperature was set to 300 K for 1 ns by using modified Berendsen thermostat. Production simulation were run for 100 ns and the trajectories were collected at every 10 ps interval.

Table 2.1: Details of the number of ILs and water molecules used in MD simulation

IL	50 mM			200 mM		
	Number of IL molecules	**Number of water molecules**	**Obtained concentration (mM)**	**Number of IL molecules**	**Number of water molecules**	**Obtained concentration (mM)**
MIC	12	13607	48.95	48	13417	198.56
EMIC	12	13576	49.06	48	13331	199.84
BMIC	12	13559	49.12	48	13229	201.37
HMIC	12	13532	49.22	47	13146	198.43
OMIC	12	13506	49.32	47	13055	199.81

2.2.7 Analysis of simulation trajectories

Analyses were carried out using various tools available in GROMACS package 5.1.4. Root mean square deviations (RMSD) and root mean square fluctuations (RMSF) for C_α-atoms

of the protein, and solvent accessible surface area (SASA) and radius of gyration (R_g) of the whole protein were determined. Radial distribution functions (RDFs) for the heavy atoms of protein against heavy atoms of water and ILs were evaluated for last 80 ns of the simulation trajectories in the presence of ILs and compared with the RDFs of protein in pure aqueous medium. The mean distribution of water and ILs around the protein was calculated for last 80 ns to evaluate the following parameters.

2.2.7.a. Number of water and ILs

Number of water molecules, IL molecules and groups of ILs (ring, butyl chain and methyl group) within cut-off 0.32 nm, 0.42 nm and 0.62 nm from the surface of protein were evaluated using gmx select command, and averaged for last 80 ns. Further, the number of water and ILs molecules around each amino acid residue were also calculated for each cut-off.

2.2.7.b. Hydration fraction

Hydration fractions (χ_{hyd}) for a given cut-off were determined to know the distribution of water and ILs around the protein, by calculating the ratio between the fraction of water molecules and ILs,

$$\chi_{hyd} = \frac{(n_w/N_w)}{(n_{IL}/N_{IL})} \tag{2.6}$$

where, n_w and n_{IL} are number of water and IL molecules within the given cut-off while N_w and N_{IL} are the total number of water and ILs in the simulation box. Hydration fractions for protein were calculated with three different cut-offs, 0.32 nm (1st hydration shell), 0.42 nm (2nd hydration shell) and 0.62 nm (1st coordination sphere of IL) which were obtained from the analysis of RDFs of water and IL.

2.2.7.c. Preferential interaction coefficient

It explains the preferential binding or exclusion of cosolvent from the vicinity of the protein with respect to water molecules in a ternary system having solute (protein), solvent (water) and cosolvent[142]. Preferential interaction coefficients of ILs with Lyz were calculated from following equation[143],

$$\Gamma_{P-IL} = \rho_{IL}\,(G_{P-w}\,(r) - G_{P-IL}\,(r)) \tag{2.7}$$

where, Γ_{P-IL} represents preferential interaction coefficient, ρ_{IL} is the number density of ILs in bulk solution and is evaluated by number of IL molecules over the volume of simulation box. Here, $G_{P-w}(r)$ and $G_{P-IL}(r)$ are Kirkwood-Buff integrals (KB integrals) for protein-water and protein-IL, respectively that was calculated at every 0.02 nm cut-off as,

$$G(r) = \int_0^r 4\pi r^2 (g(r) - 1)\, dr \tag{2.8}$$

where, (*g(r)*) is the integrated RDF values at every 0.02 nm distance interval upto 1 nm cut-off. Positive values would indicate the favourable binding of ILs to the protein surface within the cut-off distance.

2.2.7.d. Transfer free energy

It is the amount of energy required for a cosolvent (IL) molecule to reach the vicinity of the protein (Lyz) molecule from the bulk solution. Transfer free energies (ΔF^t_{P-IL}), were derived from KB integrals using the following equation[144],

$$\Delta F^t_{P-IL} = -R\,T\,G_{P-IL}(r) \tag{2.9}$$

where, *R* is the gas constant (1.98 cal mol^{-1} K^{-1}), T is temperature.

Negative values of free energy would indicate that the presence of IL molecules at the given distance is an outcome of favorable interaction with the protein.

2.2.7.e. Residue-wise interaction between Lyz and ILs

To understand the residue-level interaction of ILs with Lyz, the mean distance between IL and each amino acid (129 in Lyz) residue was evaluated using gmx distpair in Gromacs. Further, the number of times IL appeared near each amino acid within the distance cut-off 0.62 nm was counted. These numbers were converted into fraction of times the presence of IL around the protein. The obtained values were between 0 and 1, where 0 indicated no interaction of IL with a particular amino acid and 1 represented the maximum interaction. These values corresponding to each amino acid of the protein were used to assign colors on the residues of Lyz depicting the strength of binding of IL.

2.3 Results

2.3.1 Fibril formation of Lyz in ILs

Lyz forms fibrils under various denaturing conditions. Both nucleation-dependent and nucleation-independent pathways of fibrillation are reported for Lyz [122,132]. In an earlier study from our research group, it was reported that Lyz could form fibrils in the absence of any denaturant at neutral pH when its disulfide bonds were reduced using DTT and incubated at 50 ^{o}C [132]. This condition was first verified by the increase in fluorescence of thioflavin-T (ThT) which specifically binds to amyloid-like fibrils (Fig. 2.2 A). The rate of fibril formation was also followed using ThT (Fig. 2.2 B). The kinetic profile suggested that the protein underwent nucleation-independent polymerization reaction and the rate of fibrillation was calculated to be 0.08 min^{-1}. The fibril formed by Lyz in this condition was confirmed by a TEM micrograph (Fig. 2.2 C).

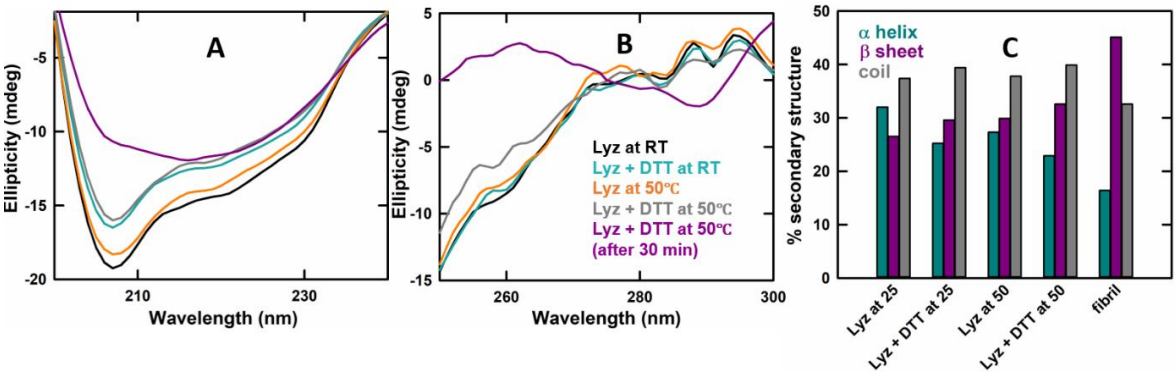

Fig 2.2 (A) Far-UV circular dichroism spectra of Lyz at room temperature (RT) in black, with DTT at RT in cyan, without DTT at 50°C in orange, at fibrillation condition, that is at 50 ^{o}C with DTT in grey and after incubation at fibrillation condition for 30 min in purple. (B) Near-UV CD spectra showing tertiary structural changes in Lyz at the given condition. (C) The secondary structural content of the protein at these conditions are derived from the far-UV CD spectra using Young's method provided in the instrument, J-1500 circular dichroism spectrophotometer.

Secondary and tertiary structural changes of Lyz under the fibrillation condition were analyzed by measuring the circular dichroism spectra in far-UV and near-UV region. Negative peaks at 222 nm and 218 nm are indicative of α-helix and β-sheet structures in a protein. Lyz showed changes in its secondary structural content with the addition of DTT at room temperature which was further more decreased when the protein was treated at higher temperature (50 °C). Additionally, β-sheet content was increased as compared to Lyz at the native conditions (Fig 2.2 A and C). Further, incubation at fibrillation condition for 30 min

showed increase in β-sheet to 45% (against 26% in the native Lyz) with the loss of α-helical content to half of the total content present in the native conformation (Fig 2.2C). The near-UV spectra collected at the same conditions (Fig 2.2B) suggested that the addition of DTT and heating at 50 ℃ lead to the loss of tertiary interactions in the protein.

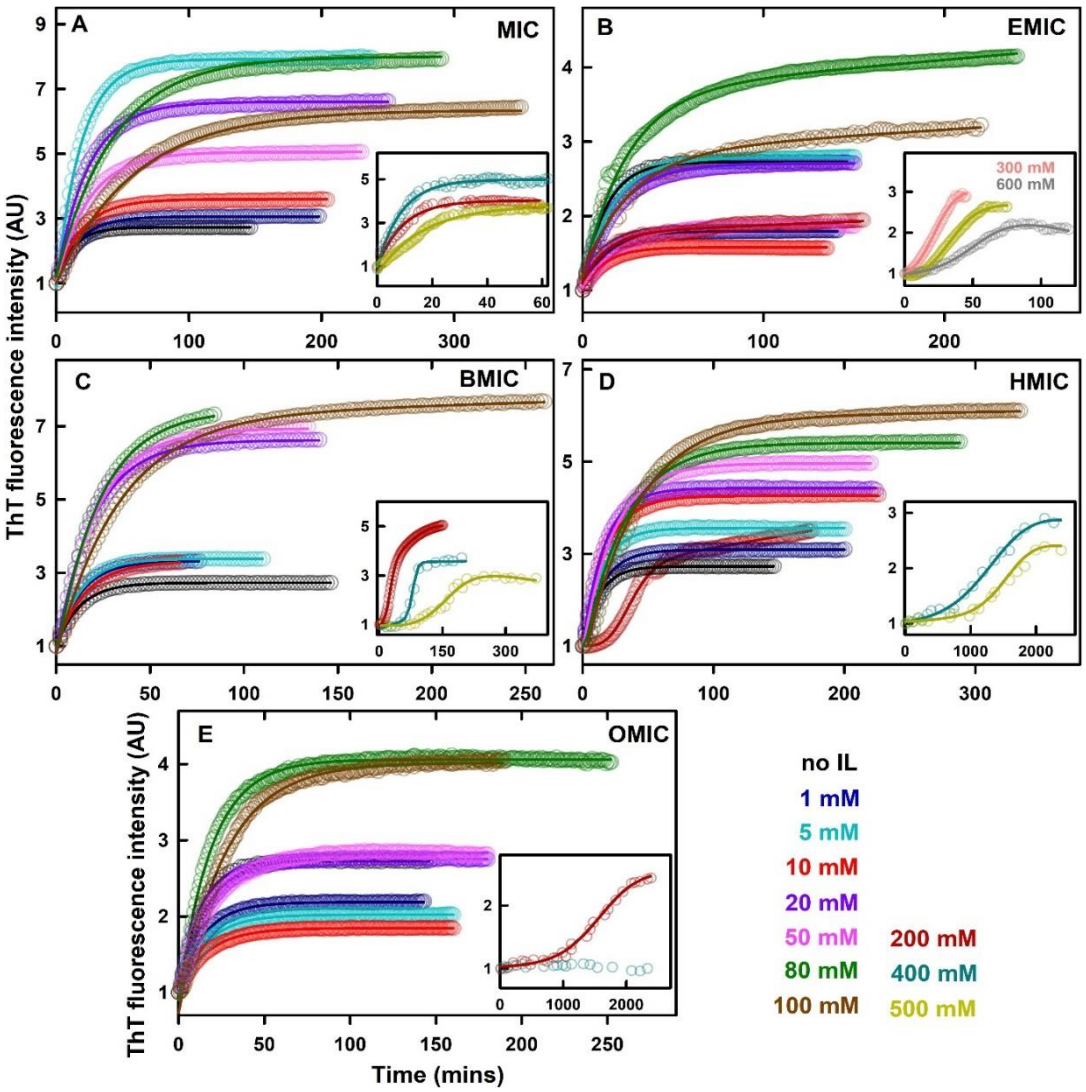

Fig. 2.3 Rate of fibril formation of Lyz followed by the change in ThT fluorescence at 485 nm in varying concentrations of Im-ILs, (A) MIC, (B) EMIC, (C) BMIC, (D) HMIC, and (E) OMIC. The concentrations above 200 mM are presented in insets. The colors represent the different concentrations of ILs as given in the legend. The solid lines represent the data-fit using equation (1) or (2) for the kinetic traces following nucleation-independent and nucleation-dependent pathways, respectively. It may be noted that during the reaction insoluble fibrils were also observed. Therefore, the fluorescence intensity could not be directly correlated with the yield of the fibrils formed.

Further, the rate of fibril formation of Lyz was calculated in the presence of varying concentrations of five different Im-ILs by monitoring the changes in the fluorescence of ThT (Fig. 2.3 & Fig. 2.4). The addition of ILs altered both the rate and fibrillation mechanism of the protein in a concentration-dependent manner.

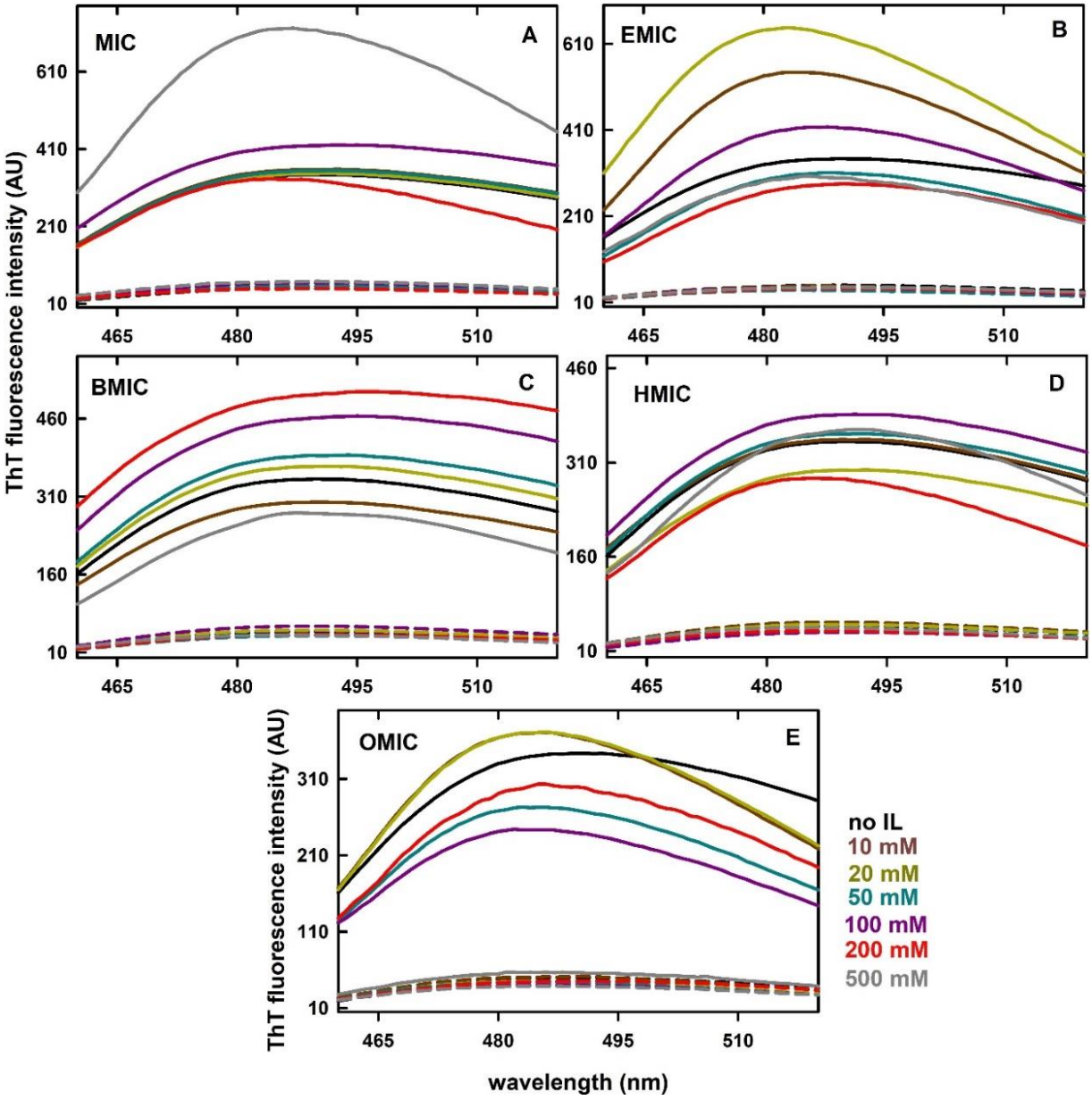

Fig. 2.4. Representative fluorescence emission spectra of ThT in DTT-reduced Lyz in varying concentrations of (A) MIC, (B), EMIC, (C) BMIC, (D) HMIC, and (E) OMIC measured before incubating at 50 ^{o}C (dotted lines) and after the incubation (solid lines). The fluorescence intensity of ThT was not significantly increased in the presence of 500 mM of OMIC (gray solid line in panel E) due to inhibition of fibril formation.

At lower concentrations, up to 100 mM, the fibrillation followed a nucleation-independent polymerization pathway without any detectable lag phase. At concentrations above 100 mM, all the ILs, except MIC, switched the fibrillation into the nucleation-dependent pathway with a notable nucleation or lag phase. These kinetic traces were analyzed using equations (2.1) and (2.2), respectively, and the obtained parameters are presented in Fig. 2.5. With increasing concentration of MIC (upto 100 mM), a gradual decrease in the rate of fibrillation of Lyz was observed. The rate was nearly unaffected by the other ILs until 20 mM, but was slightly decreased at above 20 mM. MIC showed the largest retardation of fibrillation rate in the concentration range 1-100 mM whereas OMIC and HMIC had the least effect. Increasing the concentration of IL above 100 mM (where lag phase was observed except in MIC) increased the elongation rate of fibrillation even higher than the rate observed in the buffer except in the case of OMIC. The highest increase was observed for BMIC. Further increase in the concentration of MIC and EMIC showed only a slight decrease in elongation rate. However, BMIC and HMIC strongly reduced the rate. Exceptionally, OMIC showed a drastic decrease in the elongation rate when the concentration was raised above 100 mM. Also, the protein did not show any fibril formation in the presence of OMIC at concentrations above 200 mM even after incubating for 36 hrs.

To understand how the lag time was changed with the increase in concentration of ILs, the lag time were evaluated for the nucleation-dependent kinetics using equation 2.3. The lag time (Fig. 2.5 A inset) increased with the increasing concentration of ILs. Also, the lag time increased with the increasing alkyl chain length. The extent of increase was in the order of EMIC < BMIC < HMIC. Though Lyz did not form fibrils in the presence of OMIC at concentrations above 200 mM, the lag time in 200 mM of OMIC was comparable to that observed in 500 mM of HMIC.

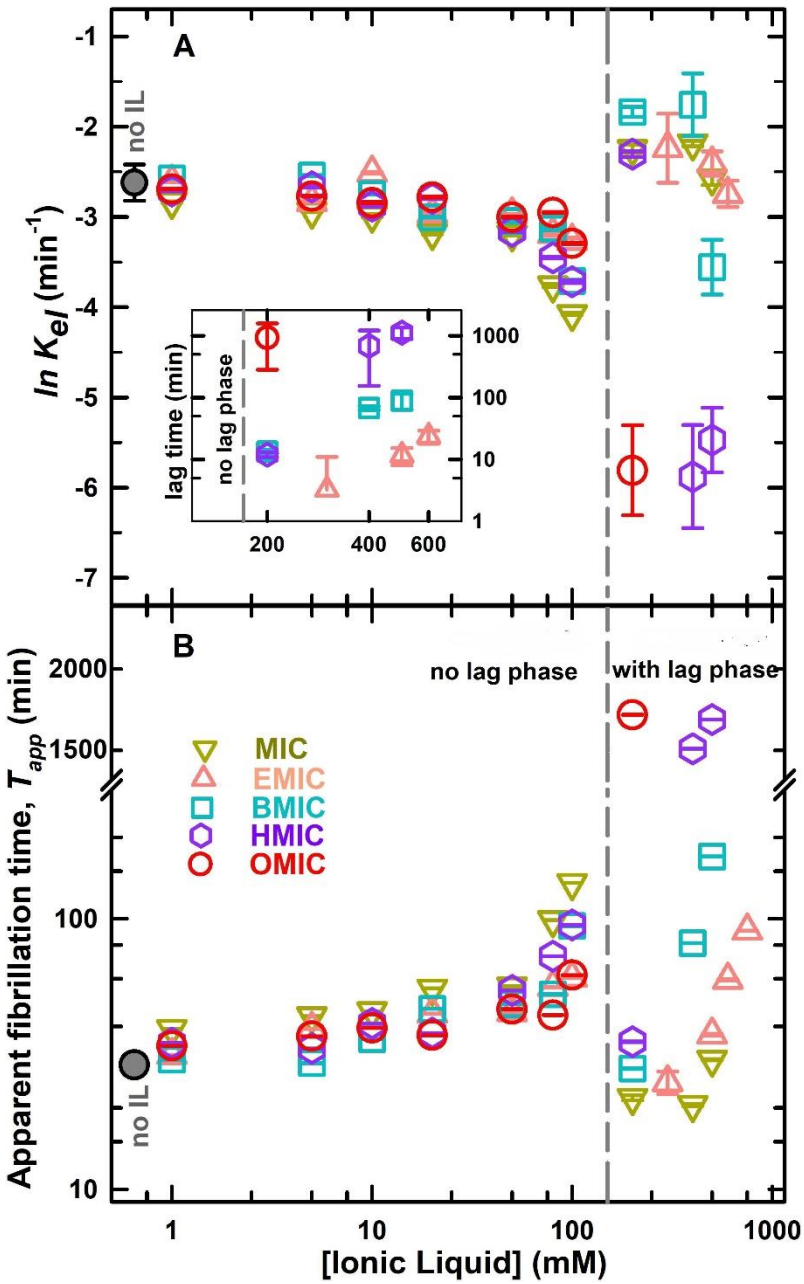

Fig. 2.5. (A) Rate of fibril formation of Lyz in the presence of varying concentrations of the ILs, MIC (green inverted triangles), EMIC (pink triangles), BMIC (cyan squares), HMIC (purple hexagons), and OMIC (red circles), obtained from the kinetic traces presented in Fig. 2.3. The lag time calculated for the conditions following nucleation-dependent mechanism are presented in the inset. (B) Apparent fibril formation time in varying concentrations of the ILs. The values of *ln* k_f and T_{app} in the absence of any IL are given as black circles. In the presence of MIC, no lag phase was observed at all the concentrations.

For further detailed interpretation, the apparent time taken by the protein to reach the saturation phase (T_{app}) in varying concentrations of ILs were evaluated using equation 2.4. This parameter can reflect the combined changes in lag time and elongation rate, thus can be used to analyze the overall effect of ILs on the fibrillation propensity. The change in T_{app} values also showed the biphasic trend (Fig. 2.5 B). At lower concentrations, the time for fibrillation was increased with increasing concentrations. At above 100 mM, fibrillation was completed in a shorter time either with or without (in MIC) lag phase, but further increase in the concentration increased the time for complete fibril formation. The extent of increase was marginal in the case of MIC whereas other ILs showed a significant increase. In case of HMIC, at the highest concentration used in the study (500 mM), the fibrillation time was nearly 55-times more than the time taken in the absence of any IL. In OMIC, even at 200 mM a similar delay was observed.

Fibril formation in the presence of ILs was confirmed by TEM images and the representative micrographs are presented in Fig. 2.6. Fibril morphology in the presence of ILs was similar to the fibrils formed in the absence of any ILs. Moreover, fibrils formed as the result of lag-independent kinetics (lower concentration, 50 mM) as well as lag-dependent kinetics

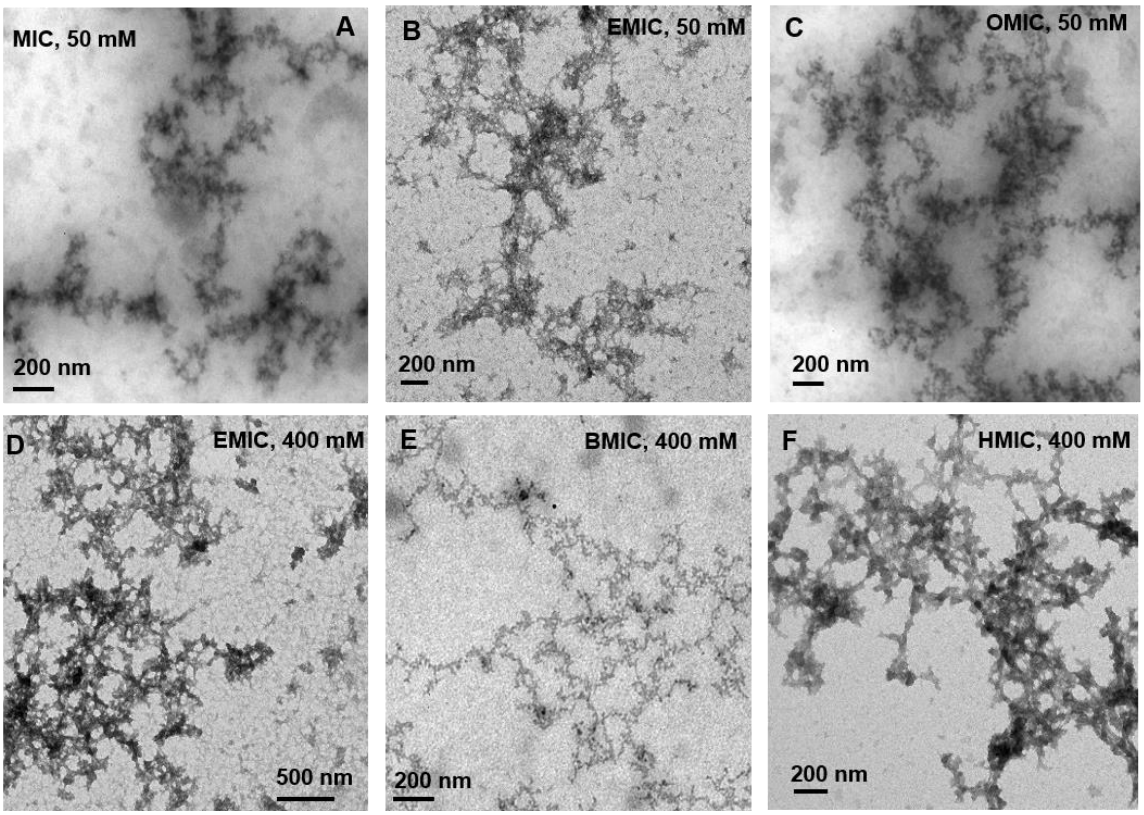

Fig 2.6 Representative TEM images of the fibrils formed by Lyz following lag-independent kinetics (top panels) in the presence of (A) 50 mM MIC, (B) 50 mM EMIC, and (C) 50 mM OMIC and lag-dependent kinetics in the presence of (D) 400 mM EMIC, (E) 400 mM BMIC and (F) 400 mM HMIC.

(higher concentration, 400 mM) showed similar morphologies. Fibrils were dense and thread-like in appearance, often seen clumped together with no distinct strands visible.

2.3.2 Thermal stability of the protein in Im-ILs

The stability of Lyz in buffer containing varying concentrations of ILs was measured by following the change in absorbance of the protein upon unfolding. The thermal denaturation process followed a two-state transition in the presence of all the ILs (Fig. 2.7). In the case of HMIC and OMIC, the thermal transitions showed non-cooperative transitions at concentrations above 200 and 50 mM, respectively, that were not included for further analysis. From other transitions, transition midpoint temperatures (T_m) and enthalpies of unfolding (ΔH_m) were calculated using equation 2.5 (Fig. 2.8).

The T_m values were less in the presence of ILs compared to the value obtained in the buffer; however, all the ILs did not exhibit a similar trend. MIC induced a larger destabilization effect at very low concentrations, (≤ 20 mM) and a further increase in IL concentration

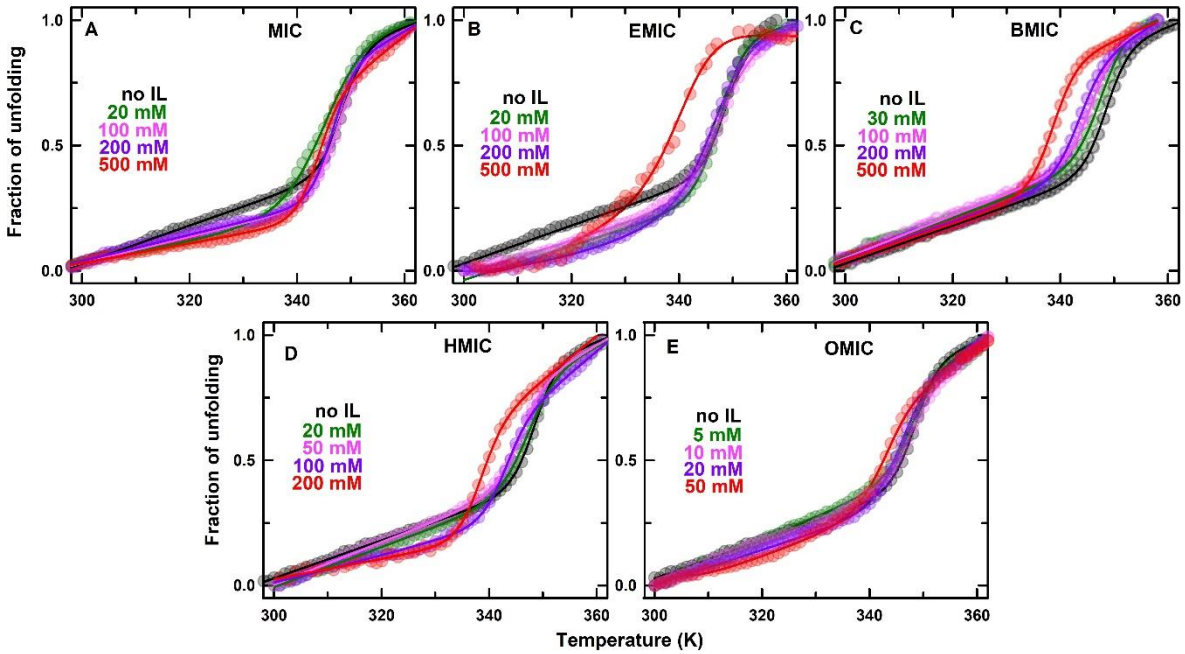

Fig. 2.7 Representative thermal denaturation transitions of Lyz measured by following the change in absorbance of the protein in the presence of varying concentrations of ILs, (A) MIC, (B) EMIC, (C) BMIC, (D) HMIC, and (E) OMIC. The solid lines represent the data fit using equation (6), for two-state transitions. The colors represent the concentration of ILs as mentioned in the legends of each panel. It may be noted that the thermal denaturation curves showed non-cooperative transitions in HMIC and OMIC at concentrations above 200 and 50 mM, respectively.

decreased its destabilization effect. At above 200 mM, the extent of destabilization was again increased. In the case of EMIC, BMIC, and HMIC, the T_m values decreased gradually. At lower concentrations, the destabilizing effect was less, but above 50 mM, there was a significant reduction in the stability. OMIC showed a larger reduction of T_m values even at lower concentrations. As the alkyl chain length increased, the destabilization effect was more pronounced by the ILs even at their lower concentration.

The enthalpy of unfolding (ΔH_m) was less in the presence of lower concentrations of the ILs which increased with the increase in their concentrations. In higher concentrations of MIC and EMIC (>200 mM and >50 mM, respectively), the ΔH_m of the protein was reduced again whereas BMIC and HMIC did not alter the ΔH_m value above 20 mM. In the presence of OMIC, the ΔH_m value was marginally decreased with increasing concentration.

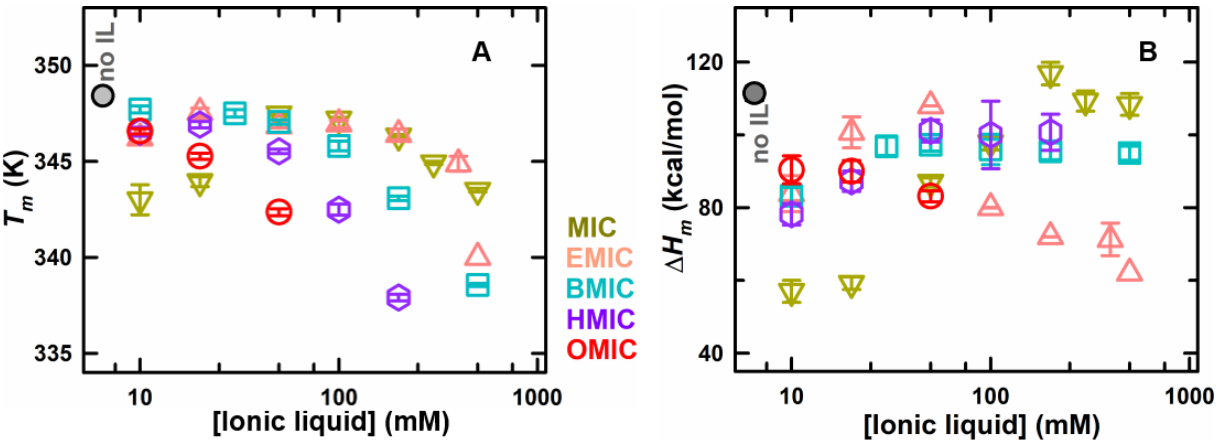

Fig. 2.8 (A) Thermal denaturation midpoint (T_m) and (B) enthalpy of unfolding (ΔH_m) of Lyz in the presence of varying concentrations of ILs, MIC (green inverted triangles), EMIC (pink triangles), BMIC (cyan squares), HMIC (purple hexagons), and OMIC (red circles) evaluated from the thermal denaturation transitions presented in Fig. 2.7. T_m and ΔH_m values in the absence of any IL are given as black circles.

2.3.3. Structural studies

2.3.3.a Absorption spectra of Lyz in ILs

The change in absorption of Lyz with the addition of varying concentrations of ILs was measured. Absorption of the protein was only marginally reduced in the presence of ILs except in HMIC (Fig. 2.9). The absorption was slightly decreased with the increasing concentration of HMIC at lower concentrations (upto 100 mM) whereas a significant reduction was observed at higher concentrations with a small red shift in the maxima from 283 to 285 nm.

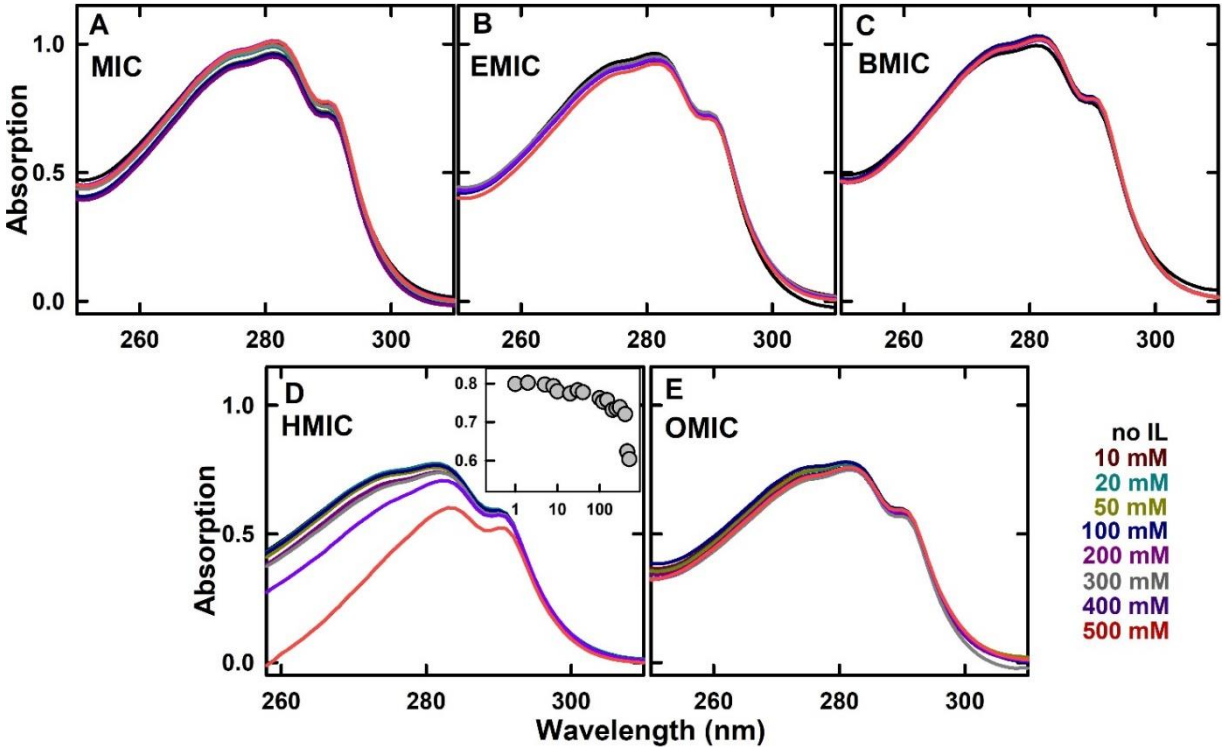

Fig. 2.9. Absorption spectra of Lyz in the presence of varying concentrations of ILs, (A) MIC, (B) EMIC, (C) BMIC, (D) HMIC, and (E) OMIC. The inset in panel (D) shows the change in absorption of Lyz at 283 nm in the presence of varying concentrations of HMIC. Colors of the spectra represent different concentrations of ILs as mentioned in the legend.

2.3.3.b Near-UV CD of Lyz in ILs

The tertiary interactions in Lyz were examined with near-UV CD spectra of the protein (Fig. 2.10). Lyz has six Trp and three Tyr residues. The native form of Lyz showed a weak triplet band arising from its Trp residues in the region of 280-295 nm as reported in earlier studies as well [145]. The band was distorted and the intensity was slightly increased with the addition of ILs. In the region around 260-280 nm, representing the conformational changes around Tyr residues, a gradual loss of ellipticity was observed. In the case of HMIC and OMIC,

at higher concentrations, the ellipticity values were close to zero indicating almost a complete loss of tertiary interactions around the Tyr residues.

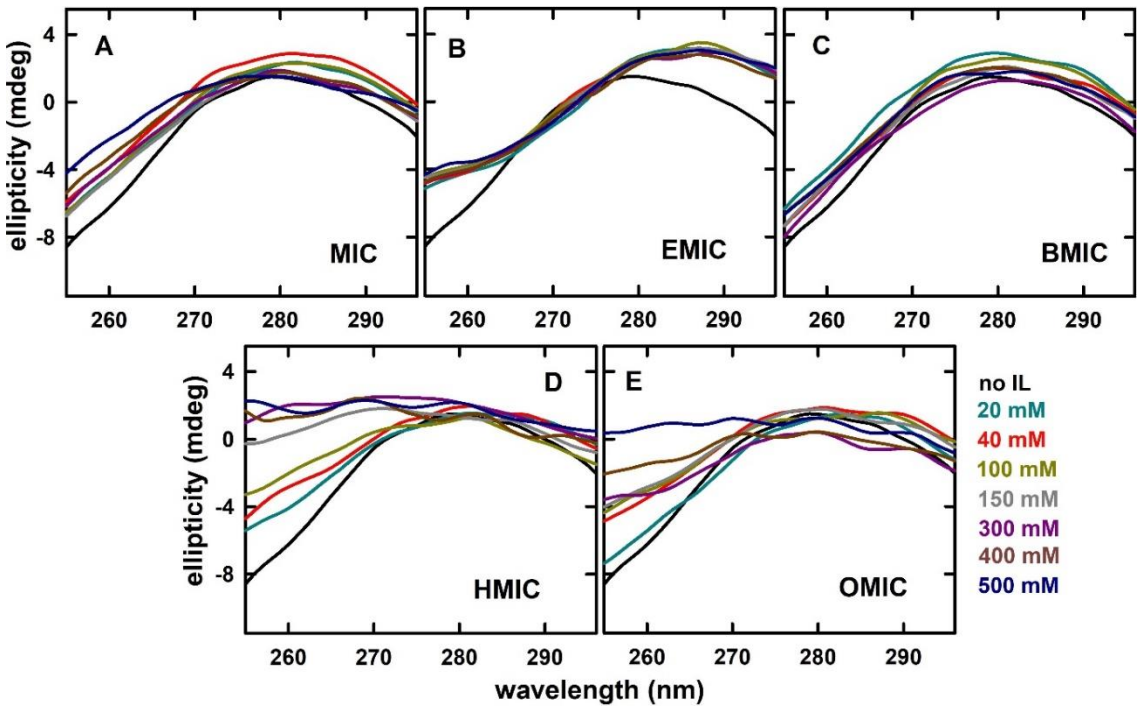

Fig. 2.10 Near-UV CD spectra of Lyz in varying concentrations of ILs (A) MIC, (B) EMIC, (C) BMIC, (D) HMIC, and (E) OMIC. The colors of the spectra represent different concentrations of ILs as mentioned in the legend.

2.3.3.c. Extrinsic fluorescence changes with ANS

The extent of denaturation induced by ILs on the protein could be probed by exposure of hydrophobic residues of the protein upon the addition of IL. ANS is a dye that specifically binds to hydrophobic patches on protein surface that increases its fluorescence emission [146]. Since ILs might alter the fluorescence of dyes, the ANS fluorescence in the ILs alone and in the presence of Lyz was measured (Fig. 2.11). In all the ILs, at concentrations above 100 mM, the ANS fluorescence was sharply increased. In the presence of Lyz, no significant difference in ANS fluorescence was observed suggesting that the exposure of hydrophobic residues by the protein was minimal.

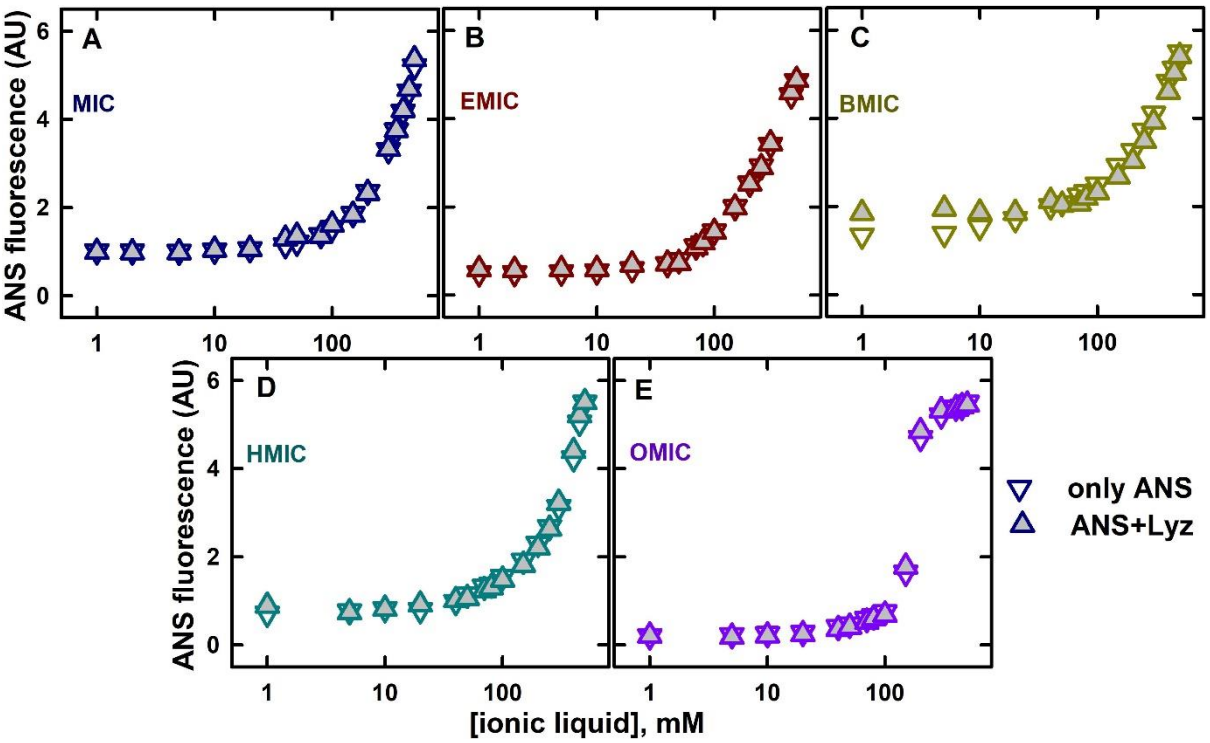

Fig. 2.11 Emission intensity of external fluorescence probe ANS at 520 nm in varying concentrations of ILs (A) MIC, (B) EMIC, (C) BMIC, (D) HMIC and (E) OMIC in the absence (inverted hollow triangles) and the presence of (gray-filled triangles) Lyz.

2.3.3.d. Intrinsic fluorescence changes in Lyz and binding affinity of IL

The change in fluorescence emission of Lyz was analyzed by exciting the protein at 280 nm (Fig. 2.12). At this wavelength, all the aromatic residues are excited [147]. In the presence of MIC, EMIC, and BMIC, fluorescence intensity was slightly decreased in lower concentration (upto 100 mM) whereas a larger decrease was noted above 100 mM concentration. The protein fluorescence was gradually decreased at concentrations above 10 mM of OMIC. HMIC showed a different pattern that at lower concentration, the fluorescence was increased and it gradually decreased when the concentration of IL was above 100 mM. The fluorescence emission maximum (WLmax) of the protein upon excitation at 280 nm was not much affected with the addition of MIC whereas higher alkyl Im-ILs showed a blue shift in WLmax with an increase in their concentration. HMIC-induced the longest blue shift in WLmax at 500 mM followed by OMIC which was larger than EMIC and BMIC at the same concentration.

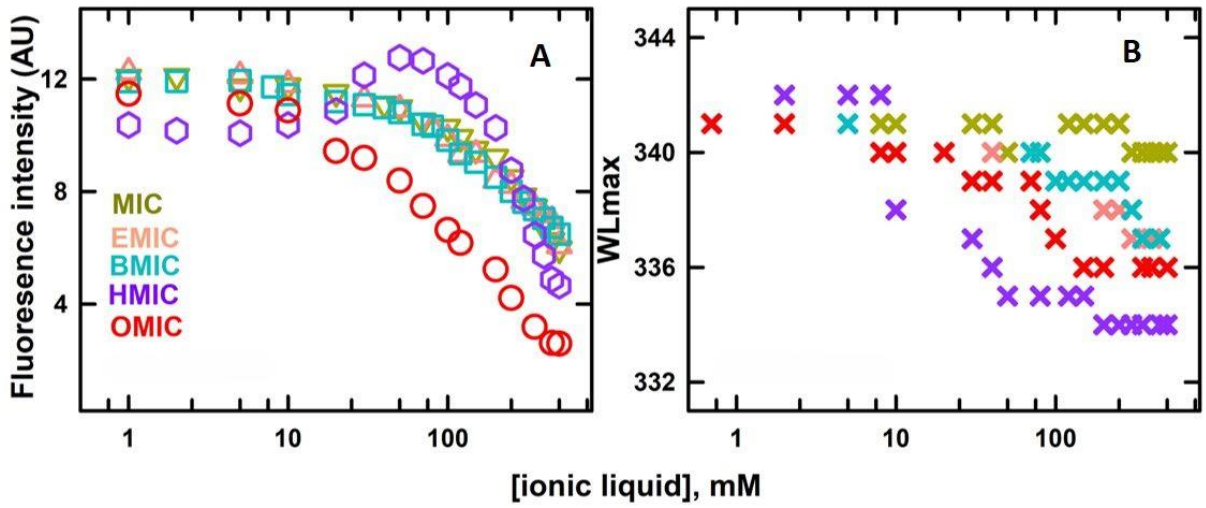

Fig. 2.12 (A) Fluorescence emission intensity of Lyz at 340 nm after exciting the protein at 280 nm in the presence of varying concentrations of the ILs, MIC (green), EMIC (pink), BMIC (cyan), HMIC (purple), and OMIC (red). (B) Emission maxima of Lyz (WLmax) while excited at 280 nm in varying concentrations of the ILs.

It was sceptical to understand the ILs binding on Lyz, as absorbance and extrinsic fluorescence data showed only marginal changes in structure, while a drastic decrease in intrinsic fluorescence with increasing concentration of ILs was observed. To investigate whether the decrease in fluorescence is due to quenching of Lyz's fluorescence by the ILs, the

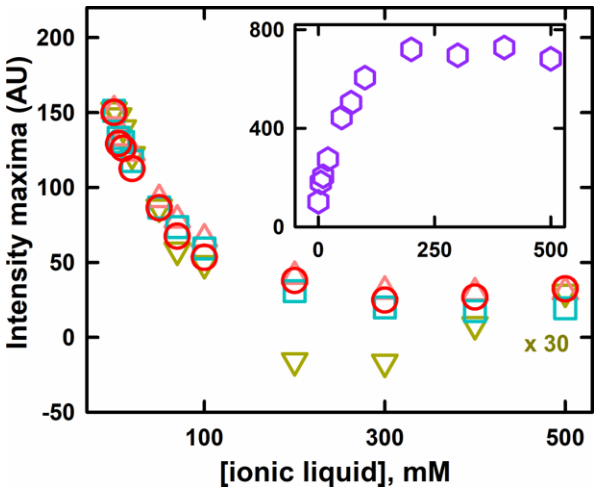

Fig. 2.13 Fluorescence emission intensity of NATA at 340 nm after exciting the dye at 280 nm in the presence of varying concentrations of the ILs, MIC (green), EMIC (pink), BMIC (cyan), and OMIC (red). Emission intensity of NATA in the presence of varying concentration of HMIC is shown in inset.

fluorescence changes of NATA in varying concentration of ILs were followed. NATA, *N*-acetyl tryptophanamide, is a structural analog of Trp residue. With the increasing concentration of ILs, NATA fluorescence was observed to decrease (Fig. 2.13). This illustrated that the decrease in fluorescence was not exclusively due to the binding of ILs with the Lyz, but could raise due to the dynamic quenching of fluorescence by the ILs. Thus, intrinsic fluorescence experiments may not be sufficient to predict the binding affinity and probable number of binding sites on Lyz. Hence, to have a better understanding about molecular level interactions and binding sites, molecular dynamics simulations were performed.

2.3.4 Molecular dynamic (MD) simulation studies

2.3.4.a Global analysis

Root mean square deviation (RMSD) determines the structural changes in three-dimensional conformation of a protein by measuring the average fluctuations in the Cα-atoms from its initial coordinates in a simulation. Here, RMSD of Lyz showed only marginal changes in the structure upon the addition of Im-ILs. The mean value of RMSD of Lyz was 0.13 ± 0.02 nm. With the addition of ILs, RMSD values were observed between 0.11 – 0.15 and 0.13-0.14 ± 0.02 nm, in 50 mM and 200 mM concentrations of ILs, respectively (Fig. 2.14 A1 & A2). Root mean square fluctuations (RMSF) reflects the average deviation of each atom from its initial position. For the analysis, Cα-atom of each residue was considered to represent the residue fluctuations from the initial position. RMSF showed major fluctuations in 4 regions of

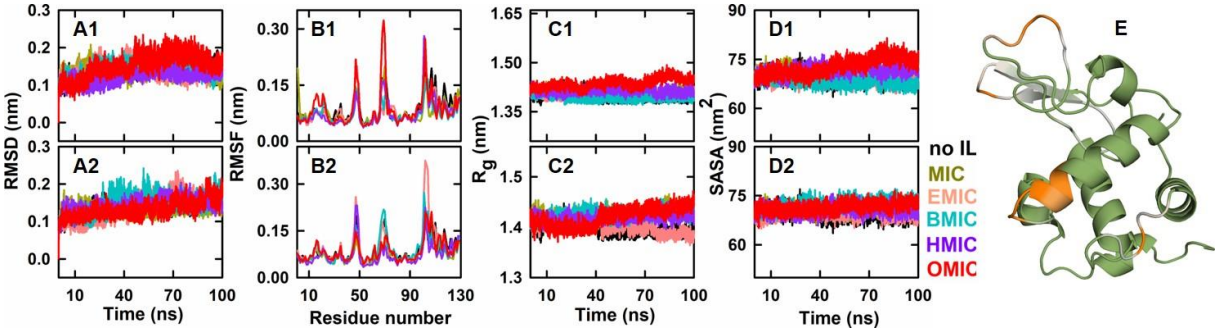

Fig. 2.14 (A1 and A2) Root mean square deviation (RMSD), (B1 andB2) root mean square fluctuation (RMSF) of Cα –atoms, (C1 and C2) radius of gyration (R_g) and (D1 and D2) solvent accessible surface area (SASA) of Lyz in the absence (black) and presence of MIC (dark yellow), EMIC (pink), BMIC (cyan), HMIC (purple) and OMIC (red). The upper (A1-D1) and lower panel (A2-D2) are in the presence of 50 mM and 200 mM ILs, respectively. (E) The structure of Lyz (green) with the regions of major fluctuations (higher RMSF values) marked in orange.

the protein consisting of the residues 16-20, 44-58, 66-71 and 99-103 (Fig. 2.14-B1 & B2). Also, radius of gyration (R_g), and solvent accessible surface area (SASA) remained unaltered with the addition of ILs at both the studied concentrations (Fig. 2.14-C1&C2 and D1&D2).

2.3.4.b Radial distribution function (RDF)

Changes in radial distribution function (RDF) of solvent and cosolvent would indicate the changes in the components of solvation layer surrounding the protein. In the RDF plot of water (Fig. 2.15), the first peak at 0.28 nm indicates the oriented tetrahedral water molecules in the first hydration shell of protein[148]. The troughs indicate the coordination spheres of the water around protein. Generally, the first water coordination sphere occurs at 0.32 nm and the second sphere at 0.42 nm from the surface of a protein.

With the addition of Im-ILs, the position and the height of peak in first hydration shell remained unaltered, but the height of peak in second hydration shell differed in the presence of different concentration of all ILs. At 50 mM concentration, distribution of water molecules around Lyz followed the order, MIC ≈ EMIC ≈ BMIC > OMIC > HMIC (Fig. 2.16 A). At 200 mM of ILs, distribution of water around Lyz was reduced the most by the addition of OMIC followed by EMIC and least changes were observed in the presence of HMIC, BMIC and MIC (Fig. 2.16 B).

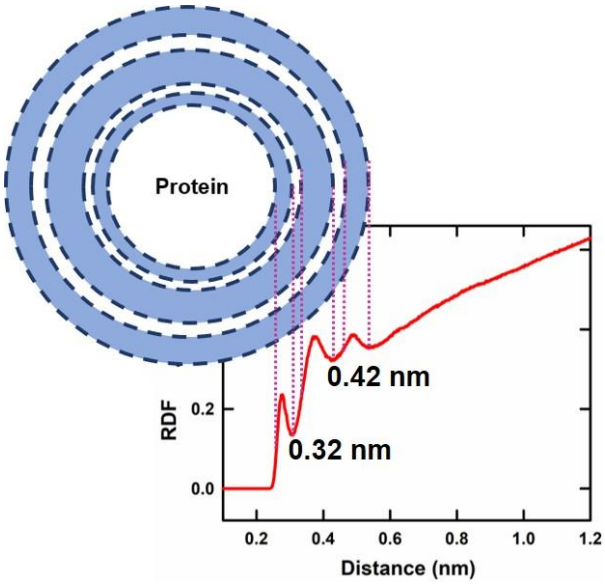

Fig. 2.15 A representative RDF plot for water around a protein.

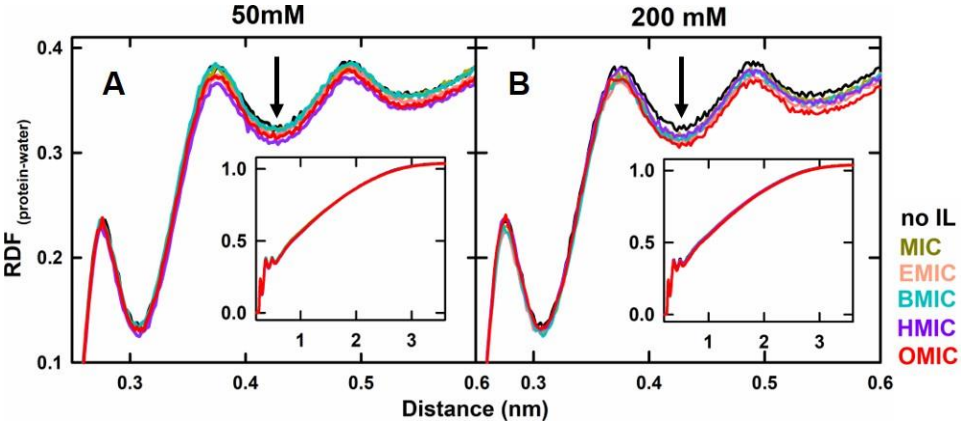

Fig. 2.16 Radial distribution function of water around Lyz in the absence (black) and presence of (A) 50 mM and (B) 200 mM of ILs, MIC (dark yellow), EMIC (pink), BMIC (cyan), HMIC (purple) and OMIC (red). Insets show the RDF values reaching to the value of 1 corresponding to the bulk solvent.

Similarly, RDFs of ILs around the protein were also analyzed. The first coordination sphere around the protein was formed at the distance of 0.62 nm from the surface of protein as shown in Fig. 2.17. At 50 mM, OMIC showed the maximum density around Lyz that was slightly more than HMIC followed by BMIC and EMIC, and least in case of MIC (Fig. 2.18 A). At 200 mM, the distribution of ILs around Lyz was in the order, OMIC ≈ MIC > HMIC > BMIC > EMIC (Fig. 2.18 B). MIC showed the exceptionally high distribution equal to OMIC around the protein which was least at 50 mM concentration.

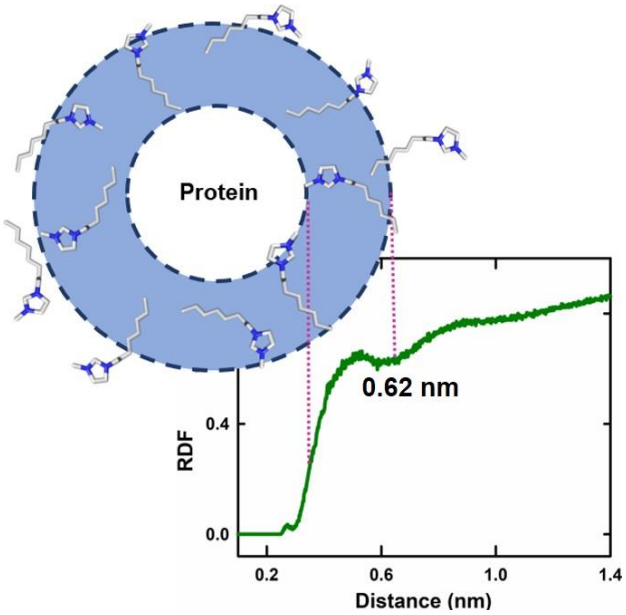

Fig. 2.17 A representative RDF plot of IL heavy atoms around the heavy atoms of Lyz.

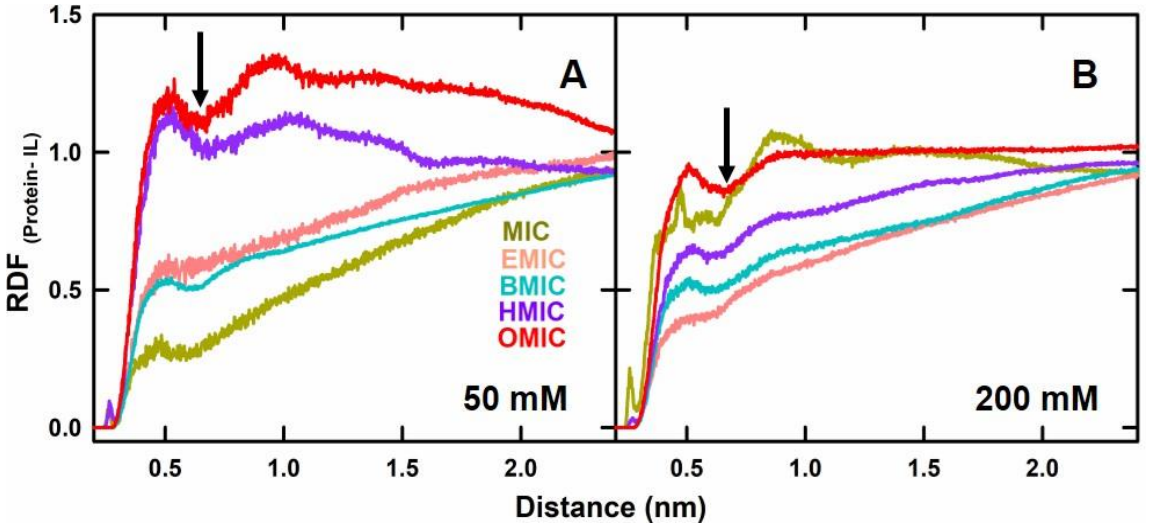

Fig. 2.18 Radial distribution function of ILs around Lyz in the presence of (A) 50 mM and (B) 200 mM ILs. MIC, EMIC, BMIC, HMIC and OMIC are shown in dark yellow, pink, cyan, purple and red, respectively. The arrows indicate the position of the first-coordination sphere of the ILs around Lyz.

2.3.4.c Number of water and IL molecules around the protein

RDF values of water showed varying distribution around the protein at 0.32 and 0.42 nm in the presence of ILs. Also, the coordination sphere of ILs was observed to be at the distance 0.62 nm from the surface of protein as similar to earlier studies[149]. Therefore, the

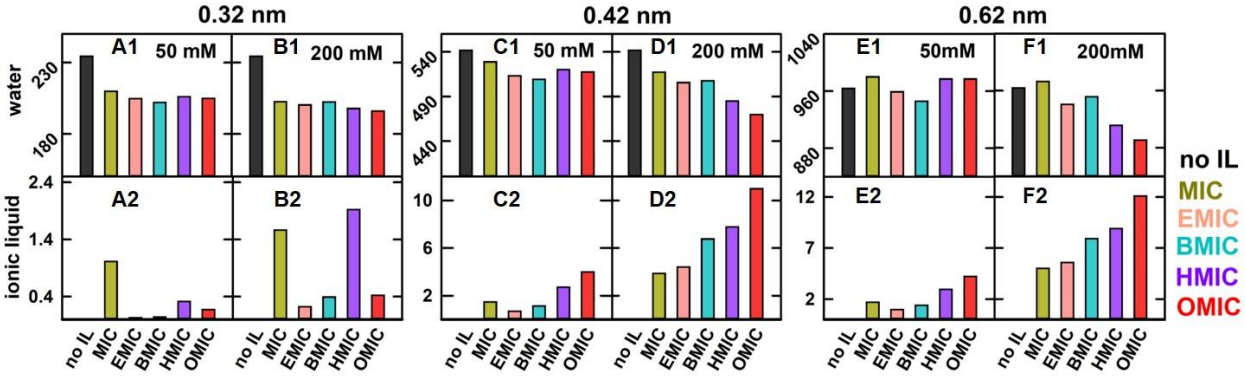

Fig. 2.19 Average number of water molecules (upper panel) and IL (lower panel) around the protein. The number of water molecules in the presence of 50 mM ILs (A1, C1, and E1) and 200 mM (B1, D1 and F1) ILs within the cut-off of 0.32, 0.42 and 0.62 nm. The number of ILs in 50 mM simulation systems are shown in A2, C2 & E2 while B2, D2 & F2 shows the number of ILs in 200 mM simulation systems. Color indications: black- no IL; dark yellow- MIC; pink- EMIC; cyan- BMIC; purple- HMIC; and red- OMIC.

number or water and IL molecules were calculated in all the simulation systems at three cut-off values viz., 0.32, 0.42 and 0.62 nm (Fig. 2.19).

At 0.32 nm and 0.42 nm cut-offs, the number of water molecules were reduced in the presence of all ILs; however, there were differences in the loss of water molecules at 50 mM and 200 mM (Fig. 2.19 A1-D1). At 50 mM, the water around Lyz was reduced more in the presence of BMIC followed by EMIC at all the distances. At higher concentration, the number of water around the protein decreased with increasing alkyl chain length of the IL except that in the presence of EMIC the reduction of water was more than BMIC. Overall, the number of water around the protein followed the trend, buffer > MIC > BMIC > EMIC > HMIC > OMIC at the higher concentrations of ILs. In complement to this, the number of ILs around the protein increased with increasing alkyl sidechain of the IL at the distances of 0.42 and 0.62 nm from the surface (Fig. 2.19 C2-F2), but at a closer cut-off of 0.32 nm, MIC and HMIC showed a higher presence than other ILs suggesting that the overall surface area and the specific length of alkyl chain could be important factors in the interactions at the closer vicinity of the protein, the first solvation shell.

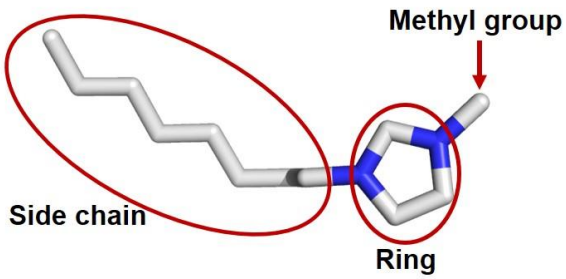

Fig. 2.20 Diagram showing the different functional groups of ILs used to understand the probable orientation of interaction with the protein.

To further investigate which moiety of IL more preferably interacts with Lyz,

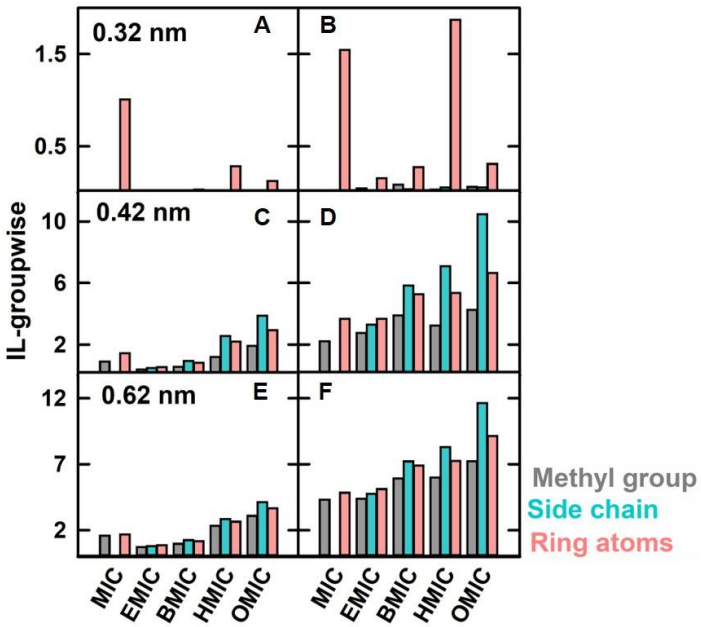

Fig. 2.21 Average number of ILs' groups around the protein in the presence of 50 mM (A, C & E) and 200 mM (B, D & F) of ILs at three different cut-off distances.

each IL was represented by three different interacting moieties, methyl, ring and side chain as shown in Fig. 2.20. The presence of each group was counted separately around the protein. The number of each group at three cut-offs would indicate the probable moiety necessary in maintaining a favourable interaction with the residues of Lyz. At 0.32 nm distance, only ring atoms were observed, while at 0.42 and 0.62 nm cut-offs, the interactions followed the order, side chains > ring atoms > methyl groups as shown in Fig. 2.21.

2.3.4.d Average number of water and IL molecules around each residue

To understand the types of amino acids interacting with the ILs, the number of IL and the number of water molecules around each amino acid were counted. The number of water molecules and ILs were very less or negligible at 0.32 nm cut-off to distinguish any preferable interactions. Thus, the results from 0.32 nm cut-off are not included. At 0.42 nm and 0.62 nm, with increasing concentration of ILs, reduction in the number of water molecules was more. The maximum reduction was observed around all the amino acids of Lyz in the presence of OMIC except around Asn. The number of water around Asn residues was the lowest in the presence of 200 mM MIC (Fig. 2.22).

Further, the number of ILs around each residue was analysed for both 50 mM and 200 mM concentrations of ILs (Fig. 2.23). Due to a smaller number of IL molecules in 50 mM simulation systems, the number of ILs around few amino acids were either very less or negligible. At 200 mM concentration, the number of lower alkyl chain ILs were found to be few or negligible around the hydrophobic amino acids such as, Ile, Val, Cys and Met. The number of ILs around the amino acids generally followed the order, OMIC > HMIC > BMIC > EMIC > MIC. However, the interaction around Met, Glu, Gln and Asp showed some differences. Met had greater number of BMIC around it as compared to HMIC, while Glu, Gln and Asp had a greater number of MIC as compared to EMIC.

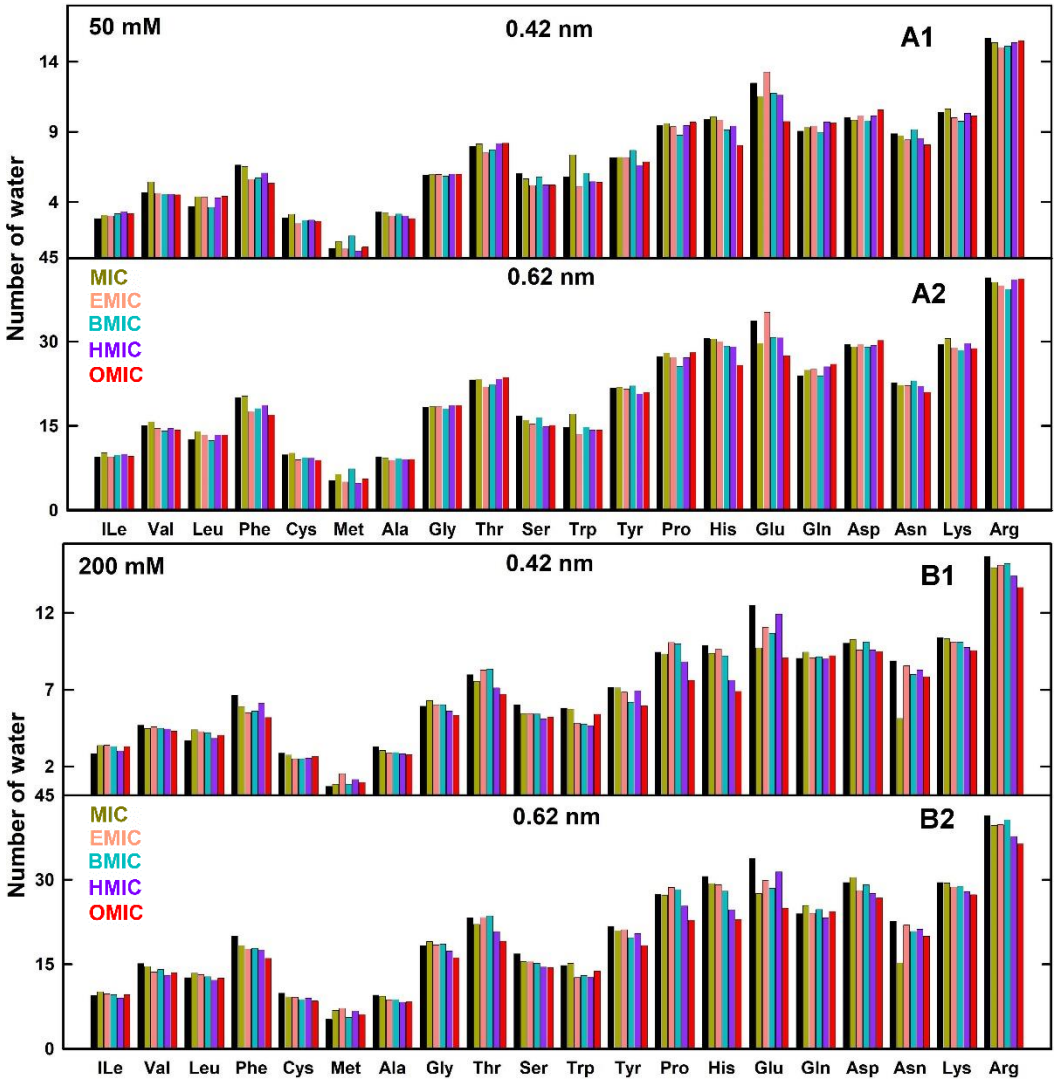

Fig. 2.22 Average number of water molecules around each residue of Lyz in the presence of 50 mM of ILs at a distance cut-off of (A1) 0.42 nm and (A2) 0.62 nm, and in the presence of 200 mM ILs at a distance cut-off of (B1) 0.42 nm and (B2) 0.62 nm. Black bars indicate the number of water around the residues in the absence of ILs, whereas dark yellow, pink, cyan, purple and red bars indicate the presence of MIC, EMIC, BMIC, HMIC and OMIC, respectively.

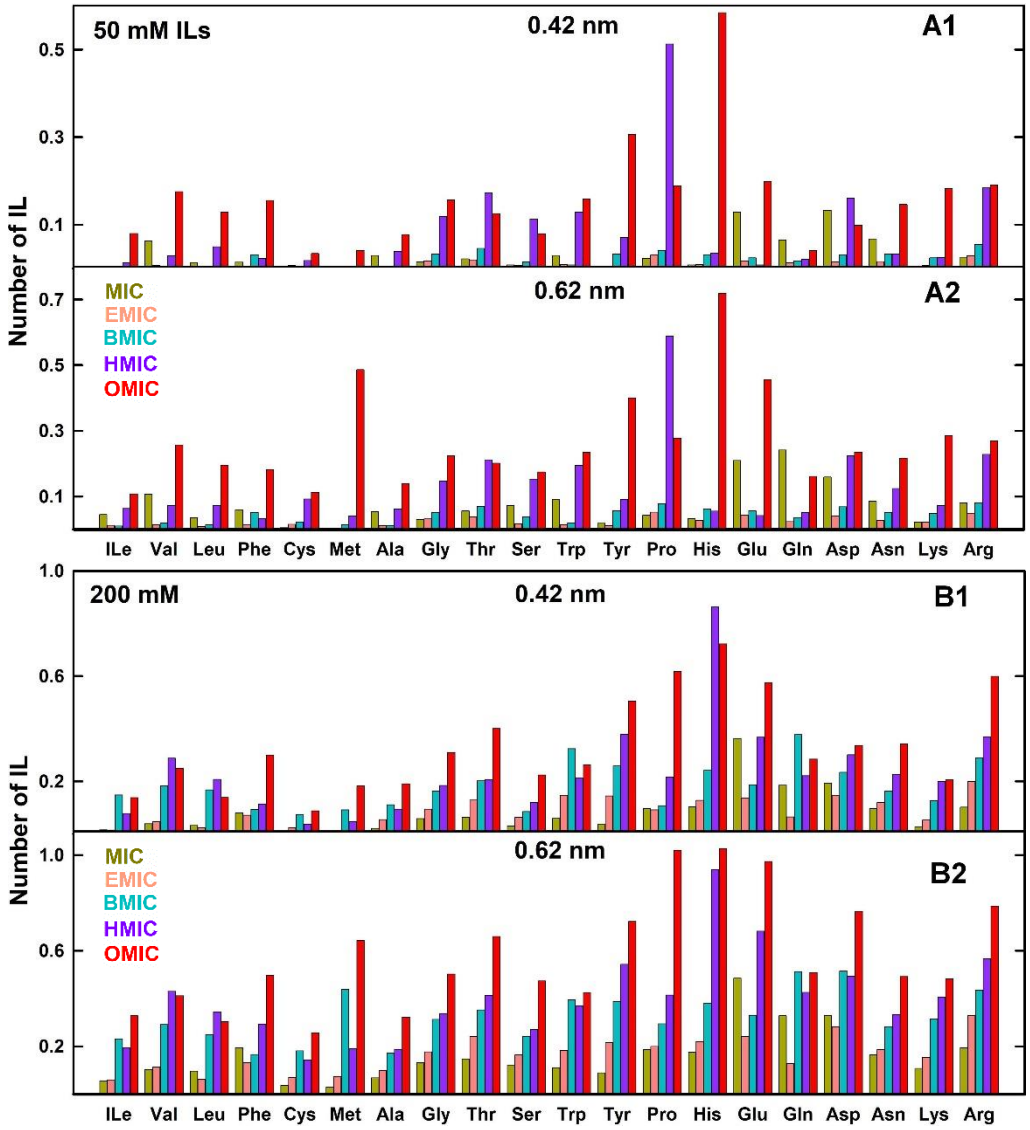

Fig. 2.23 Average number of IL molecules around each residue of Lyz in the presence of 50 mM ILs within cut-off of (A1) 0.42 nm & (A2) 0.62 nm, and 200 mM ILs at a distance cut-off (B1) 0.42 nm & (B2) 0.62 nm. Bars in dark yellow, pink, cyan, purple and red color indicate the number of MIC, EMIC, BMIC, HMIC and OMIC, respectively.

2.3.4.e Solvation properties

To gauge the solvation effects, hydration fractions (χ_{hyd}) around the protein were evaluated in the presence of the ILs. It was determined to know the relative distribution of water and IL in the vicinity of the protein compared to their distribution in the bulk. It was calculated from the last 80 ns of the MD simulation trajectories for each IL using equation 2.6, described in section 2.2.7.b. The extent of hydration in first hydration shell was maximum reduced in the presence of MIC and HMIC at 50 and 200 mM, respectively while maximum in the presence of EMIC at both concentrations (Fig. 2.24 A1 & A2). In the presence of 50 mM ILs, hydration fraction followed the following order, EMIC > BMIC > MIC > HMIC > OMIC, at 0.42 and 0.62 nm cut-off (Fig. 2.24 B1 & C1). At higher concentration of ILs, the hydration fraction was reduced as the length of alkyl side chain increased (Fig. 2.24 B2 & C2).

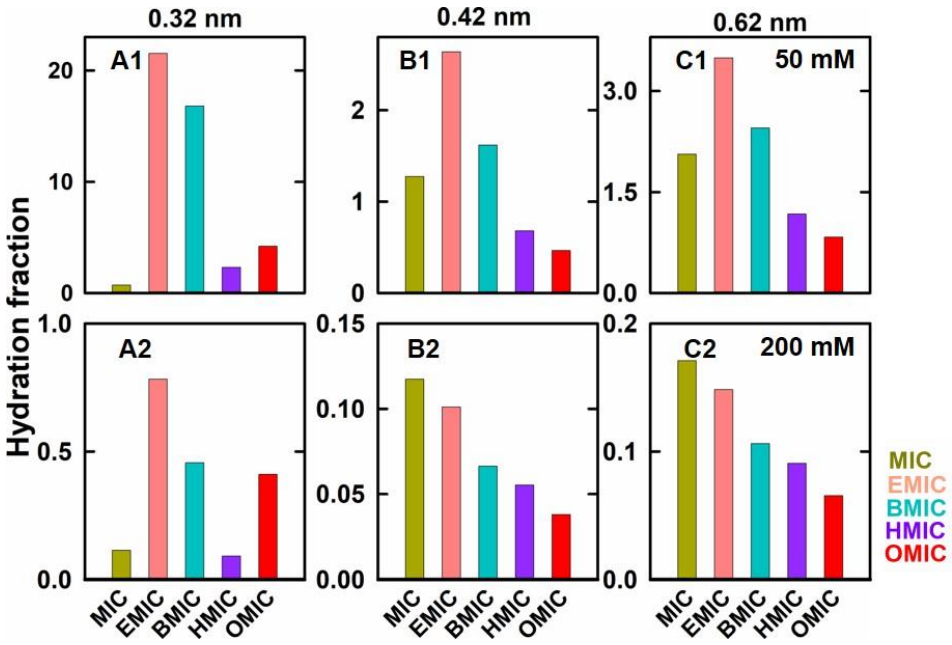

Fig. 2.24 Hydrations fractions calculated at the cut-off values 0.32 nm (A1 and A2), 0.42 nm (B1 and B2), and 0.62 nm (C1 and C2) around Lyz in the presence of 50 mM (upper panel) and 200 mM (lower panel) of ILs (dark yellow- MIC, grey- EMIC, cyan- BMIC, purple- HMIC and red- OMIC).

2.3.4.f Preferential interaction coefficient (PIC) and transfer free energy (TFE)

Preferential interaction coefficients of ILs were calculated by Kirkwood-Buff type integral using equation 2.8 (Fig. 2.25 A & B). The preferential interaction of all the ILs was positive suggesting that interaction between protein and ILs was favourable. Interaction of ILs with Lyz increased with increasing concentrations of ILs. Values of preferential interaction

coefficient were observed maximum in the presence of EMIC, but a distance farthest from the surface of Lyz which indicate the bulk like properties of EMIC. ILs favouring the interaction with Lyz would tend to stay in the vicinity of protein, i.e., near the surface of protein. At higher concentration of ILs, peaks were observed at varying distances and followed the order, MIC > OMIC > HMIC > BMIC > EMIC. However, the height of peak for preferential interaction coefficient was the following order, EMIC >> BMIC > HMIC > OMIC >> MIC. Favourability of interaction depends on both the factors, height of the peak and the distance at which it is appearing. Thus, the PIC graphs indicate, ILs with longer alkyl chain tend to establish stronger interaction with Lyz and stay in the vicinity of the protein.

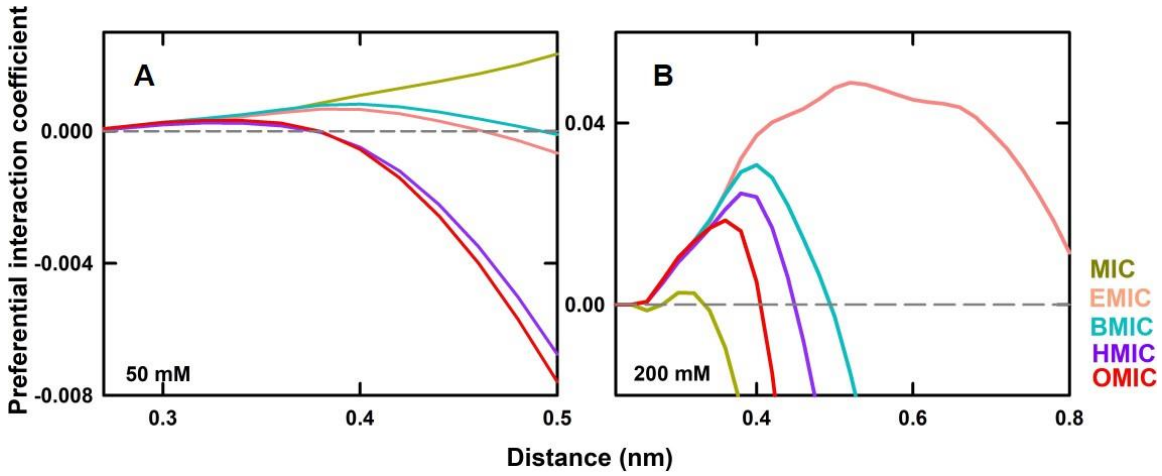

Fig. 2.25 Variation in preferential interaction coefficients calculated for Lyz with increasing distance from the protein surface in the presence of (A) 50 mM and (B) 200 mM of ILs. (Dark yellow- MIC, pink- EMIC, cyan- BMIC, purple- HMIC, red- OMIC).

The results were further supported by the negative transfer free energies (TFE) derived from the preferential interaction coefficient values at every 0.02 nm distance from the surface of protein (Fig .2.26 A & B). TFE is the amount of energy required for an IL to reach the vicinity of the protein molecule from the bulk solution[144]. The TFE values followed the similar order as observed for PIC. This indicated that ILs with longer alkyl chain interact with Lyz more preferentially.

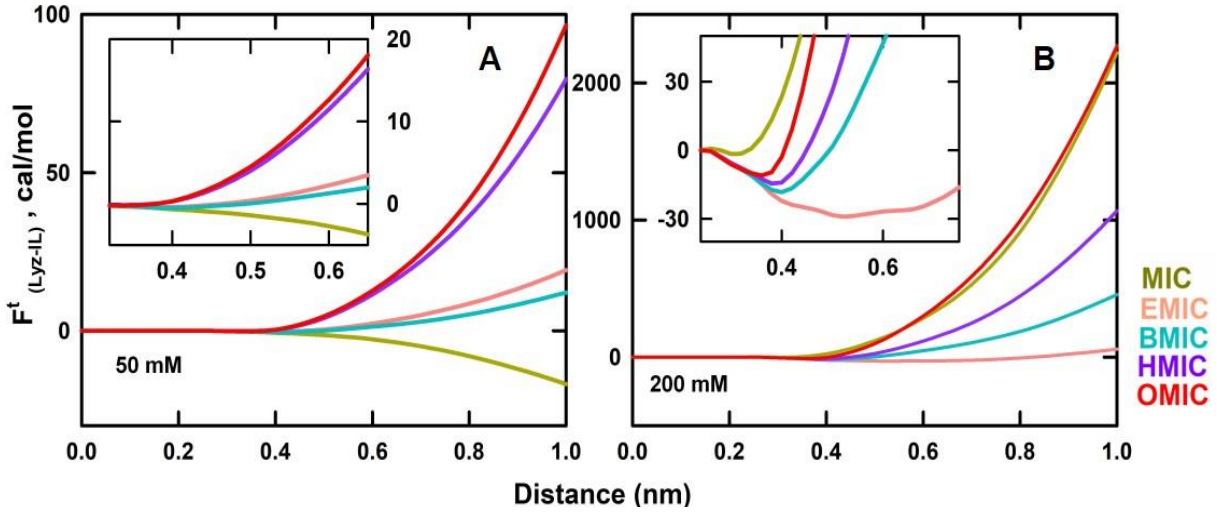

Fig. 2.26 Transfer free energies derived from preferential interaction coefficients for Lyz in the presence of (A) 50 mM and (B) 200 mM of MIC (dark yellow), EMIC (pink), BMIC (cyan), HMIC (purple) and OMIC (red).

2.3.4.g Residue-wise interaction between Lyz and ILs

A specific folding conformation of a native protein allows few residues to be buried to the core of the structure and remaining residues interact with the surrounding solvent and cosolvent molecules in a ternary system. Therefore, knowing the specific residues involved in the interaction with ILs would extend the depth of information about underlying mechanism leading to (de)stabilization and thus fibrillation of Lyz. At 50 mM concentration, all the ILs showed their strongly interacting residues in N-terminal region (Fig. 2.27 A-E). Moreover, ILs with longer alkyl chain, HMIC and OMIC showed maximum regions of interaction on Lyz as shown in Fig. 2.17 D and E. At higher concentration, regions of interaction are more for all ILs. Regions involved in interaction with each IL are shown in Table 2.2.

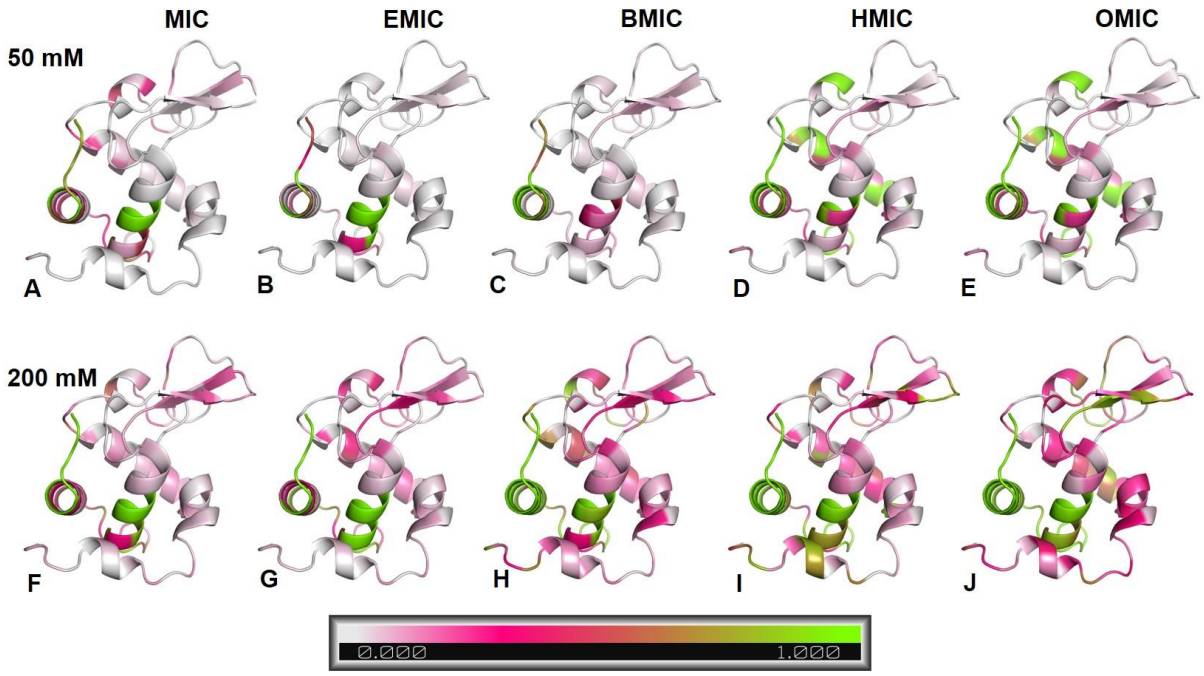

Fig. 2.27 Cartoon diagram depicting the regions of interaction of Lyz with MIC (A & F), EMIC (B & G), BMIC (C & H), HMIC (D & I) and OMIC (E & J) at 50 mM (A-E) and 200 mM (F-J) concentrations of each IL. Non-interactive regions are shown in white color. Green color shows stronger interaction, while pink color indicates moderate interactions between Lyz residues and IL.

Table 2.2 Regions of Lyz showing stronger interaction (shown in green in Fig. 2.28) with Im-ILs at 50 mM and 200 mM concentrations.

IL	50 mM	200 mM
MIC	K1 - A11, S24 – A31	K1 – E7, S24 – A31
EMIC	G4 – C6, S24 – A31	K1 – C6, L13 – L17, Y23 – A31
BMIC	K1 – A11	K1 – A31, S86 – N93, R125 – R129
HMIC	K1 – A11, N19 – S24, W28 – V29, I78 – S81, A90 – S91, V99 – G102	K1 – A31, N46 – T51, A122 – C127
OMIC	K1 – A11, N19 – S24, W28 – A31, I78 – S81, T89 – S91, V99 – G102	K1 – A31, R45 – N46, D52 – G55, W62 – D66, L75 – C80, I98 – S100

2.4 Discussion

2.4.1 Rate and fibrillation pathway in ILs

Fibril assembly of globular proteins is generally initiated from a partially unfolded conformation[24]. In the present study, the effect of varying concentrations of Im-ILs, with increasing alkyl side chain length, on the fibrillation of Lyz is investigated at the condition where Lyz follows the nucleation-independent polymerization pathway. Lyz shows a significant loss of secondary structure at the fibril initiating condition, that is addition of DTT and incubation at 50 ºC (Fig. 2.2 A &C), as reported earlier[132]. This partially unfolded conformation has higher β-sheet content than the native state which might facilitate the formation of fibrils. The fibrillation rate of Lyz at this condition is found to be faster compared to the rates obtained at various other conditions[119,120,122]. Mostly, cosolvents are known to affect the kinetic parameters without altering the aggregation mechanism itself. However, the fibrillation is shown to switch from nucleation-independent polymerization to nucleation-dependent mechanism with the increase in initial concentration of lysozyme, when the fibrillation is initiated in the presence of 4 M urea[150]. Similarly, a change in the aggregation mechanism is noted for serum albumin when salt or guanidinium hydrochloride is added to the solution[115,151]. It is proposed that charge repulsion could drive the proteins to follow the nucleation-independent polymerization pathway. Also, proteins may undergo a nucleation-independent pathway when the initial concentration is above a certain 'supercritical concentration[152].

In continuation of these observations, the present study suggests that even the hydrophobic interactions of cosolvents can alter the mechanism of fibril formation. At lower concentrations (≤50 mM), the binding of ILs is weak and shows less structural changes (as discussed below), thus exhibiting marginal changes on the fibrillation. ILs with alkyl side chains induce nucleation-dependent fibril formation at higher concentrations, whereas MIC does not alter the mechanism. Also, the lag phase is observed to be longer for the ILs with longer alkyl side chain. At higher concentrations, binding of ILs might prevent the inter-chain hydrophobic interactions in Lyz. Thus, the nucleus formation could become an energy barrier at these conditions preventing downhill polymerization of protein chains and switch the fibrillation into nucleation-dependent pathway. The apparent fibrillation time, (T_{app}) calculated to assess the overall effect of ILs on the time taken by the protein to attain the fibrillar state (Fig. 2.5), clearly indicates that in lower concentrations, MIC is most effective in retarding the

fibril formation followed by BMIC and HMIC. However, in higher concentrations, HMIC and OMIC increase the fibrillation time by nearly 55-fold.

2.4.2 Structural changes and stability of Lyz

The absorbance of Lyz in the presence of ILs suggests that there is no significant change in the conformation of the protein. Only in the presence of HMIC, the absorption region dominated by Tyr, absorbance is reduced (Fig. 2.9 D). The absence of any notable change in the fluorescence of ANS implies that the binding of ILs does not significantly unfold the protein (Fig. 2.11). However, the decrease in ellipticity observed in near-UV CD (Fig. 2.10) infers that there could be a loss of tertiary interactions locally around the binding regions. Thus, the binding of ILs might occur on the surface of Lyz through the interactions with the partially exposed hydrophobic residues and polar residues. The intrinsic fluorescence of Lyz decreases when the concentrations of ILs are above 100 mM (above 50 mM for HMIC and OMIC) with a notable blue shift (Fig. 2.12). Analysis of fluorescence changes of NATA in the presence of varying concentrations of ILs indicated that reduced fluorescence could not be exclusively attributed to the binding of ILs with Lyz, but could arise from dynamic quenching effect.

From MD simulation, RMSF analysis reveal that there are mainly four regions showing larger fluctuations upon addition of ILs (Fig. 2.14-B1 and B2). These regions mostly belong to the residues different from the six hydrophobic clusters in Lyz. Moreover, the fluctuations observed are maximum in the presence of OMIC and HMIC. These results correlate well with the near-UV CD observations and suggest that the ILs with longer alkyl chain viz., increased hydrophobicity tend to interact more with hydrophobic regions of Lyz, leaving unbound residues with greater flexibility.

Though all the five ILs destabilize the protein, MIC shows a stronger destabilization effect at lower concentrations (≤20 mM) than the other ILs at the same concentration. However, at concentrations above 20 mM, the destabilization effect is more pronounced with longer alkyl chain ILs. To evaluate the enthalpy-entropy compensation on the destabilization effect, the difference in the enthalpy of unfolding ($\Delta\Delta H_m$= enthalpy of unfolding in buffer at T_m - enthalpy of unfolding in IL at T_m) is plotted against the difference in the entropy of unfolding ($T.\Delta\Delta S_m$ = entropy of unfolding in buffer at T_m - entropy of unfolding in IL at T_m). The enthalpy–entropy plot can be divided into four regions[39,153] which can explain the energetics of osmolyte-induced effect on the stability of the protein [154,155]. The plot (Fig. 2.28) clearly indicates that the

destabilization of ILs is enthalpy-driven in all the cases. This could be attributed to the binding of ILs with the proteins. The earlier reports reveal that there is a direct interaction between the protein and Im-ILs similar to guanidinium ions which might drive the destabilization effect of ILs [156]. Preferential binding of Im-ILs with the unfolded states of the protein may be further facilitated by exposed hydrophobic residues; thus, the effect of denaturation is more for the ILs with longer alkyl chains. Increased destabilization effect with increasing hydrophobicity of Im-ILs is reported in the cases of cytochrome *c* [156], hemoglobin (Jha et al., 2015), and azurin [158] as well.

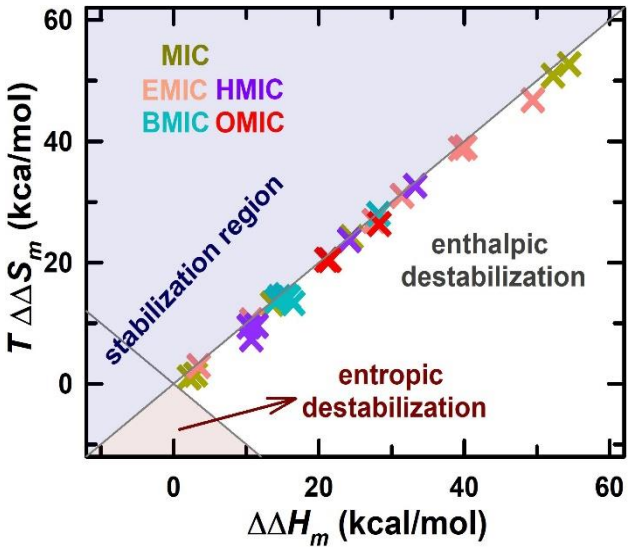

Fig. 2.28 Enthalpy-entropy compensation plot: $\Delta\Delta H_m$ (difference between the enthalpy of unfolding in buffer and in IL at T_m) is plotted against $T.\Delta\Delta S_m$ (difference between the entropy of unfolding in buffer and in IL at T_m) for Lyz in the presence of varying concentration of ILs. The enthalpy and entropy values were evaluated from the thermal denaturation studies presented in Fig. 2.8. The cosolvent-induced stabilization (blue-shaded) and destabilization (red-shaded and transparent) regions are marked for reference.

2.4.3 Surface solvation of Lyz and moieties of ILs involved

RDFs of water in the presence of ILs show that the distribution of water molecules in the first hydration shell remains unchanged. However, in the second hydration shell, the distribution of water is considerably reduced in the presence of all ILs and maximum reduction is observed with OMIC followed by HMIC (Fig. 2.16). A similar observation is reported earlier in the presence of Im-IL with pentyl side chain (PMImBr) at a distance of 4 Å (from the surface of Lyz) which showed reduced water content around the protein[159]. The increased ILs density

around Lyz explains that ILs tend to interact with the protein by replacing water molecules. RDFs calculated between Lyz and ILs indicate that the coordination sphere of ILs could be up to 0.62 nm from the surface of the protein. This can be attributed to the size of the ILs which is larger than water molecules. Again, the increasing hydrophobicity displays greater distribution of ILs around Lyz, with OMIC and HMIC showing the highest distribution (Fig. 2.18).

Hydration fractions calculated in the presence of all Im-ILs support the molecular distribution of water and ILs around Lyz. In the second hydration shell and the coordination sphere of ILs, the hydration fraction reduces as the alkyl chain length of IL is increased (Fig. 2.24). The results from RDFs and hydration fraction explain that ILs probably tend to interact with exposed hydrophobic residues on Lyz via alkyl side chains. Thus, more the hydrophobicity, more the interaction between IL and Lyz. These interactions are formed as a result of breaking native contacts between the protein and surface water molecules leading to the unfolding of Lyz, which slightly exposes the hydrophobic residues.

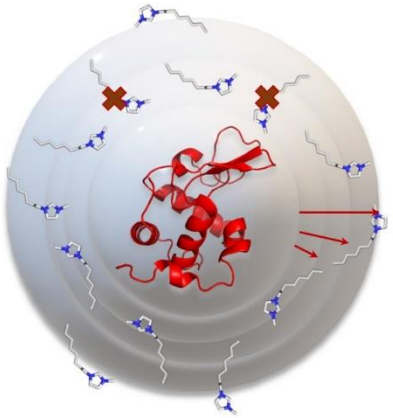

Fig. 2.29 Model diagram showing the probable orientation of ILs around the protein. The red crosses over the ILs denote the least possible orientations.

The calculated number of water and ILs around each amino acids support the above results. The number of ILs around each residue type increases with increased hydrophobicity. To understand the type of interactions between the protein and cosolvent in a ternary system, it was pertinent to know the orientation of ILs required, i.e., which moiety is interacting with protein. Analysis of groupwise distribution of ILs moieties explain the significance of the side chain for interaction with the protein as shown in Fig. 2.21. A representative model diagram for the orientation of ILs on the surface of Lyz is presented in Fig 2.29. Interactions are more favorable as the hydrophobic side chain is longer as depicted by the positive values of preferential interaction coefficient and negative transfer-free energy.

2.4.4 Binding of ILs, perturbation in structure and inhibition of fibrillation with increasing hydrophobicity

At lower concentration, only few regions of interaction were observed on Lyz. But the ILs with more hydrophobicity show more regions of interactions even at this concentration (Fig.

2.27 A-E). At higher concentration, the interactions are global with some regions having stronger interactions. These interaction profile of Lyz with ILs having varying hydrophobicity illustrates that the ILs with longer alkyl side chain tend to interact more with Lyz, leading to the perturbation in structure. The binding of ILs with hexyl (HMIC) and octyl alkyl chains (OMIC) distorts the tertiary contacts of the residues in the site locally; however, the protein is not globally denatured. During thermal denaturation, the protein exposes the buried hydrophobic residues which might facilitate the binding of ILs, thus stabilizing the denatured state more compared to the native state. The extent of destabilization is larger for the ILs with longer alkyl side chains due to this preferential binding.

Hydrophobic interaction is one of the critical factors influencing the self-aggregation of protein molecules [160,161]. The fibril formation in Lyz is driven by long-range interaction between the hydrophobic clusters 3 and 5. All the ionic liquids bind to clusters 1 and 2 invariably. However, the longer alkyl chain ILs, HMIC and OMIC has stronger potential to interact with clusters 3 and 5 compared to the other ILs. It is proposed that the region covering the long loop connecting the α- and β-domains, and helix-C (residues 57 to 107) is the highly amyloidogenic region in Lyz [121,123,162]. These observations indicate that increasing hydrophobic interaction between the protein and IL could weaken the amyloid formation of the protein. Further, this might increase the energy barrier for downhill polymerization and switch the pathway into nucleation-dependent mechanism. The indifference in the mechanism of fibrillation in the presence of MIC and the longest lag times observed with the ILs with longer alkyl chains (OMIC and HMIC) evidence for the same.

Globular proteins require a specific partially-unfolded conformation to attain their fibril structure. Any changes in the conformation might alter their fibrillation propensity. Though ILs destabilize Lyz, the more destabilizing ILs, HMIC and OMIC, are found to retard the fibrillation more. The alternate conformations attained by the protein upon binding of ILs could be less prone to adapt a fibrillation pathway. Destabilized conformations of proteins induced by ILs which could inhibit the fibrillation process is observed in other proteins as well [108]. The inhibition can also be attributed to the binding of ILs to hydrophobic regions which are essential for driving the inter-chain interaction to form fibrils. The 55-fold increase in fibrillation time in HMIC and the inhibition of fibrillation by OMIC might be due to their strong binding interaction with Lyz through hydrophobic interactions, thus, driving the protein to attain a non-favorable conformation for fibrillation.

2.5. Conclusion

Protein stability and self-association is influenced by its interaction with small molecules. Ionic liquids having different cationic and anionic moieties affect the proteins differently. Effect of increasing hydrophobicity of cationic moiety of IL on a model protein, Lyz, is investigated with chloride as a common anion. At lower concentrations, ILs mostly do not affect the stability or fibrillation propensity of the protein significantly. However, at concentrations above 50 mM, they destabilize the protein and alter the fibrillation propensity. As the alkyl chain length increases, number of water molecules decrease and number of ILs increase around the protein. The extent of destabilization is more with the longer alkyl side chain ILs. Though at the concentration around 100 mM, almost all the ILs show a sharp increase in the rate of fibrillation, further increase in their concentration retards the rate. HMIC delays the fibril formation by nearly 55-fold and OMIC at above 200 mM inhibits the fibrillation completely. Also, all the ILs switch the mechanism of fibrillation to nucleation-dependent pathway at the concentrations above 100 mM except MIC, in which Lyz follows nucleation-independent mechanism at all the concentrations. The structural changes, destabilization, reduced hydration of Lyz, delay in fibril formation and inhibition follows the order, OMIC > HMIC > BMIC > EMIC > MIC. Thus, the study emphasizes that hydrophobic interaction of ILs with proteins could result in a significant change in their stability, and fibrillation propensity and pathway as well as the complete inhibition of fibrillation pathway at higher concentration as hydrophobic factor is increased.

Chapter 3
Alicyclic and aromatic moieties-induced hydrophobicity on the stability and fibrillation propensity of lysozyme

3.1 Introduction

Ionic liquids consist of organic cations and organic or inorganic anions[163]. The exceptional physicochemical properties of ILs, such as low melting point and very low vapor pressure might arise from the asymmetry in the constituting ions, charge delocalization and weak intermolecular interactions[164]. These properties are sensitive to trivial changes in the functional groups on both the ions, thus significantly alter the ionization, hydrophobicity, solubility, and intermolecular interactions of the ILs. The increase in alkyl chain length of cation decreases the hydrophobicity, thus the solubility of the IL. The branching in the alkyl chain also decreases the solubility of ILs, for instance isobutyl substitutions are less soluble compared to n-butyl, which might arise from the less entropy of solution for the branched chains compared to linear chains[165]. Also, in ILs with aromatic cations, the positional isomerism alters the mutual solubility of IL and water. The radial distribution functions of water in ILs calculated from MD simulation studies indicate that the *meta* substitution in the cationic rings hinders the water interaction more compared to *ortho* and *para* substitutions. This might reduce the solubility of ILs in water[166].

ILs with non-aromatic cations show slightly lesser solubility in water. For instance, the mutual solubility of 1-methyl-1-propylpyrrolidinium and 1-methyl-1-propylpiperidinium in water is less than 1-methyl-1-propylimidazolium at STP conditions[167]. This generally correlates with the hydrophobic tendency of the cationic group. Further, the increase in the number of atoms in the cationic ring might also reduce the solubility of ILs in water[168]. Though the surface volume of the functional groups could be a factor influencing the solubility in case of alkyl sidechains, the thermochemical properties of aromatic and alicyclic cationic groups show poor correlation with the molar volume. This indicates that the electronic distribution of these groups could be the primary factor in determining their properties[165].

The studies on the interaction of ILs with individual amino acids suggest that the hydrophobic amino acids weaken the hydration of ILs, whereas the hydrophilic amino acids enhance the solvation of ILs[169]. The hydrophobic amino acids preferably interact with the alkyl sidechains of the cationic moiety of ILs. Polar amino acids show a stronger salting-out effect for ILs which generally decreases with increasing sidechain length. Arg and Lys has moderate effect whereas Glu and Asp effects on the mutual solubility of ILs in water is insignificant[170].

Proteins in their native three-dimensional conformation consist of amino acids with varying solvent accessibility and their interactions with ILs depend on the surface residues. The

functional groups on the ILs also determine the extent of interaction. The less hydrophobic ILs are found to enhance the refolding whereas highly hydrophobic ILs might destabilize the proteins in a concentration-dependent manner[171]. The stability of RNase A is reported to be altered by the addition of ILs while the 1-butyl-3-methylimidazolium destabilizes the protein more than 1-butyl-1-methylpyrrolidinium[172]. Differences in the cations alter the protein self-aggregation efficiency as well. Ethylammonium nitrate inhibits the aggregation of β-lactoglobulin whereas 1-butyl-3-methylimidazolium increases the aggregation[173]. Similarly, ethylammonium nitrate shows higher protection against aggregation of insulin[174]. These observations suggest that the differences in the functional moieties of cationic species of ILs could change their interaction with the proteins and alter their stability and aggregation properties.

In the previous chapter, the effect of alkyl chain length on the stability and fibril formation of lysozyme was examined. As discussed above, there are significant differences in the hydrophobicity of ILs having aromatic and alicyclic cations, and the number of carbon atoms in the cyclic ring also affects their hydrophobicity. In the present chapter, the effect of such differences in the ILs on the stability and fibrillation propensity of Lyz is analyzed. In order to achieve this, two ILs with aromatic cationic groups and two ILs with alicyclic cationic groups (Fig. 3.1) were chosen. The study suggests that ILs with aromatic moiety show more preferential binding with the protein and induce more destabilization. In contrast, the ILs with aliphatic moiety show preferential hydration of the protein and their destabilization effect is less. Though both type of ILs delay the fibrillation of Lyz, the aliphatic ILs delayed the overall fibrillation longer than aromatic ILs.

3.2 Materials and methods

3.2.1 Materials

Hen-egg white lysozyme (Lyz), thioflavin-T (ThT), 8-anilinonaphthalene-1-sulphonic acid (ANS), *N*-acetyl tryptophanamide (NATA) and 1-butyl-3-methylimidazolium bromide (BImBr) were purchased from Sigma-Aldrich. 1-butyl-1-methylpyrrolidinium bromide (BPyroBr; CAS No. 93457-69-3), 1-butyl-1-methylpiperidinium bromide (BPipBr; CAS No. 94280-72-5), 1-butyl-4-methylpyridinium bromide (BPyrdBr; CAS No. 65350-59-6) were purchased from TCI chemicals. Dithiothreitol (DTT) and phosphate buffer salts were purchased from SRL, India. All the chemicals were used without any further purification. The structures of ILs used in the study are shown in Fig. 3.1.

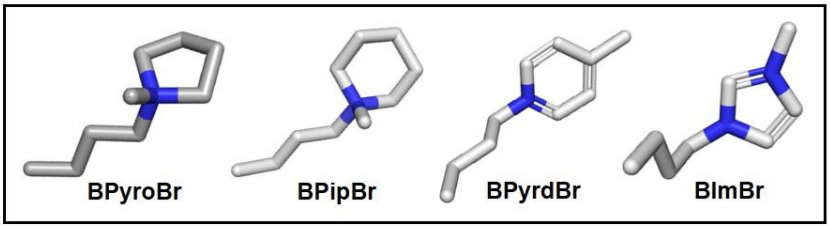

Fig 3.1 Alicyclic and aromatic ILs used in the study: 1-butyl-1-methylpyrrolidinium bromide (BPyroBr), 1-butyl-1-methylpiperidinium bromide (BPipBr), 1-butyl-4-methylpyridinium bromide (BPyrdBr) and 1-butyl-3-methylimidazolium bromide (BImBr). Carbon atoms are in grey and nitrogen atoms are in blue.

3.2.2 Fibrillation experiments and analysis

Method for fibril formation was adapted from our earlier work[39,40] and the same is described in section 2.2.2. Fibrillation kinetics were carried out in the absence and presence of varying concentration of afore mentioned ILs. TEM images of the fibrils were collected using the same method described in section 2.2.5.

3.2.3 Structural Studies

Fluorescence spectra of Lyz (15 µM) were obtained in Jasco FP-8500 in the absence and presence of varying concentrations of ILs. Intrinsic fluorescence changes of tryptophan (Trp) in Lyz were followed in the wavelength region 310-400 nm after exciting the samples at 280 nm. ANS fluorescence changes were recorded in the range from 400-600 nm upon excitation at 380 nm. ANS with 50 µM concentration was added in all the samples.

Fluorescence of NATA (10 µM) with the chosen ILs were performed to verify the quenching Trp fluorescence by ILs. Tertiary structural changes in Lyz (50 µM) were studied in Jasco J-1500 spectropolarimeter connected to a circulating water bath. Baseline corrected near-UV CD spectra were obtained in the range of 250-300 nm in the absence and presence of varying concentrations of ILs (0 - 500 mM). At far-UV region, due to high voltage in the presence of ILs, studies for secondary structural changes could not be carried out. All the experiments were performed using 1 cm pathlength quartz cuvette and the samples were prepared in 20 mM phosphate buffer at pH 7.0 (± 0.1).

3.2.4 Thermal denaturation studies

Thermal denaturation of Lyz in the absence and presence of ILs were carried out using the method discussed in section 2.2.4. Obtained thermal transitions were fitted to equation 2.5 to evaluate the change in melting temperature (T_m) and the enthalpy of unfolding at the transition mid-point (ΔH_m).

3.2.5 Molecular dynamics (MD) simulation

All the simulations were carried out using GROMACS package 5.1.4. The parameters for simulations were same as discussed in section 2.2.6. Lyz molecule was placed in a cubic box extended to 1.2 nm from its surface with the volume of 414.223 nm^3. Number of water and IL molecules used in each simulation are presented in Table 3.1.

Table 3.1: Details of the number of ILs and water molecules used in MD simulation

IL	50 mM			200 mM		
	Number of IL molecules	**Number of water molecules**	**Obtained concentration**	**Number of IL molecules**	**Number of water molecules**	**Obtained concentration**
BPyroBr	12	12855	51.81	45	12519	199.50
BPipBr	12	12848	51.84	45	12474	200.22
BPyrdBr	12	12857	51.80	45	12524	199.40
BImBr	12	12864	51.78	45	12556	198.90

The MD simulation trajectories were analyzed to obtain global changes in the structure and the interaction of water and ILs with the protein using the same procedures mentioned in section 2.2.7.

3.3 Results

3.3.1 Fibrillation studies

Lyz (140 µM at pH 7.0) follows a nucleation-independent fibrillation pathway (Fig. 3.2A), in the presence of 14 mM DTT, when incubated for 45 min at 50 ℃. Gradual increase in ThT fluorescence was recorded at every two minutes at 480 nm. The fluorescence spectrum of ThT collected after incubation showed higher fluorescence compared to the spectrum collected before incubation (Fig. 3.2A-inset). The rate of reaction was calculated using equation. 2.1 and found to be 0.08 min^{-1}. Far-UV spectra in circular dichroism is an effective way to detect the secondary structural content in any protein while near-UV spectra describe the tertiary interactions in a protein. Far UV-CD spectra of Lyz revealed changes in secondary structure of the protein after incubation in fibrillation conditions. Negative peaks at 208 nm and 222 nm, indicative of α-helical structure in a protein, disappeared (Fig. 3.2B), while an appearance of weak negative band at 217 nm characterizing β-sheet content was observed. A strong band at 295 nm corresponding to Trp-108[175] and two weak bands at 288 nm and 278 nm arising from other Trp and Tyr residues in the active site of Lyz, were not visible in the near-UV spectra recorded after incubation at fibrillation conditions (inset in Fig 3.2B). Further, the fibril formation of Lyz was confirmed by TEM images (Fig 3.2 C) and the width was measured to be nearly 50 nm (inset Fig. 3.2 C).

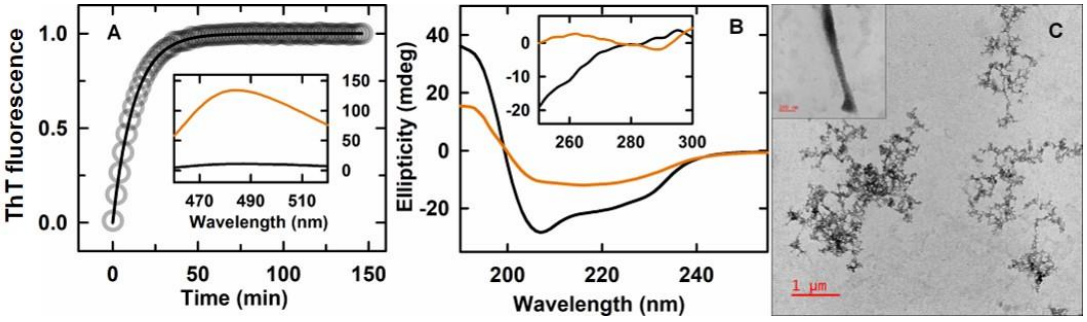

Fig. 3.2. (A) Fibril formation of Lyz in the presence of DTT at 50°C probed with the change in ThT fluorescence. Inset shows the fluorescence spectra of ThT in native (black) and fibrillar (orange) protein. (B) Far-UV CD spectra of lysozyme in native (black) and fibril (orange) conformations. Inset shows near-UV CD spectra of the same samples. (C) TEM micrograph of the fibril formed by Lyz.

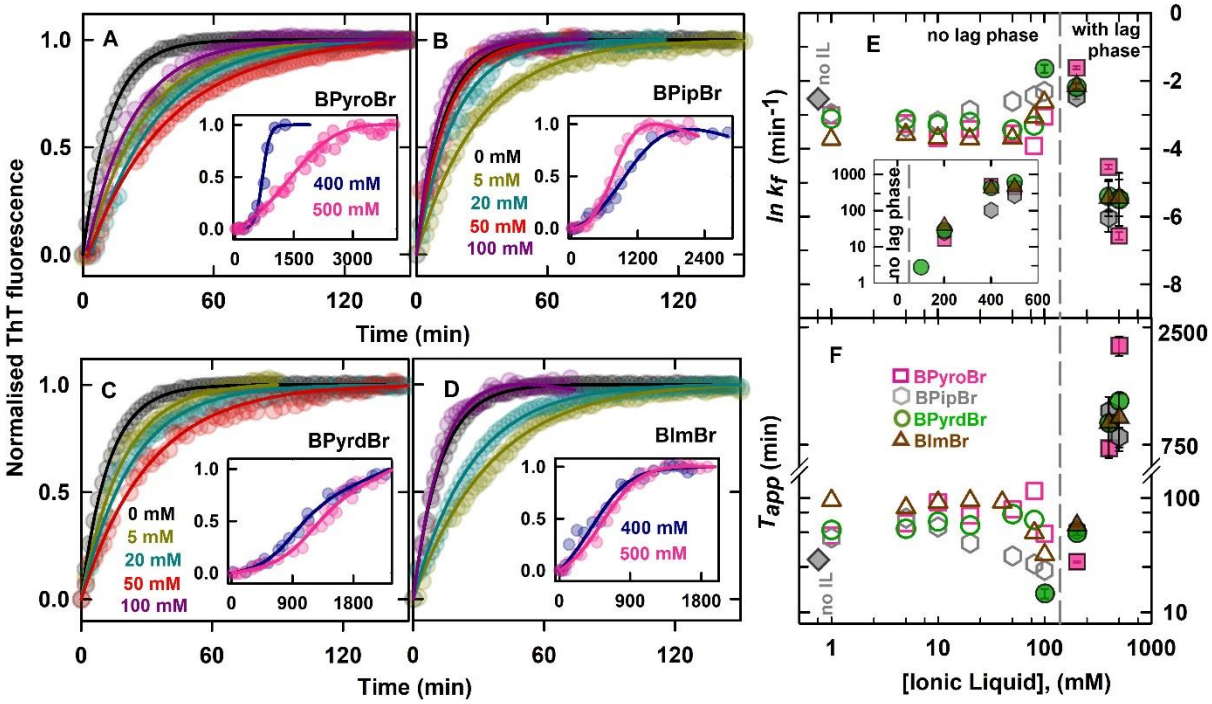

Fig 3.3. Representative kinetic graphs showing change in ThT fluorescence during the fibrillation of Lyz in varying concentrations of different ionic liquids, (A) BPyroBr, (B) BPipBr, (C) BPyrdBr, and (D) BImBr. The solid lines are data-fit using equation 2.1 or 2.2 for nucleation -independent and nucleation-dependent kinetics, respectively. (E) Rate of fibril formation of Lyz in the presence of various concentrations of the ILs: BPyroBr (pink squares), BPipBr (grey hexagons), BPyrdBr (green circles), and BImBr (brown triangles). Inset shows lag times calculated for the concentrations following nucleation-dependent mechanism. (F) Apparent fibril formation time (T_{app}) in various concentrations of the ILs. The values of ln k_f and T_{app} in the absence of any IL are given as black diamonds.

The fibrillation experiments were also performed in the presence of varying concentrations of the selected four ILs. Fig. 3.3 (A-D) shows the representative kinetic traces for the increase in ThT-fluorescence upon Lyz fibril formation in the presence of different ILs. Fibrillation pathway switched from a nucleation-independent to nucleation- dependent mechanism, with a noticeable lag time, when the concentration of ILs was ≥200 mM, except in the presence of BPyrdBr, which switched the mechanism at the concentrations ≥100 mM. The lag time and elongation rates were evaluated using equations 2.1 and 2.2. Elongation rates decreased with increasing concentrations of ILs (Fig. 3.3E). At lower concentrations of ILs with alicyclic ring moiety (BPyroBr and BPipBr), the rate was reduced by ~1.6 times. While the addition of aromatic ILs (BPyrdBr and BImBr), the fibrillation rate was reduced to a greater extent. At 1 mM concentration, fibrillation rate was reduced by ~1.8 and ~3.3 times in the

presence of BPyrdBr and BImBr, respectively. In BImBr, the rate was found to be the least among all ILs at concentrations <100 mM. While the rate was slightly increased between 100 and 200 mM of ILs, only in the presence of BPipBr the rates started increasing from 20 mM. With an increase in the IL concentration above 200 mM, the elongation rate was drastically reduced with BPyroBr showing the slowest rate at 500 mM. The lag time observed in the presence of higher concentrations of ILs increased with increasing IL concentration.

To evaluate the total time taken to form fibrils in different conditions, apparent fibrillation time (T_{app}) was derived using equation 2.4. In lower concentrations of ILs, the time taken by Lyz to form fibrils was slightly increased which was later reduced at above 100 mM. In the ILs concentrations of around 100-200 mM, the fibrillation time was comparable with that of Lyz in buffer alone. When the concentration was above 200 mM, all the ILs enormously delayed the fibrillation process by 30 to 70-fold. In 500 mM of IL, the apparent fibrillation time followed the order as, BPyroBr > BPyrdBr > BImBr > BPipBr.

To gain further insights into the effects of ILs on the fibrils morphology of Lyz, TEM micrographs of the fibrils formed under different conditions were collected (Fig. 3.4). Lyz fibril formed in the absence of any IL was thread-like in appearance and often clumped together (Fig. 3.4A). Fibrils were visibly dense and formed blob-like thick and dark structures at regular intervals with an estimated width of ~50.3±6 nm for an individual filament (Fig 3.4F). In the presence of BPyroBr (Fig. 3.4 B), the fibrils formed were micrometres long, unbranched and flexible with an average width of 36.6±3 nm. Thin fibrils were arranged parallel to each other and loosely interwind to form a bundle-like appearance. Fibrils formed in the presence of BPipBr had similar morphology as in the presence of BPyroBr with slight differences in their twists of individual filaments (Fig. 3.4 C). The length of the fibrils was nearly 15 to 20 µM with an average width of 49.4 ± 6 nm. The fibrils formed in the presence of BPyrdBr (Fig. 3.4 D) were long, flexible and unbranched, and were twisted around each other in doublets or triplets with the short nodes appearing at regular intervals of 17-20 nm distance. The average width of a single fibril was found to be 59.6 ± 2 nm. The morphology of fibrils formed in the presence of BImBr (Fig. 3.4 E) was similar to the Lyz fibrils formed in buffer with slightly lesser average width of 20.7 ± 3 nm.

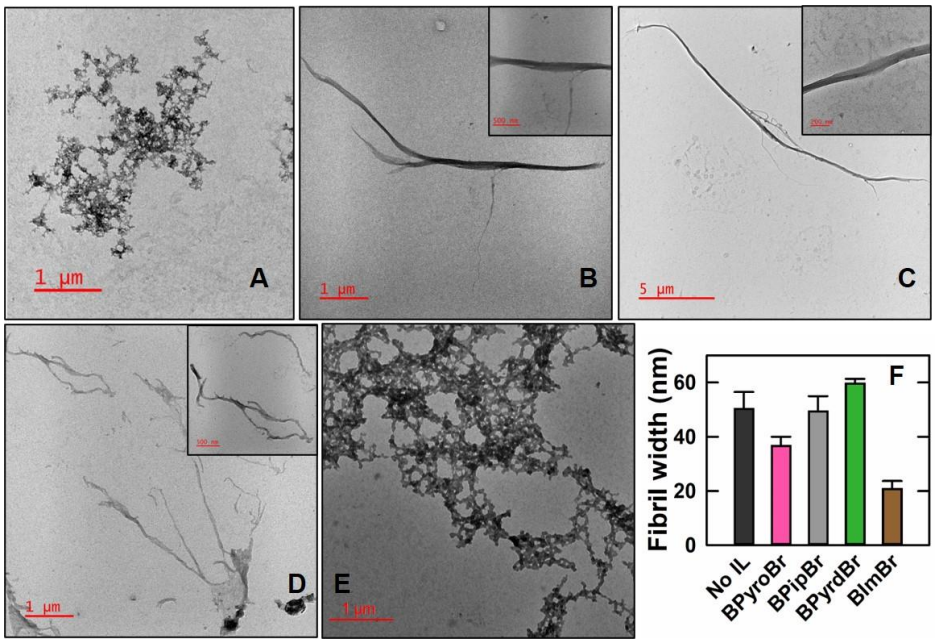

Fig. 3.4 Representative TEM images of the Lyz fibrils in (A) the absence of any IL and in the presence of (B) 100 mM BPyroBr, (C) 400 mM BPipBr (D) 100 mM BPyrdBr, and (E) 400 mM BImBr. (F) Width of fibrils formed in different ILs is calculated from the TEM micrographs.

3.3.2 Thermal stability

Change in the absorbance of Lyz with an increase in temperature was measured to study the stability of the protein in the presence of different ILs. The thermal transitions obtained in the absence and the presence of all the ILs exhibited sigmoidal curves representing two-state unfolding transitions (Fig. 3.5 A-D). With increasing concentrations of all the ILs, the protein was gradually destabilized. Exceptionally, non-cooperative transitions were obtained in the presence of BImBr above 200 mM that were not considered for analysis. Other thermal unfolding curves were analysed using equation 2.5 to calculate transition mid-point temperatures (T_m) and enthalpy of unfolding (ΔH_m) and the values are presented in Fig. 3.5 (E & F). There was a marginal reduction in T_m value in the presence of ILs up to 50 mM. At higher concentrations, the extent of reduction in the T_m value was more, except in the case of BImBr which showed a gradual loss of stability up to 200 mM. The lowest T_m of Lyz was observed in the presence of 500 mM BPyrdBr and the order of destabilization in the presence of ILs at the highest concentration was BPyrdBr > BPyroBr > BPipBr. ΔH_m value of Lyz was gradually

decreased with the increasing concentrations of all the ILs. However, ΔH_m slightly increased in BPipBr and substantially higher in BPyrdBr at the concentrations above 200 mM.

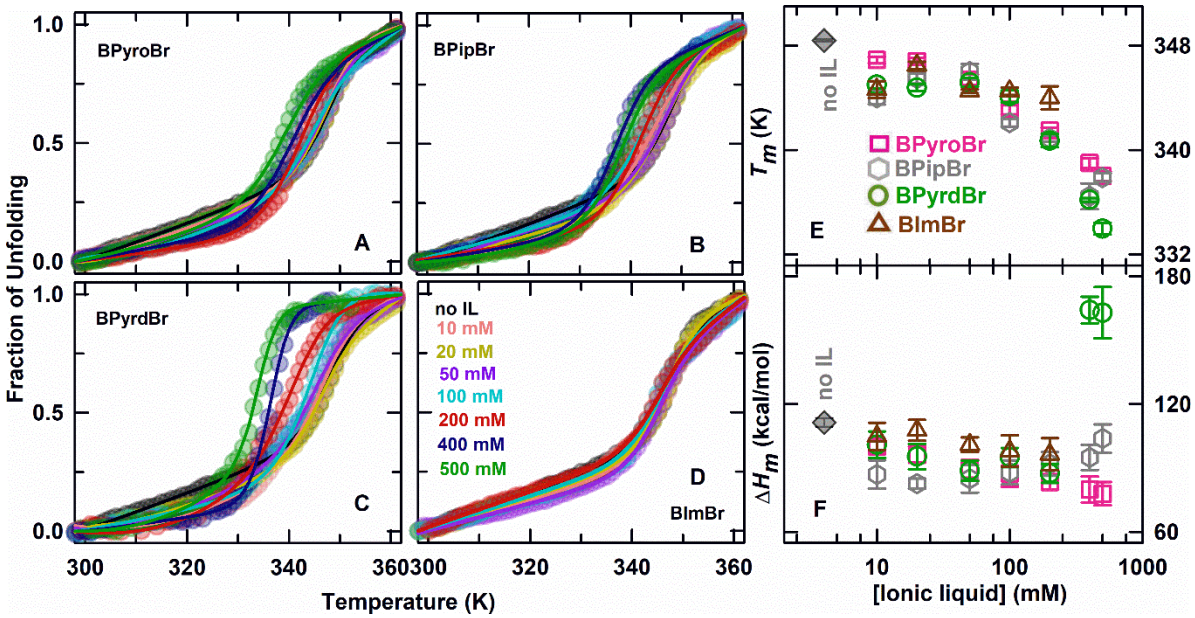

Fig. 3.5. Representative thermal denaturation transitions of Lyz measured by following the change in absorbance of the protein in the presence of varying concentrations of ILs, (A) BPyroBr, (B) BPipBr, (C) BPyrdBr, and (D) BImBr. The solid lines represent the data-fit using equation 2.5. (E) Thermal denaturation midpoint (T_m) and (B) enthalpy of unfolding (ΔH_m) of Lyz in the presence of various concentrations of ILs: BPyroBr (pink squares), BPipBr (grey hexagons), BPyrdBr (green circles), and BImBr (brown triangles). The T_m and ΔH_m values in the absence of any IL are given as black diamonds.

3.3.3 Structural changes in Lyz

The conformational features of a protein can be studied with the help of circular dichroism (CD) spectroscopy. Characteristic peaks in far-UV region (180-250 nm) at 190 nm (strong band) and 210 nm (weak band) attribute to the peptide bonds, negative peaks at 208 nm and 222 nm corresponds to α-helical content and peak between 216 – 218 nm arises due to β-sheet content in a protein[176]. On the other hand, tertiary structural changes in native proteins can be deduced from the spectra collected in the range between 250 – 300 nm. Aromatic amino acids (Trp, Tyr and Phe) as well as disulphide bonds show characteristic peaks in this region[176]. With the change in residue composition and the environment around the residues, notable differences in the spectral patterns can be observed. Lyz has six tryptophan residues, three tyrosine and four disulfide bonds to maintain the structural integrity of the protein[177]. Two weak

positive bands at 282 nm, 288 nm, and a sharp positive peak at ~294 nm in arises due to the Trp residues in the binding site of the protein. A peak at 294 nm is particularly due to Trp-108 in Lyz. Any alterations in the protein conformation around Tyr can be characterized by the peaks in range of 260-280 nm. Differences in the ellipticities at three wavelengths, 278, 284 and 294 nm were observed for varying concentrations of ILs before and after incubation of Lyz in fibrillation conditions. There were marginal changes in the ellipticities at these wavelengths in the presence of BPyroBr (Fig. 3.6-A2&A3) and BPipBr (Fig. 3.6-B2&B3). However, a significant decrease in ellipticities was seen in the presence of BImBr (Fig. 3.6-C2 & C3).

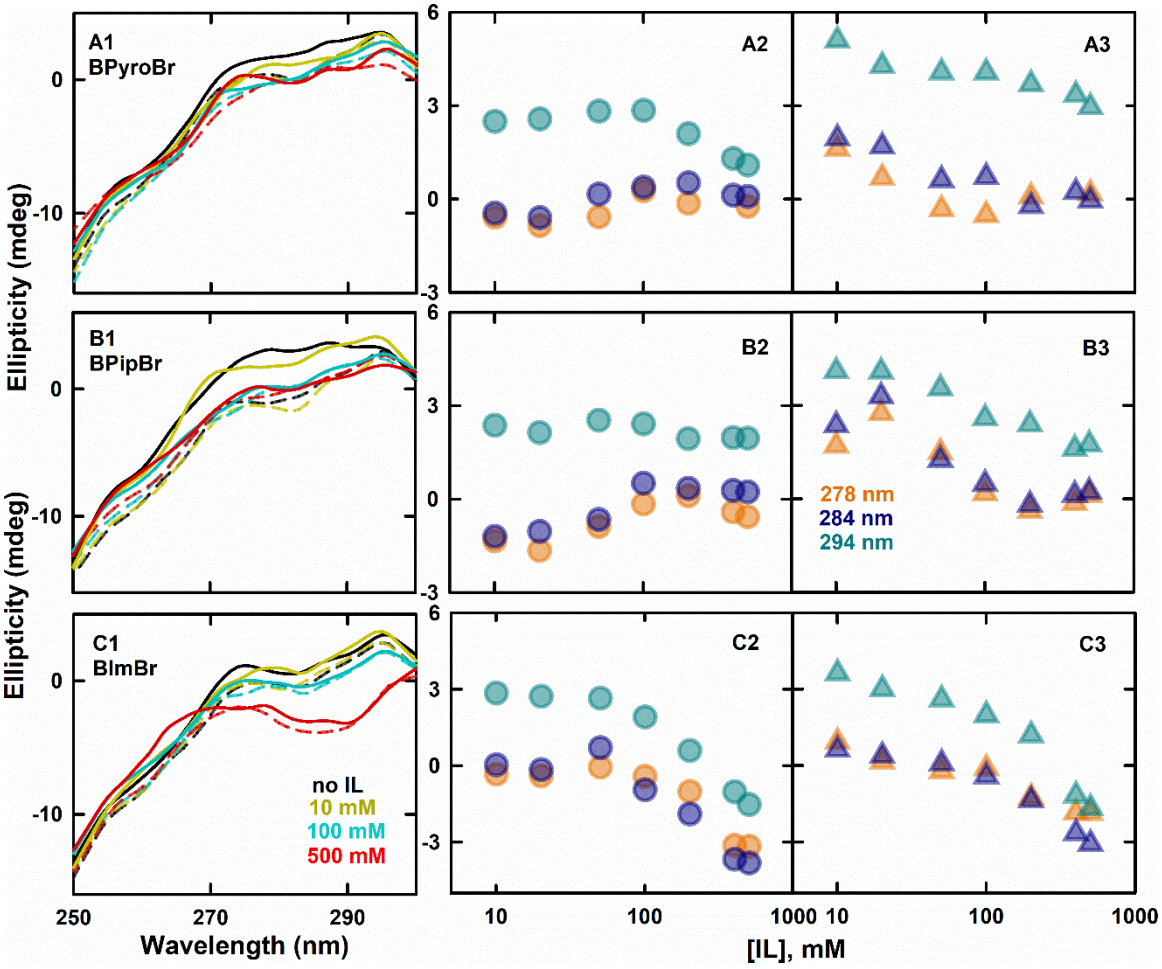

Fig. 3.6. Near UV-CD spectra of Lyz in the absence (black) and the presence of 10 mM (dark yellow), 100 mM (cyan), and 500 mM (red) of (A1) BPyroBr, (B1) BPipBr, and (C1) BImBr. Dashed and solid lines represent before and after incubation of Lyz at fibrillation condition. Ellipticity changes in the protein in the presence of varying concentrations of ILs before (circles) (A2-C2) and after incubation (triangles) (A3-C3) at fibrillation conditions followed at 278 nm (orange), 284 nm (dark blue), and 294 nm (cyan).

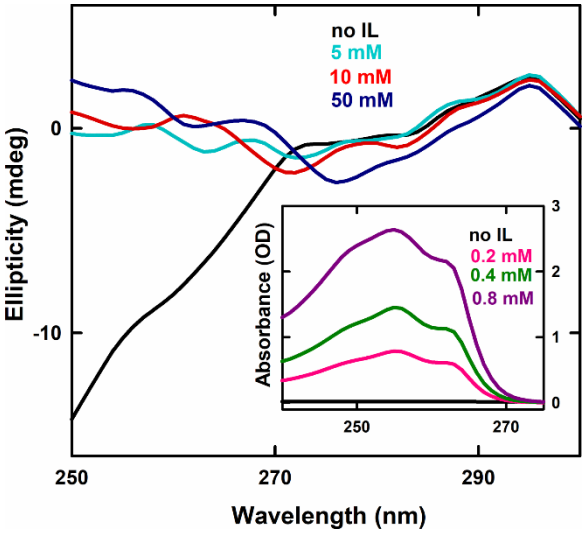

Fig. 3.7. Near-UV CD spectra of Lyz in the absence (black) and presence of 5 mM (blue), 10 mM (red) and 50 mM (dark blue) of BPyrdBr. Inset shows absorption spectra of BPyrdBr at 0.0 mM (black), 0.2 mM (pink), 0.4 mM (green) and 0.8 mM (purple)

Contrarily, a sharp reduction in the ellipticities for Trp and Tyr residues was seen in the presence of BPyrdBr even at the lowest concentration (Fig. 3.7). This could be due to the high absorption of BPyrdBr in this region (inset of Fig 3.7). There were changes in ellipticities upon incubation of Lyz at fibrillation conditions in the absence as well as presence of varying concentrations of ILs. With increasing concentrations of ILs, ellipticity changes were differentiable, with maximum changes in the presence of BImBr followed by BPipBr and least in the case of BPyroBr.

Intrinsic fluorescence spectra of Lyz in the presence of varying concentrations of

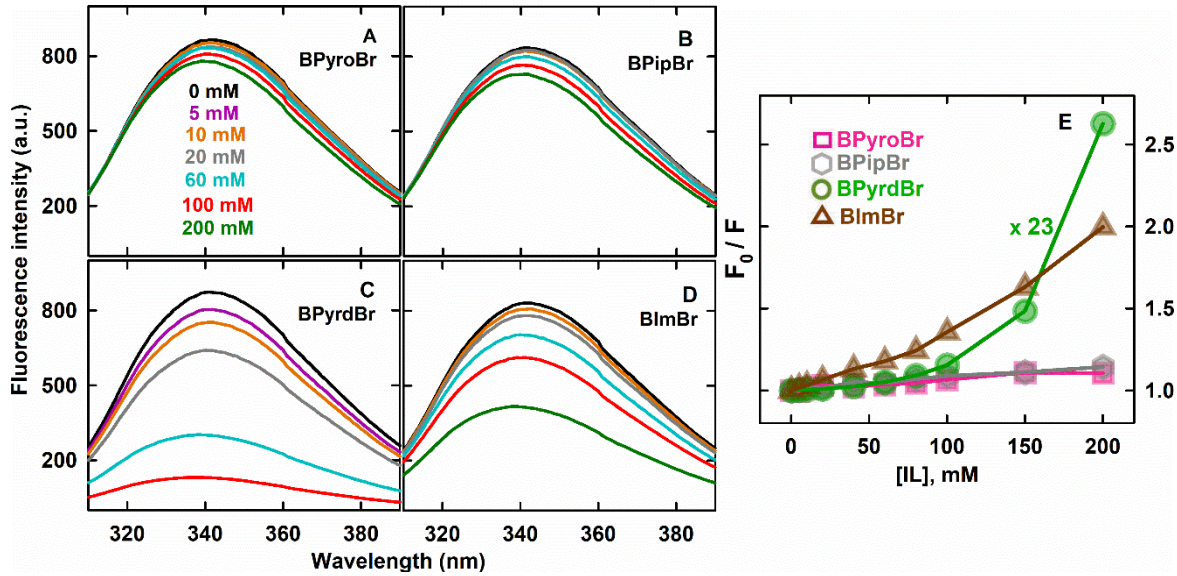

Fig. 3.8. Fluorescence emission spectra of Lyz in the absence (black) and in the presence of varying concentrations of (A) BPyroBr, (B) BPipBr, (C) BPyrdBr, and (D) BImBr upon excitation at 280 nm. (E) Stern-Volmer plots for the fluorescence at 340 nm (derived from spectra given in panels A-D) in the presence of BPyroBr (pink square), BPipBr (grey hexagon), BPyrdBr (green circle), and BImBr (brown triangle).

ILs showed a fall in spectral fluorescence in the order as follows, BPyrdBr >> BImBr > BPipBr > BPyroBr (Fig. 3.8 A-D). Stern – Volmer plots derived from fluorescence emission at 340 nm showed a non-linear curve for all the ILs indicative of possible static quenching (Fig. 3.8E). To verify whether the fluorescence quenching occurred as a result of ground state complex formed between protein and ILs, spectra for N-acetyl tryptophanamide (NATA, a model compound for protein tryptophan residues) were collected in varying concentrations of ILs (Fig. 3.9). Decrease in the fluorescence intensity of NATA was observed in the presence of ILs and showed similar trends as Lyz. Notably. The fluorescence intensity of both Lyz and NATA was completely lost in the presence of higher concentrations of BPyrdBr. Therefore, it could be assumed that the observed fluoresce quenching might not exclusively arise due to the binding of IL with the protein.

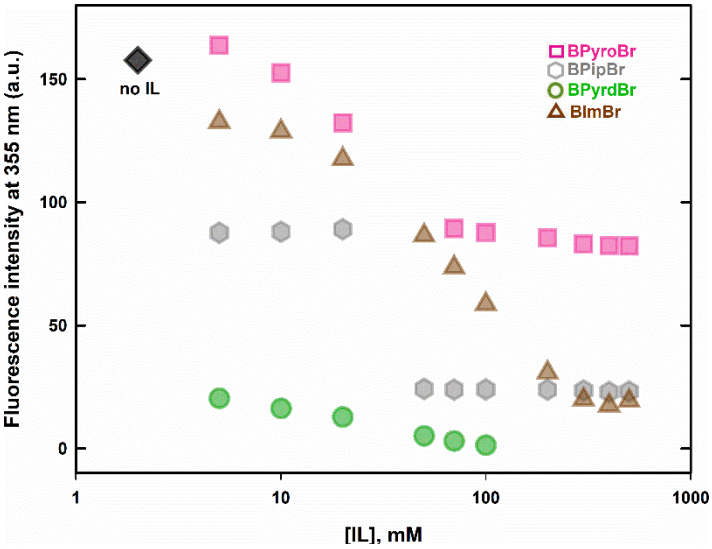

Fig. 3.9. Fluorescence emission intensity of NATA at 355 nm after exciting the dye at 280 nm in the presence of varying concentrations of the ILs, BPyroBr (pink squares), BPipBr (grey hexagons), BPyrdBr (green circles), and BImBr (brown triangles).

Protein undergoing conformational changes in the presence of any cosolvent may expose a few hydrophobic residues on the surface, such that, they are accessible to the solvent molecules. ANS, a dye that shows elevated fluorescence on getting bound to the hydrophobic residues is thus employed to study the conformational changes of the protein. Any perturbations in the microenvironment of these residues may lead to a blue or red shift in the wavelength emission maxima accompanied by the changes in fluorescence intensity of ANS. The ANS fluorescence in ILs in the presence and the absence of Lyz was similar except in the case of lower concentrations (≤50 mM) of BPyrdBr (Fig. 3.10). Though changes in tertiary structure were observed through CD spectra, intrinsic and extrinsic fluorescence studies demonstrated opposite imprints of protein conformation upon addition of varying concentrations of ILs. This suggests that the conformational changes might be restricted to local environments. For further residue-level insight, molecular dynamic simulations were performed.

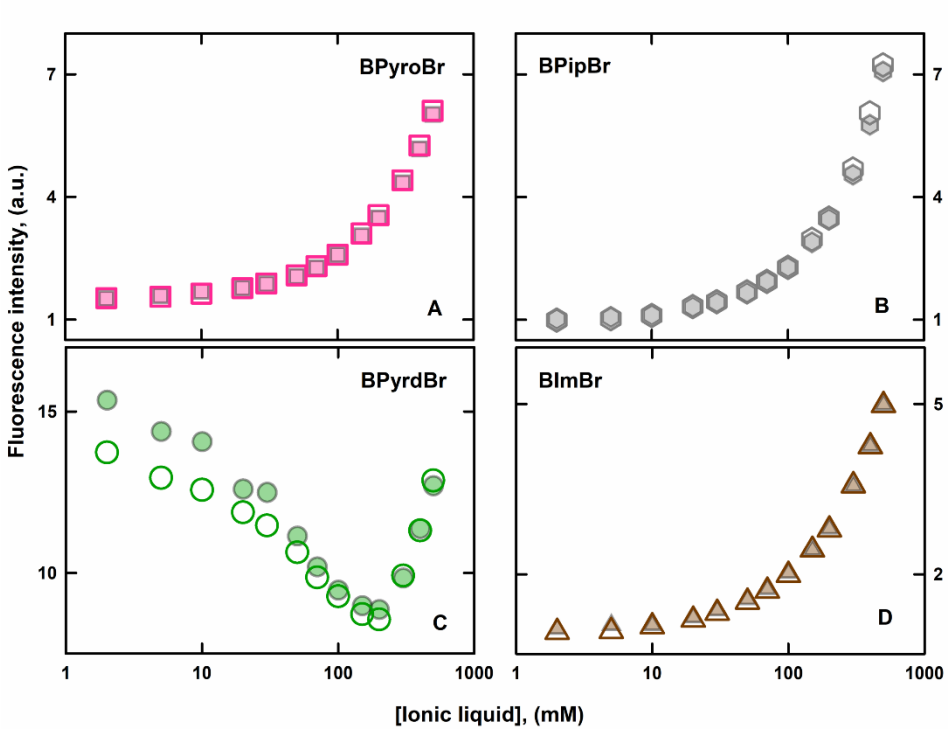

Fig. 3.10 The fluorescence intensity of ANS at 520 nm after exciting the dye at 380 nm in varying concentrations of (A) BPyroBr, (B) BPipBr, (C) BPyrdBr and (D) BImBr in the absence (hollow symbols) and the presence (filled symbols) of Lyz.

3.3.4 Molecular dynamic simulations studies

3.3.4.a Residue fluctuations and compactness

Root mean square deviation (RMSD) of the protein chain, root mean square fluctuations (RMSF) of individual residues, radius of gyration (R_g) and solvent accessible surface area (SASA) of Lyz were calculated from the MD simulations of the protein performed in the absence and the presence of all four ILs at two different concentrations, 50 mM and 200 mM (Fig. 3.11). RMSD analysis reflects the average amount of movement of backbone atoms throughout the entire protein structure while RMSF values show the localised flexibility of individual amino acids throughout the protein. R_g is the extent of compactness a protein undergoes in the given conditions while SASA is the surface area of protein accessible to solvent molecules[178]. RMSD values of Lyz had only marginal changes in the presence of 50 mM of ILs as compared to Lyz in water. In 200 mM concentration of ILs, RMSD values were reduced and the extent of reduction followed the order, BPyrdBr > BPipBr > BPyroBr > BImBr (Fig. 3.11 A1 & B1). RMSF values in the absence and presence of ILs showed differential residue-wise fluctuations throughout the protein as shown in Fig. 3.11 (A1 & A2). The

fluctuations were more around the residues 44-50, 65-74 and 98-119. In general, the residue fluctuations were reduced in the presence of 200 mM of ILs compared to 50 mM. Radius of gyration (R_g) and SASA values did not show any significant differences with the addition of ILs (Fig. 3.11 A3-B4).

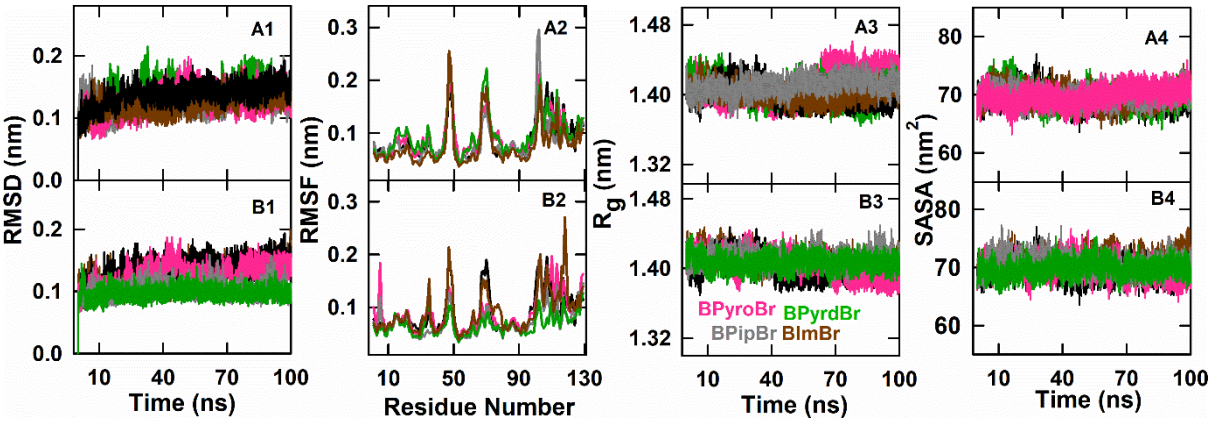

Fig. 3.11. Upper panels: (A1) Root mean square deviation of the protein chain (RMSD), (A2) root mean square fluctuations (RMSF) of residues, (A3) radius of gyration (R_g) and (A4) solvent accessible surface areas (SASA) of Lyz in the absence (black) and presence of 50 mM BPyroBr (pink), BPipBr (grey), BPyrdBr (green) and BImBr (brown). Lower panels (B1-B4) show similar results in the presence of 200 mM of the ILs.

3.3.4.b Radial distribution function (RDF)

The distribution of water and ILs around the protein were calculated using radial distribution function (Fig. 3.12). The RDFs calculated for water showed three maxima which appeared at 0.28 nm, 0.38 nm and 0.48 nm representing the first, second and third hydration shells around the protein. It may be noted that the peak positions were not changed upon the addition of ILs but maxima values were altered. In the presence of 50 mM ILs, the changes were almost negligible in all cases, while in 200 mM concentration, there were visible differences in the values. With the addition of BPyroBr and BPipBr, the maxima values were increased in the second and third hydration shells, but almost remained unchanged for the first hydration shell. This implied that both the ILs tend to increase the water density around the protein surface. On the other hand, in the presence of BPyrdBr, the values were decreased, but only marginally reduced in the presence of BImBr. Reduction in peak height possibly relates to reduced water molecules in the respective hydration shells.

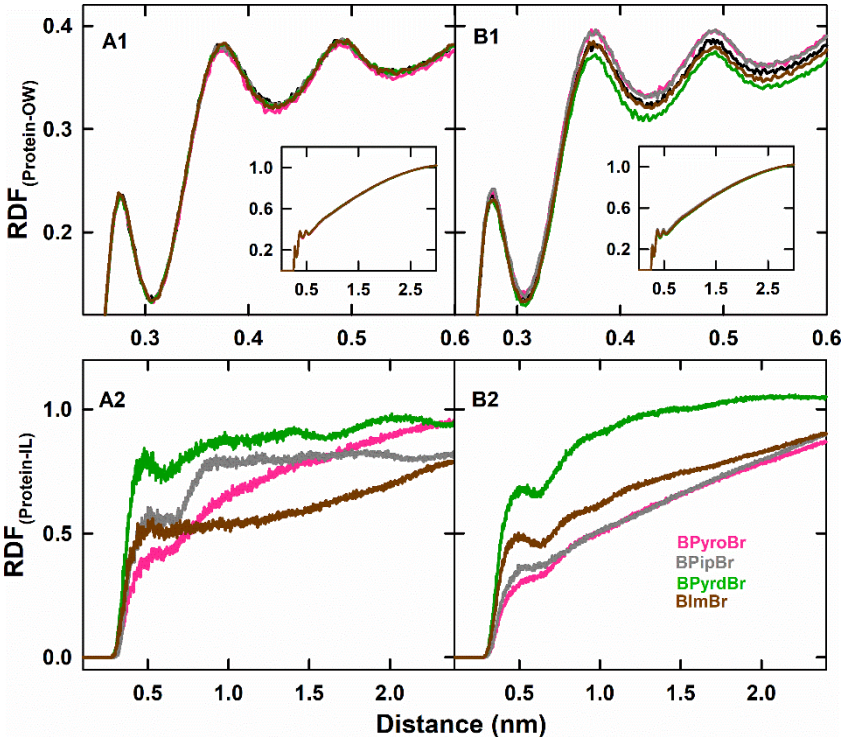

Fig. 3.12. Radial distribution function of water (upper panels) and ILs (lower panels) in the absence (black) and presence of 50 mM (A1 and A2) and 200 mM (B1 and B2) of BPyroBr (pink), BPipBr (grey), BPyrdBr (green), and BImBr (brown).

The RDF plots for ILs around the protein showed that the first coordination sphere of the ILs around the protein could be at ~0.48 nm. The peak heights followed the order, BPyrdBr > BImBr > BPipBr ≈ BPyroBr, indicating that the density of BPyrdBr around the protein was maximum and it is minimum for BPyroBr among the four ILs.

3.3.4.c Distribution of water and ILs around Lyz and residues

The number of water and ILs were evaluated at three different cut-offs 0.32, 0.42 and 0.62 nm from the protein surface by the same procedure followed in section 2.3.4.c. of the previous chapter. In the presence of 50 mM of ILs, the average number of water molecules in all three regions showed marginal reduction as compared to the number of waters in the absence of any ILs (Fig. 3.13-A1, B1 & C1). In the presence of 200 mM of ILs, the decrease in the water molecules around the protein was higher at all three cut-offs. The decrease in water molecules followed the order, BImBr > BPyrdBr > BPyroBr > BPipBr (Fig. 3.13-A2, B2 & C2). The number of ILs around the protein showed only a small fraction in first hydration shell and had significant values at 0.42 and 0.62 nm. The occupancy of BPyrdBr and BImBr was more around the protein whereas BPyroBr was the least at all three distance cut-offs (Fig. 3.13-B2, B4 &

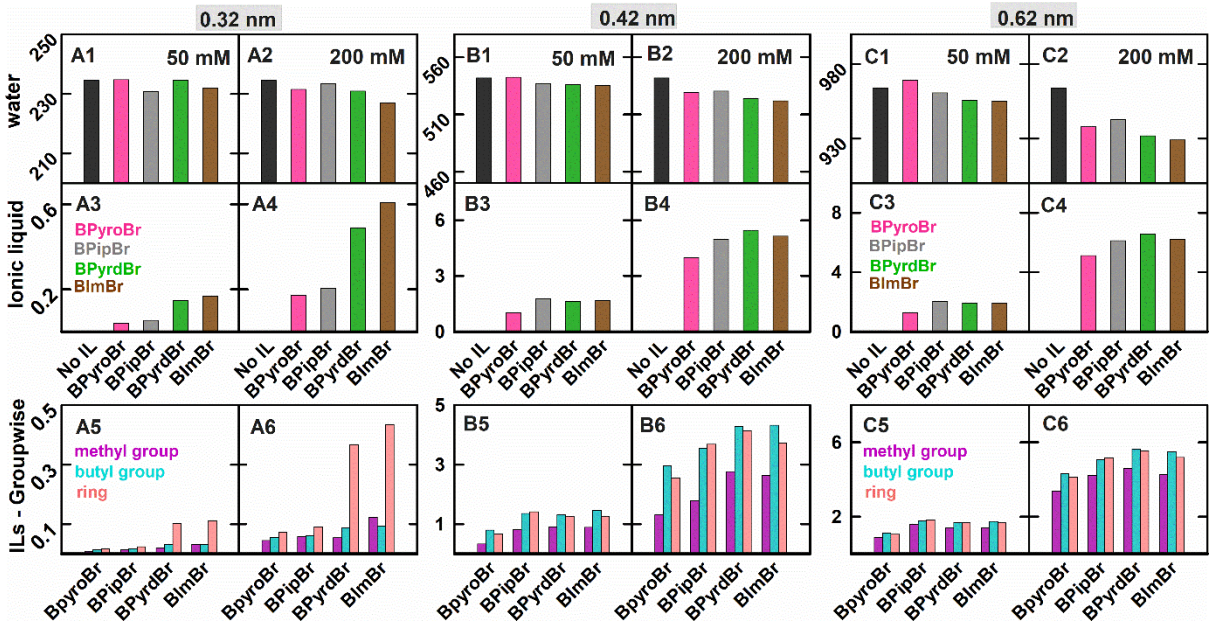

Fig. 3.13 Average number of water molecules (top row), IL (middle row), and ILs' groups (bottom row) around the protein in the absence and presence of 50 mM (A1, A3, A5, B1, B3, B5, C1, C3, C5) and 200 mM (A2, A4, A6, B2, B4, B6, C2, C4 and C6) of ILs within the cut-offs of 0.32 nm (panel A), 0.42 nm (panel B) and 0.62 nm (panel C). Black bars indicate the absence of any IL (top row), pink for BPyroBr, grey for BPipBr, green for BPyrdBr, and brown for BImBr (top and middle row). Methyl groups, butyl groups and ring moiety of each ILs are shown in violet, cyan and orange bars (bottom row), respectively.

C4). To understand the preferable orientation of interaction of the ILs with Lyz, ILs were separated into three groups, methyl, butyl sidechain and ring moiety and the interaction of each group around the protein was analysed (Fig. 3.13-A5, A6, B5, B6, C5 and C6). It was observed that the ring moiety and butyl sidechain of the ILs are closer to the protein surface than the methyl group for all four ILs.

To garner the residue-level interaction of Lyz with the ILs, the numbers of water molecules and ILs around each type of amino acid were evaluated (Fig. 3.14 and 3.15). This would provide information on which amino acids were more often involved in the interactions with ILs. The number of water and IL molecules at the distance cut-offs of 0.42 and 0.62 nm were only discussed, because of the negligible fraction of IL molecules around the protein in the first hydration shell. It was observed that in the presence of all the ILs, the water molecules around Phe and Trp were reduced except for BImBr (Fig. 3.14). There was only slight reduction in the water molecules for Ser, Thr, Pro, His, Asp, Asn, Lys and Arg with the addition of all ILs. In the presence of BPipBr and BImBr there was a larger reduction in water molecules

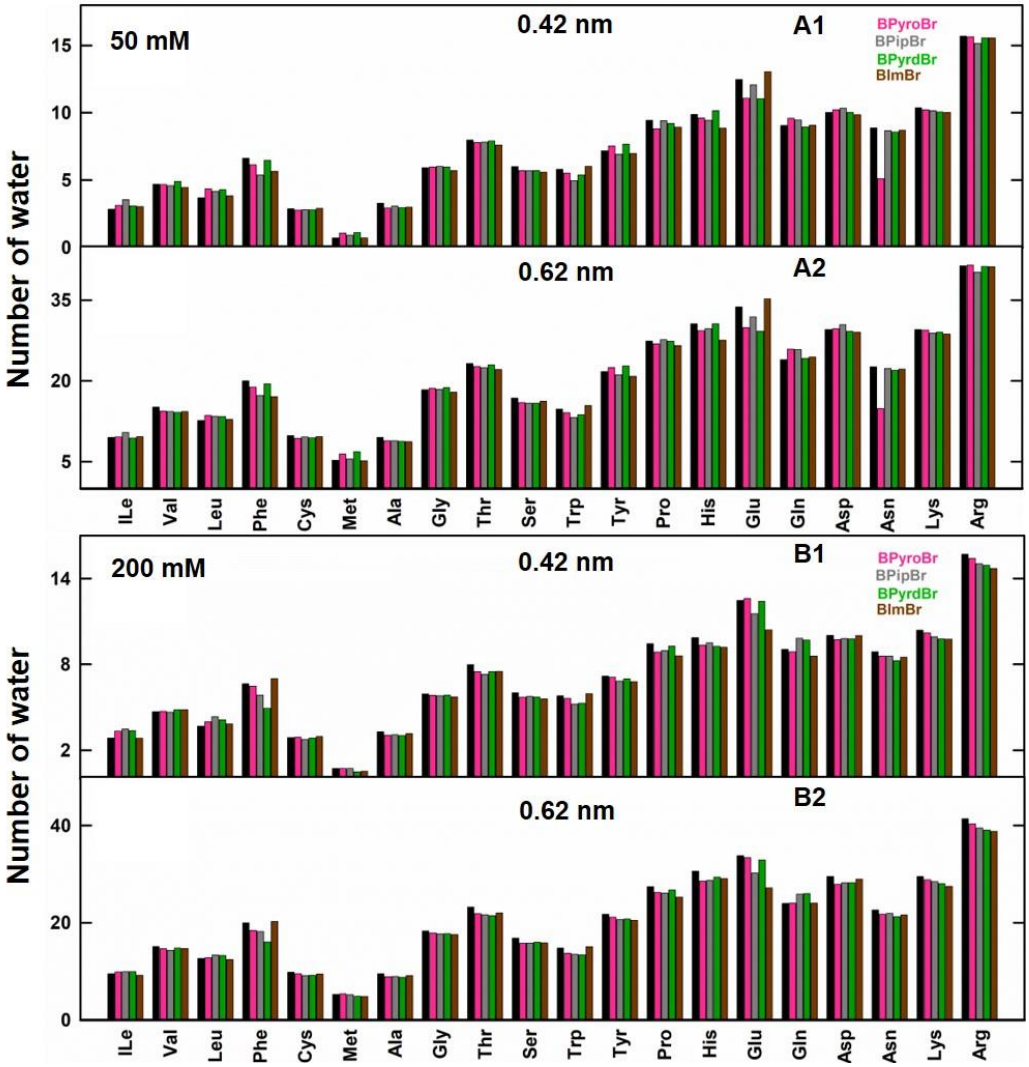

Fig. 3.14 Average number of water molecules around each residue of Lyz in the presence of 50 mM of ILs at a distance cut-off of (A1) 0.42 nm and (A2) 0.62 nm, and in the presence of 200 mM ILs at a distance cut-off of (B1) 0.42 nm and (B2) 0.62 nm. Black bars indicate the number of water around the residues in the absence of any IL, whereas pink, grey, green and brown bars indicate the presence of BPyroBr, BPipBr, BPyrdBr and BImBr, respectively.

around Glu as well. A slight increase in the number of water molecules around Gln was observed with the addition of BPipBr and BPyrdBr. From the number of ILs around the residues (Fig. 3.15), it was noted that BPipBr and BImBr had more interaction with hydrophobic residues such as Ile, Val, Phe and Met. While BPyrdBr was found more in the vicinity of polar or charged residues, such as Cys, Glu, Arg and Lys, BImBr molecules were found to be in the proximity of Thr, Ser, Pro, Gln and Phe residues and showed less interaction towards His and Lys as compared to BPipBr and BPyrdBr.

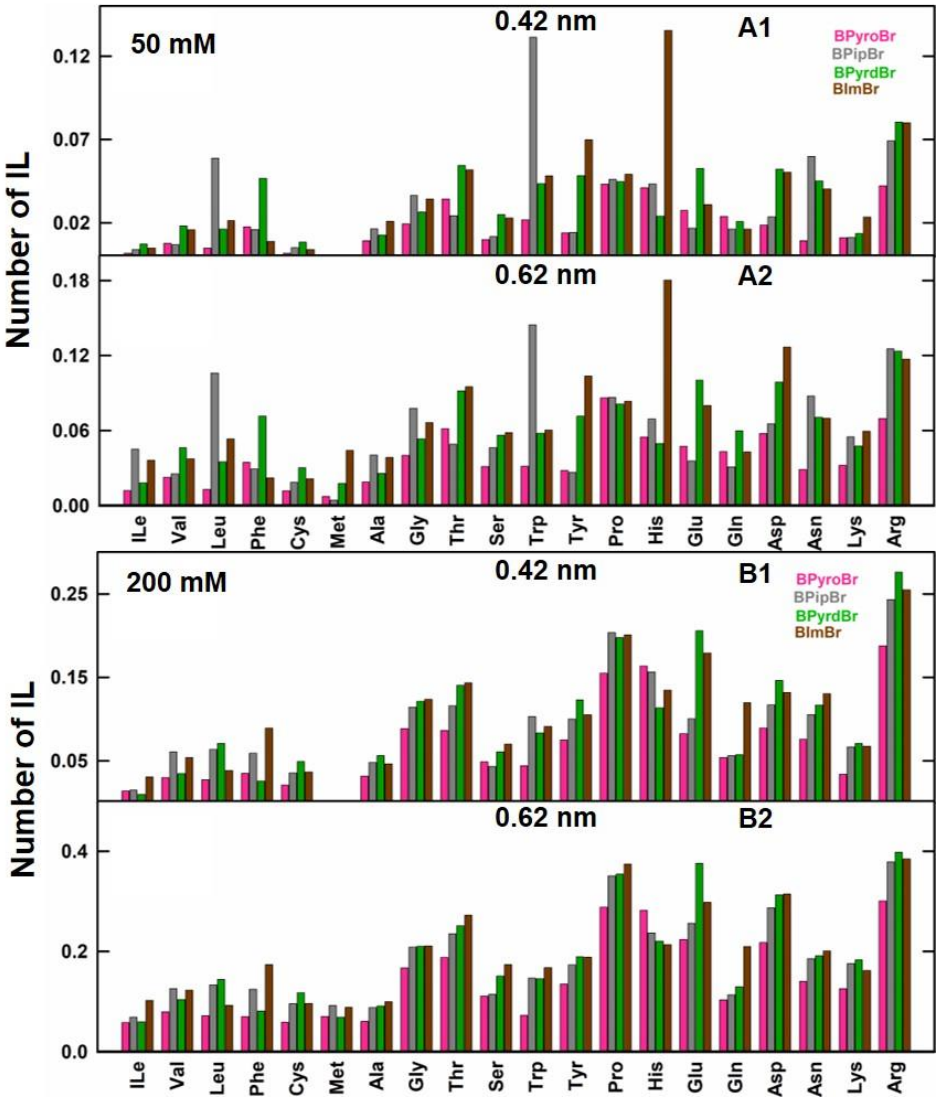

Fig. 3.15 Average number of IL molecules around each residue of Lyz in the presence of 50 mM of ILs at a distance cut-off of (A1) 0.42 nm and (A2) 0.62 nm, and in the presence of 200 mM ILs at a distance cut-off of (B1) 0.42 nm and (B2) 0.62 nm. Bars in pink, grey, green and brown color indicate the presence of BPyroBr, BPipBr, BPyrdBr and BImBr, respectively.

3.3.4.d Solvation properties and associated free energies

The hydration fraction was calculated at three different cut-offs using equation 2.6 as mentioned in the previous chapter. The values of hydration fraction (χ_{hyd}) in the presence of 50 mM and 200 mM ILs are shown in Fig. 3.16. At both concentrations, hydration fraction was in all three regions. In 50 mM ILs, χ_{hyd} values were the highest for BPyroBr followed by BPipBr and BPyrdBr for the first hydration shell (0.32 nm cut-off). In the regions underlying 0.42 nm and 0.62 nm, the hydration fraction was again maximum for BPyroBr, but the value was almost

similar in other three ILs. In 200 mM as well, χ_{hyd} followed the same trend that the value was maximum of BPyroBr at all three distance cut-offs.

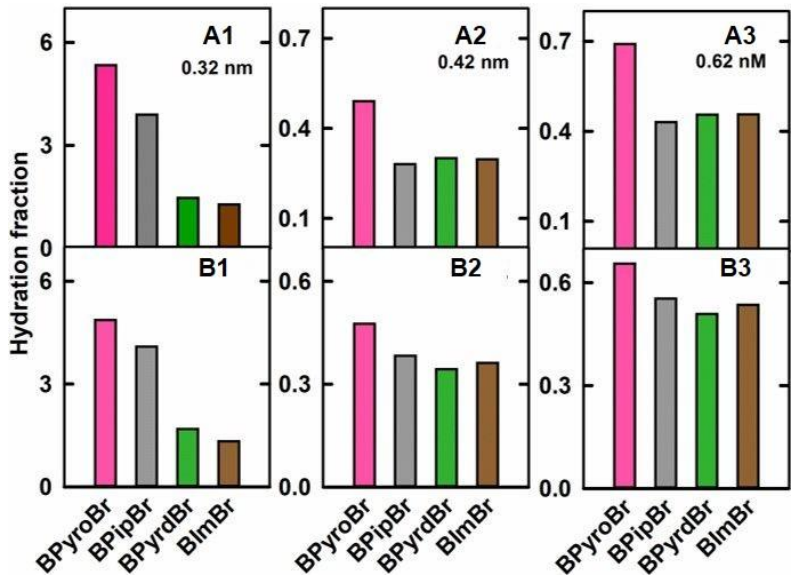

Fig. 3.16 Hydrations fractions calculated at the distance cut-off of 0.32 nm (A1 and B1), 0.42 nm (A2 and B2), and 0.62 nm (A3 and B3) around Lyz in the presence of 50 mM (A1-A3) and 200 mM (B1-B3) of ILs (pink: BPyroBr, grey: BPipBr, green: BPyrdBr, and brown: BImBr).

Further, preferential interaction coefficient ($\Gamma_{P\text{-}IL}$) was calculated based on Kirkwood-Buff integral method using radial distribution functions as described in section 2.2.7.c (Fig. 3.17-A1 & B1). At both 50 and 200 mM concentrations, BPyrdBr showed the highest values beyond 0.32 nm cut-off. At lower concentration, for the other three ILs, the values were close to zero or slightly negative implying that at lower concentration only BPyrdBr tends to interact with Lyz. At higher concentration, BPyrdBr and BImBr showed positive values beyond the second-hydration shell, whereas BPyroBr and BPipBr had negative values at all the distances. These results suggest that BPyrdBr, followed by BImBr, had more preferential interaction over water molecules around the protein, whereas in the presence of ILs with alicyclic moieties, BPyroBr and BPipBr, the protein surface is preferentially hydrated. For any interaction to be a favorable event, free energies of binding or interaction should be negative. Fig. 3.17 (A2 and B2) show the negative transfer free energy for BPyrdBr and BImBr while positive values were noted for BPyroBr and BPipBr.

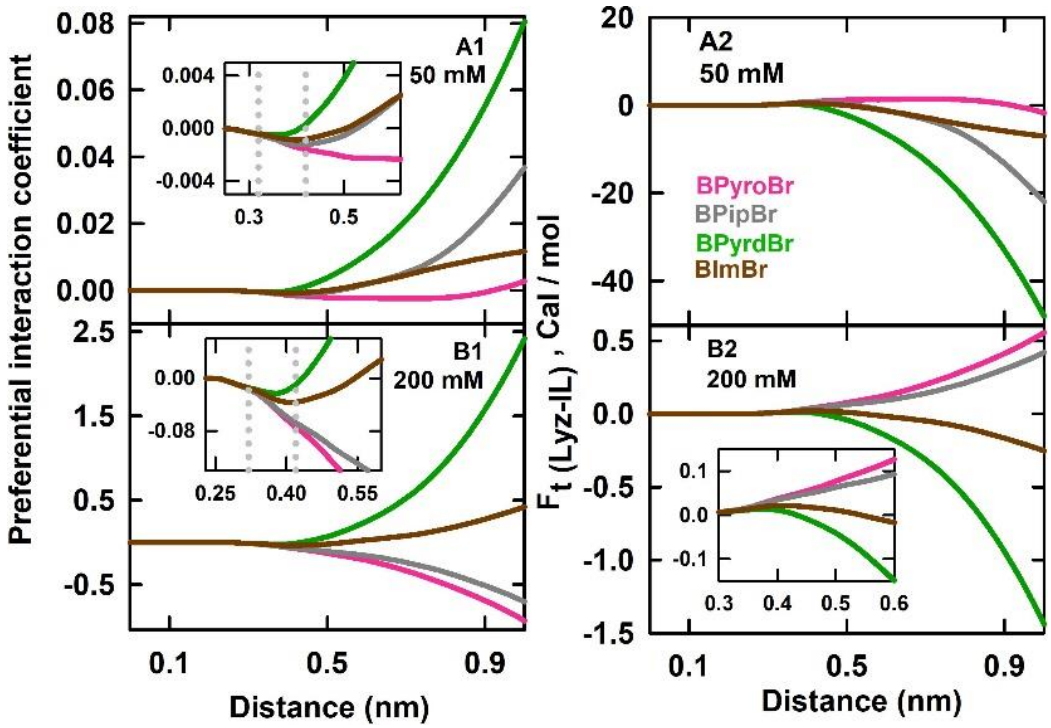

Fig. 3.17 Preferential interaction coefficients calculated for Lyz with increasing distance from the protein surface in the presence of 50 mM (A1) and 200 mM (B1) of BPyroBr (pink), BPipBr (grey), BPyrdBr (green) and BImBr (brown). Insets show a closer view to the preferential interaction coefficients and the distances 0.32 nm and 0.42 nm from the protein surface are indicated with grey dotted vertical lines. Transfer free energies derived from preferential interaction coefficients for Lyz in the presence of (A2) 50 mM and (B2) 200 mM of the ILs.

3.3.4.e Probable ligand binding sites on Lyz

As the protein is folded in a particular conformation, not all the residues are exposed to the solvent molecules to interact. Therefore, knowing how and to what extent each residue would be involved in the interactions with a particular IL type is highly significant to predict the probable binding sites. The degree of interaction between each residue and IL was evaluated used the same method discussed in the previous chapter (section 2.2.7.e). Residues were assigned color on the basis of their interaction tendency with ILs. Fig. 3.18 shows the interaction profile of Lyz with all ILs at 50 and 200 mM concentrations. In the presence of 50 mM of ILs, the major interacting site was on the N-terminal of Lyz and a few other regions showed weak interactions (Fig. 3.18 A-D). While at higher concentration, apart from N-terminal residues, few other sites show moderate to high interactions with ILs shown in Fig. 3.17 (E-H). The

overall representation of all the probable binding sites for all four ILs is discussed in detail below in section 3.4.4. and Fig.3.21.

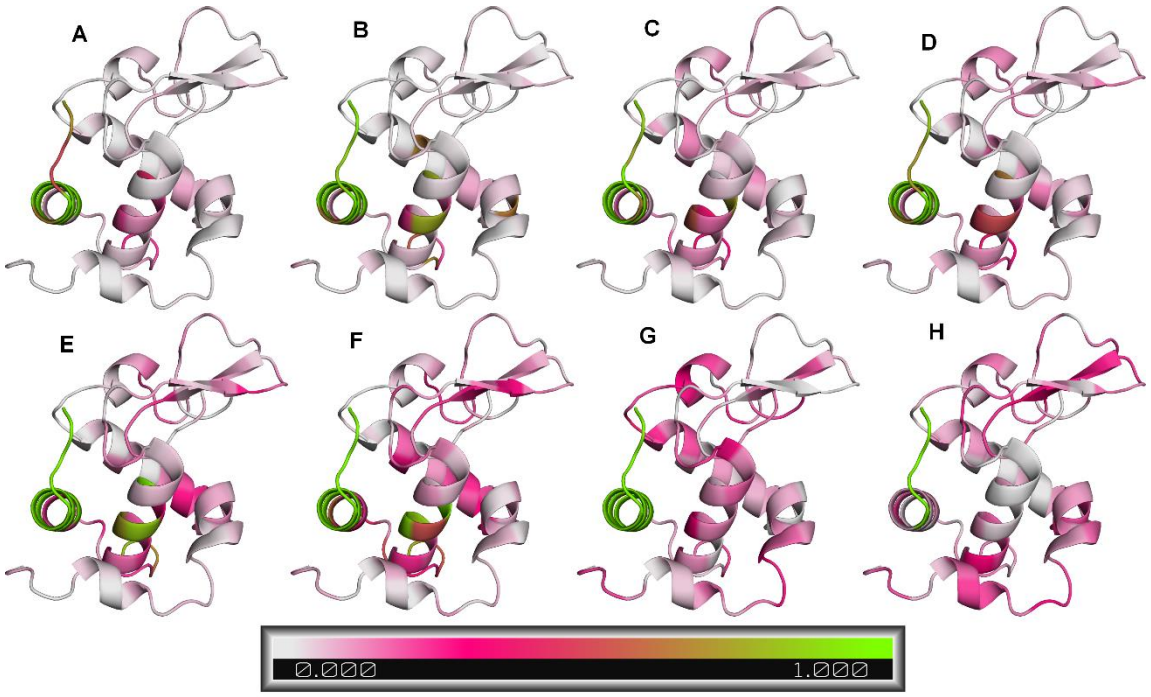

Fig. 3.18 Cartoon diagram depicting the fraction of time (A) BPyroBr, (B) BPipBr, (C) BPyrdBr and (D) BImBr occurred in the vicinity of each residue of Lyz throughout the simulation in the presence of 50 mM (upper panels) and 200 mM (lower panels) of the ILs. The color gradients from white to green indicate non-interactive regions to most interacting regions on the protein, while regions shown in pink are indicative of moderate interactions with the ILs.

3.4 Discussion

3.4.1 Fibrillation rate, mechanism and morphology

Lyz forms fibrils by following a nucleation-independent mechanism under the condition adapted in this study (Fig. 3.2 B). With the addition of ILs, apparent fibrillation time is delayed in a concentration-dependent manner (Fig.3.3). At lower concentrations, the rate is slightly reduced. When the concentration of ILs is above 100 mM (80 mM for BPyrdBr), the fibrillation switched from nucleation-independent to nucleation-dependent mechanism. At the concentrations above 200 mM, the rate is drastically reduced in the presence of all the ILs. Also, the lag time was increased in a concentration-dependent manner almost linearly. To understand the overall effect of aromatic and alicyclic ILs on the fibrillation propensity of Lyz, apparent fibrillation time (T_{app}) was calculated. The maximum delay in fibril formation is provided by 500 mM of BPyroBr that is nearly 70-fold longer that the fibrillation time in buffer. 500 mM

of BPipBr induces minimum delay among all the four ILs which is nearly 30-fold longer than the control. The delay in fibrillation by all four ILs followed the order, BPyroBr > BPyrdBr > BImBr > BPipBr. TEM micrographs reveal that the morphology of fibrils are different in the presence of BPyroBr, BPyrdBr and BPipBr, whereas in BImBr, the morphology is similar to the fibrils formed in buffer (Fig. 3.4). The width of fibrils is maximum in the presence of BPyrdBr, while in all other ILs the width is similar to the control.

3.4.2 Structural changes and thermal stability of Lyz

All the ILs destabilized the protein and the maximum destabilization is noted in the presence of aromatic ILs. 500 mM of BPyrdBr lowers the T_m by 14 K as compared to the T_m of Lyz in buffer, which is the maximum among all the ILs. Interestingly, destabilization is significant in the presence of BImBr as well, though slightly lesser than BPyrdBr. However, BImBr shows non-cooperative transitions at above 200 mM. Similar transitions are observed also in the presence of higher concentrations of HMIC and OMIC (Im-ILs with longer alkyl chains) in the previous chapter. On the other hand, the destabilization effect of alicyclic ILs is relatively less. The enthalpy of unfolding (ΔH_m) has only marginal reduction with increasing concentration of BPyroBr, BPipBr and BImBr which corresponds to the reduced T_m of Lyz. However, BPyrdBr shows exceptionally higher values of ΔH_m at concentrations above 200 mM. Enthalpy-entropy compensation plot for the thermal transitions in the presence of all four ILs is shown in Fig. 3.19.

All the ILs induce enthalpically-driven destabilization of Lyz, except in the presence of higher concentrations of BPyrdBr. Overall, the results indicated that the destabilizing effect of ILs with aromatic moiety is more than the ILs with alicyclic moiety, particularly at concentrations above 100 mM. There are only marginal structural changes in the ellipticity measured at near-UV region in the presence of alicyclic ILs (BPipBr and BPyroBr) at room temperature as well as at the fibrillation conditions. Whereas aromatic ILs (BPyrdBr and BImBr) show significant changes in the structure of Lyz at both conditions (Fig. 3.6). Also, the intrinsic fluorescence has only slight reduction indicating less structural differences in Lyz. BImBr, an aromatic IL, shows slight reduction in ellipticity and fluorescence at lower concentrations (upto 20 mM) but with increasing concentration, there is a drastic reduction in both. These findings are indicative of the fact that BImBr interacts effectively with the protein at higher concentrations and induce structural changes. BPyrdBr completely reduces the

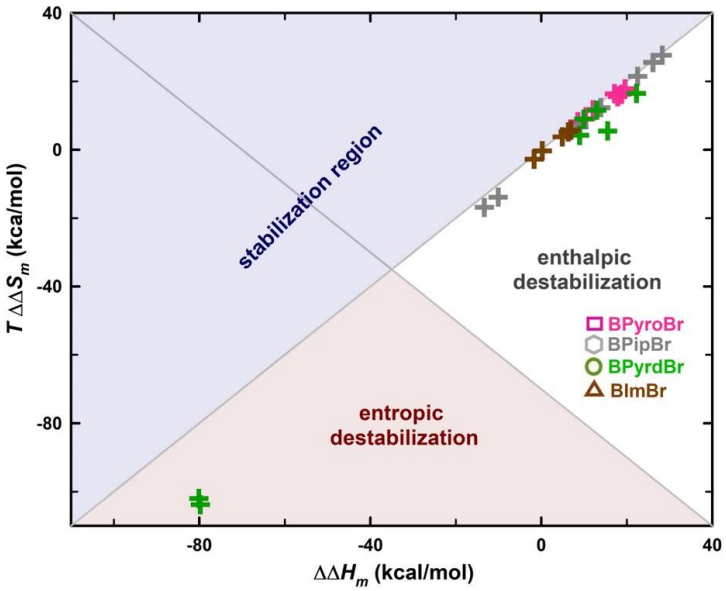

Fig. 3.19 Enthalpy-entropy compensation plot evaluated from the thermal denaturation studies presented in Fig. 3.5. The cosolvent-induced stabilization (blue-shaded) and destabilization (red-shaded and transparent) regions are marked for reference.

ellipticity at all concentrations. This can be due to its characteristic absorption at wavelength 255 nm (Fig. 3.7 inset), which falls in near-UV region. Further, the excessive reduction of fluorescence intensity, also complemented by NATA fluorescence quenching (Fig. 3.9), explains that structural changes in Lyz cannot be predicted only based on ellipticity and fluorescence data of BPyrdBr .

The structural changes and interaction between Lyz and ILs were evaluated through MD simulations. Global parameters, RMSD, radius of gyration and SASA has only marginal changes. However, RMSF values show more fluctuations in the presence of ILs compared to Lyz in water which are higher in the presence of aromatic ILs (Fig. 3.20). Such differences in RMSF of protein can be related to different interaction strengths of ILs with the protein.

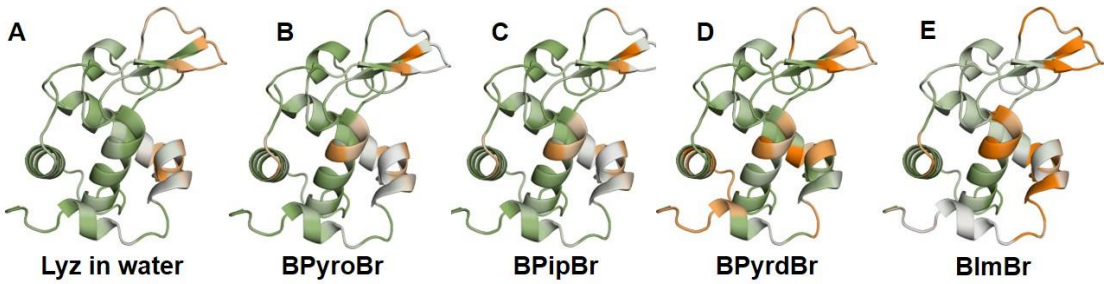

Fig. 3.20 Structure of Lyz highlighting the regions with higher RMSF values (orange) in the (A) absence of any IL and in the presence of (B) BPyroBr, (C) BPipBr, (D) BPyrdBr, and (E) BImBr.

3.4.3 Solvation properties of Lyz in the presence of ILs

Reduction in RDFs of water with the addition of aromatic ILs is more pronounced as compared to alicyclic ILs. This is complemented with the increased RDFs of aromatic ILs (Fig. 3.12). This suggests that the probability of finding an aromatic IL around the protein is more than an alicyclic IL. RDF result is also corroborated with the number of water and ILs calculated around the protein. More water molecules are reduced in the presence of aromatic ILs (Fig. 3.13) and a greater reduction in hydration fraction is observed (Fig. 3.16) indicating that the tendency of BPyrdBr, followed by BImBr, to be in the vicinity of the protein is more compared to BPyroBr and BPipBr. This implies that aromatic ILs show more interaction by replacing the water molecules in the vicinity of protein.

3.4.4 Interaction, structural changes and delayed fibrillation

Type of molecular interaction between protein and ligand depends on the functional group moiety of ligand and the surface-exposed residues in the protein. Therefore, we tried to know the orientation of each IL present in the vicinity of the protein. All four ILs preferably interact with Lyz through butyl sidechain and ring moiety. Residue-wise interaction of ILs with Lyz (Fig. 3.18) shows that the number of binding sites are more for aromatic ILs than the alicyclic IL. It is also observed that the destabilizing effect of BPyrdBr is the most among all four ILs and it also shows the longest lag time during fibril formation of Lyz. Whereas BPyroBr shows minimum destabilization effect and maximum T_{app} value during the fibril formation of Lyz.

BPyroBr, though least in number around the protein, shows stronger binding to the protein, in the regions far away from the hydrophobic clusters 3 and 5, which is crucial for fibril assembly. The loss of number of water molecules around Lyz is less with the addition of BPyroBr as compared to the addition of aromatic ILs. This might suggest that the hydrophobic core of protein remains less-exposed to initiate fibril assembly, hence leading to the delay in fibrillation. On the other hand, BPyrdBr shows many regions of binding on Lyz including the hydrophobic clusters 3 and 5. The reduced number of water molecules on the surface of Lyz and its greater destabilization indicate that BPyrdBr interact with the protein globally and destabilizes it. This does not allow the misfolded conformations to form a nucleus of critical size which is crucial to effectively initiate fibril elongation. This might result in a prolonged lag time in the presence of higher concentrations of BPyrdBr. Overall, four regions were identified

on Lyz for the interaction of ILs as shown in the Fig. 3.21. All the ILs show the strongest interaction on the N-terminal region of Lyz. All the identified binding regions on Lyz are mostly composed of hydrophobic residues.

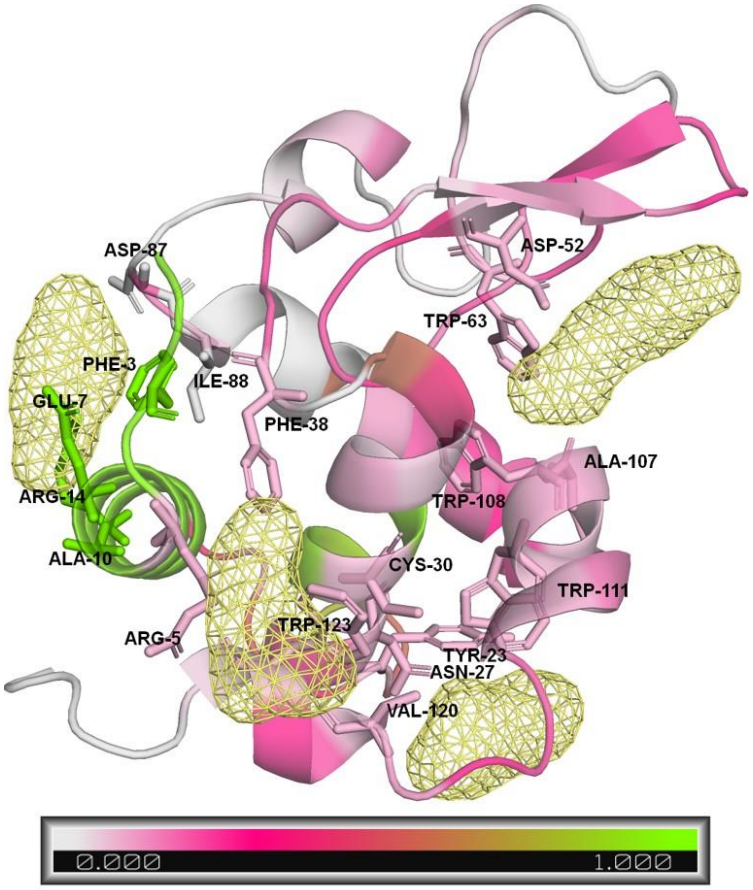

Fig. 3.21 A cumulative representation of the binding regions of ILs on Lyz obtained from MD simulation of the protein with 50 mM and 200 mM of all the ILs. The color gradients from white to green indicate non-interactive regions to most interacting regions on the protein, while regions shown in pink are indicative of moderate interactions with the ILs. ILs are represented with yellow colored surface-mesh. The major residues in the binding pockets are shown in sticks and are labeled.

3.5 Conclusion

Packing of hydrophobic residues to the core of a protein is the key to stabilizing its native conformation. However, any molecule added to the protein-solvent binary system, which can alter the native conformation of the protein such that the hydrophobic residues are partially exposed might lead the protein to aggregation or fibrillation. Thus, molecules having different degrees of hydrophobicity, by the nature of presence of aromatic or alicyclic moieties, are used to study their effect on the stability and fibrillation propensity. Fibrillation was delayed by all the ILs, while different mechanisms were involved in forming the fibrillar assemblies of Lyz in the presence of alicyclic and aromatic ILs. Higher concentration of BPyrdBr induced maximum destabilization which was entropically-driven. Aromatic ILs induced fibrillation by destabilizing the protein, i.e., by replacing more water molecules in the vicinity of Lyz. Whereas, alicyclic ILs showed less destabilization by preferential hydration of Lyz. Overall, aromatic ILs show more interaction with protein as compared to alicyclic ILs and ILs with alicyclic moiety inhibits fibrillation more effectively.

Chapter 4
Combinatorial effect of different hydrophobic moieties on the stability and fibrillation propensity of lysozyme

4.1 Introduction

Proteins, the most abundant molecules, are the principal entities in all the molecular functions in a cell[11]. It is well known that functional maturity of a protein is governed by its three-dimensional structure guided by the sequence of amino acids[2]. Though misfolded proteins undergo proteasomal degradation in the cellular milieu, thermodynamically low energy conformations may coexist in the system. Such misfolded conformations might become precursors to form aggregated or fibrillar structures leading to protein conformation disorders (PCDs)[69]. Hence, it is crucial to understand the mechanisms involved in the formation of non-native conformations and the remedies to stabilize the proteins. Also, the misfolding of proteins in *in vitro* systems can harbor numerous challenges in the field of biotechnology and pharma industries which employ enzymes (proteins) to catalyze various biochemical pathways to obtain the desired end products[179,180].

Stability of proteins can be affected by various conditions such as cold, heat, non-native pH and ionic strength of the solvent, etc. To overcome the effects of these destabilizing factors various methods are adapted. For instance, genetic engineering, mutations, fusion strategies, modulation of solvents, addition of preservatives, surfactants and additives are most commonly used in bio-pharma industries[179]. Of all these methods, the modification of solvent systems occupies the major attention of biophysical community because of its non-invasive approach and does not affect the three-dimensional spatial arrangements of proteins[181]. Generally, the addition of cosolvents to the binary systems, protein in solvent, are studied to increase the stability, enhance their activity, and prevent or protect them from aggregation or fibril formation[182,183]. Such cosolvent systems, generally called as chemical chaperones, leverage the folding and stability by affecting the unfolding transitions of the proteins[69].

There are many reports on the use of cosolvents such as sugars[180,184], polyols[185], amino acids[186], salts[187], and ionic liquids[188,189] that help in elevating the thermal stability of proteins. These molecules are studied in mixtures[69,181] with certain molar ratio to understand whether such modulations of solvent systems improve the stability of the proteins and/or further help in delaying or completely inhibiting the formation of fibrillar assemblies. For example, the equimolar mixture of proline and sorbitol can delay the fibrillation of insulin and lysozyme by many folds in a synergistic manner compared to their individual effects on the fibrillation of these proteins[69]. A study on the mixtures of amino acids shows that the combination of glycine

and arginine can significantly stabilize the catalase enzyme while spray drying and is able to retain its activity for longer duration[179,180].

Ionic liquids, also known as green solvents, are proven to be a bio-compatible solvents as they possess the ability to stabilize proteins[190]. For example, BMIC acts as the stabilizer for α-chymotrypsin[191], though it may slightly destabilize some of the proteins like myoglobin[192]. Studies also suggest that ionic liquids are efficient in preventing aggregation and fibrillation of proteins when added in appropriate concentrations[193], while in some cases ionic liquids enhance the fibrillation process. For instance, 1-butyl-3-methylimidazolium nitrate is found to reduce the aggregation of Lyz but promotes the aggregation of β-lactoglobulin[173]. These findings suggest that the same ionic liquid may behave differently with different proteins.

It is also an interesting quest to know whether the mixture of ionic liquids can offer better stability and reduce the fibrillation propensity of proteins as observed in the case of osmolyte molecules. There are a few studies suggesting that ILs when used in combination show enhanced stability of proteins as compared to their individual presence. It is reported that 1-butyl-3-methylimidazolium chloride (BMIC), an enzyme deactivating agent, and butyltrimethylammonium bis(trifluoromethylsulfonyl)imide ([N1114][NTf2]), an enzyme destabilizer, manifest increased stability on cellulase when added simultaneously to the protein buffer system[194]. Another study has witnessed the enhanced stability and activity of immobilized lipase in the presence of mixtures of 1-ethyl-3-methylimidazolium tetrafluoroborate ([EMIM][BF_4]) and 1-hexadecyl-3-methylimidazolium bis(trifluoromethylsulfonyl)imide [C_{16}MIM] [Tf_2N] rather than when used individually. It is also demonstrated that the denaturing effect of [BMIM][I] on α-chymotrypsin can be counteracted by the presence of [BMIM][Br][195]. This is quite surprising to note that the behaviour of the ILs in combination is entirely different since it is already well-known that bromide or iodide containing ILs denature the proteins when used alone as cosolvents[196–198].

As the mixture of ILs alter the stability of proteins in a synergistic way, one may expect that studying their effects on the fibrillation propensity of proteins could bring more insightful results and might help to solve many dreadful issues arising due to the self-aggregation of proteins. In this chapter, mixtures of ionic liquids were chosen by systematically varying their hydrophobicity. A protic ionic liquid with aromatic cation (MIC) was mixed with either aromatic-shorter alkyl chain IL (BMIC), aromatic-longer alkyl chain IL (HMIC) or alicyclic IL (BPyroBr). In another series of combinations, an aromatic-shorter alkyl chain (BMIC) IL was

mixed with either aromatic-longer alkyl chain IL (HMIC) or an alicyclic IL (BPyroBr). The effect of the aforementioned IL mixtures on the thermal stability, structure and fibrillation propensity of Lyz were studied. Also, molecular dynamic simulations were carried out to analyse the interactions between the protein and each IL, individually and in combinations as well. The results show that the longer alkyl chain IL in combination with the other ILs could delay fibril formation. Further, they destabilize the protein more than their individual effect. The simulation studies predict that a longer alkyl chain increases the preferential binding of IL on the protein surface.

4.2 Materials and methods

4.2.1. Materials

Hen egg lysozyme (Lyz), thioflavin-T (ThT), 1-methylimidazolium chloride (MIC, CAS No. 35487-17-3), 1-butyl-3-methylimidazolium chloride (BMIC, CAS No. 79917-90-1), 1-hexyl-3-methylimidazolium chloride (HMIC, CAS No. 171058-17-6) and 1-methyl-3- were purchased from Sigma-Aldrich. 1-butyl-1-methylpyrrolidinium bromide (BPyroBr; CAS No. 93457-69-3) was purchased from TCI chemicals. Dithiothreitol (DTT) and phosphate buffer salts were obtained from SRL, India.

4.2.2. Sample preparation

The combinations of ILs used in the study and their molar ratios are depicted in Fig. 4.1. and Table 4.1., respectively.

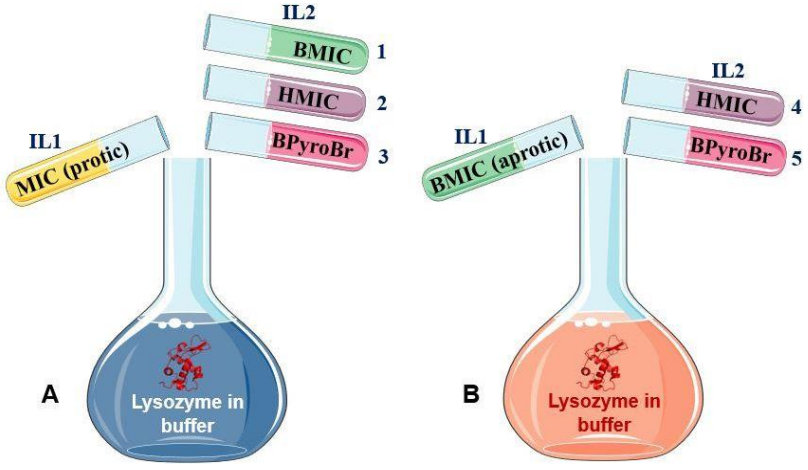

Fig. 4.1 A schematic showing the combinations of ILs used in the present study. Combinations of (A) MIC (protic IL with aromatic group): (1) MIC + BMIC, (2) MIC + HMIC, (3) MIC + BPyroBr, and (B) BMIC (aprotic IL with aromatic group and an alkyl side chain) (4) BMIC + HMIC, and (5) BMIC + BPyroBr.

Table 4.1 Ratios of IL combinations used in the studies.

IL1	IL2
0.25	1
0.50	1
1	**1‡**
2	1
1	0.25
1	0.50
1	2

‡100 mM of each IL

4.2.3. Fibrillation studies

Fibrillation studies were performed using the method mentioned in section 2.2.2 of chapter 2 with a slight modification that the reaction was carried out at 40 ℃. The fibrillation of Lyz was measured in the mixture of ILs as shown in Fig. 4.1. and also, in the presence of individual ILs at 100 mM concentration. All the experiments were carried out in a 96-well microtiter plate in duplicates. Kinetics were recorded in Jasco FP-8500 spectrofluorometer connected to FMP-825 microplate reader and a Peltier temperature controller. Rate of fibrillation was evaluated using equation 2.2, as mentioned in chapter 2. Apparent fibrillation time (T_{app}) was calculated using equation 2.4. TEM images of fibrils were obtained using the protocol mentioned in section 2.2.5 of chapter 2.

4.2.4. Thermal denaturation and structural studies

Thermal denaturation of Lyz was performed in the absence and presence of individual and mixtures of ILs in the ratios mentioned in Table 4.1. The methodology followed was same as described in section 2.2.4 in chapter 2. Structural changes in Lyz were monitored using absorbance, circular dichroism and fluorescence spectroscopy as explained in section 2.2.3 of chapter 2. Changes in absorbance, ellipticities at 273 and 294 nm, and intrinsic fluorescence at 340 nm having excited the protein at 280 nm were monitored to study the protein conformational changes in the ILs.

4.2.6. Molecular dynamic simulations

GROMACS package 5.1.4. with OPLS AA/L forcefield and TIP3P water model were used to carry out all the simulations at 300 K. The crystal structure of lysozyme (Lyz) (PDB ID: 5K2P) was obtained from the Protein Data Bank (www.rcsb.org). Co-crystallized ligands and water molecules were removed prior to the simulations in the absence and the presence of 100 mM of individual or an equimolar ratio of mixed ILs. Ionic liquids parameters were obtained from LigParGen, OPLS/CM1A Parameter Generator for organic ligands (http://zarbi.chem.yale.edu/ligpargen)[139–141]. Lyz molecule was placed in a cubic box extended by 1.3 nm from its surface with a total volume of 448.47 nm^3. Number of water and IL molecules used in the simulations are shown in Table 4.2. Number of water and IL molecules in the mixed ILs simulations are shown in Table 4.3. All the simulation systems were energy minimised using 10,000 steps of steepest descent algorithm. Pressure and temperature were

kept constant at 1 atm and 300 K for 1 ns using same methods described in section 2.2.6 of chapter 2. Production simulations were carried out for 200 ns and the trajectories were collected at every 10 ps interval for further analysis.

Table 4.2. The number of ILs and water molecules in individual ILs simulations

IL	Number of IL molecules	Number of water molecules	Obtained concentration (mM)
MIC	24	13544	98.27
BMIC	24	13433	99.08
HMIC	24	13383	99.45
BPyroBr	24	13436	99.06

Table 4.3. Details of the number of ILs and water molecules in mixed ILs simulations

IL combination	Number of each IL molecules	Number of water molecules	Obtained concentration (mM)
MIC + BMIC	24	13452	98.76
MIC + HMIC	24	13544	98.09
MIC + BPyroBr	24	13399	99.15
BMIC + HMIC	24	13424	98.97
BMIC + BPyroBr	24	13424	98.97

4.2.6.a. Analysis

Parameters such as RMSD, RMSF, R_g and SASA were determined to evaluate the fluctuations in the protein backbone in the presence of mixtures of ILs and compared with the structural deviations in the absence and presence of individual ILs. RDFs for heavy atoms of water and ILs were evaluated in all the cases. Number of water molecules and ILs around the protein and each 20 amino acids, hydration fraction, preferential interaction coefficient, transfer free energy and ILs interaction profile with Lyz in all the simulation systems were determined with the same methods mentioned in section 2.2.6 of chapter 2. For these analyses, the last 150 ns of their respective simulation trajectories were used.

4.3 Results

4.3.1. Fibril formation of Lyz in the mixtures of ILs

Lyz fibril formation was initiated by the addition of DTT and incubating the sample at 40 ℃ with ThT. ThT fluorescence at 485 nm was recorded at every two minutes after exciting at 440 nm. After an initial lag period of 20 min, fluorescence intensity was increased with time. Fibrillation was completed in an hour and followed a lag-dependent kinetics as shown in Fig. 4.2. Fibril elongation rate was evaluated using equation 2 mentioned in chapter 2 and calculated to be 0.19 min^{-1}. Further, fibrillation of Lyz was carried out in the presence of different ratios of IL mixtures. Fig. 4.3 shows the normalized ThT fluorescence profiles of the measured kinetic traces.

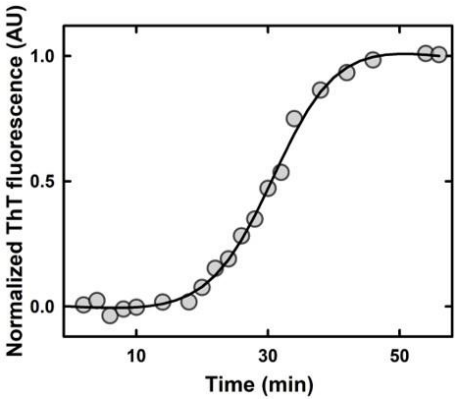

Fig. 4.2 ThT fluorescence at 485 nm after exciting the molecule at 440 nm in the presence of DTT-reduced lysozyme at 40℃.

The lag time and rate of elongation were calculated from the kinetic profiles using equation 2.3 and apparent fibrillation time was calculated using equation 2.4. Calculated parameters were compared with the rate, lag time and apparent time obtained in the presence of 100 mM of

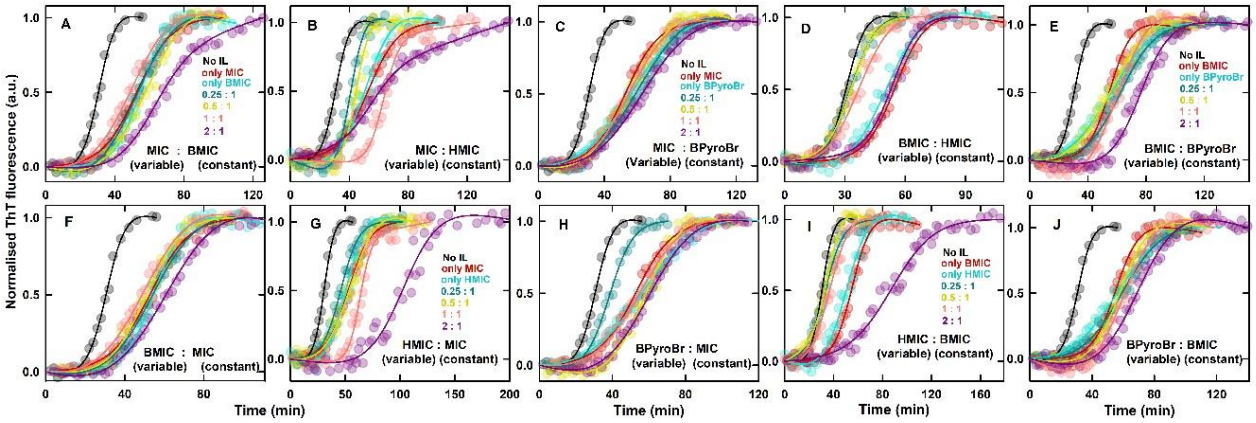

Fig. 4.3 Kinetics of Lyz fibrillation followed by the change in ThT fluorescence in the presence of combinations of MIC+BMIC (A & F), MIC+HMIC (B & G) and MIC+BPyroBr (C & H), BMIC+HMIC (D & I) and HMIC+BPyroBr (E & J). In the legends, 'constant' represents the concentration of corresponding IL as 100 mM whereas 'variable' represents different concentrations according to the molar ratios presented in each panel. The solid lines represent the data-fit using equation 2.2. given in chapter 2.

corresponding individual ILs used in the combinatorial study. It was noted that in the presence of all the combinations of ILs, fibril formation followed the lag-dependent kinetics.

4.3.1.a. Combinations of MIC

Elongation rate was reduced in the presence of all the combinations except in the presence of MIC+ HMIC added in the ratio 0.5:1. Interestingly, the rate was highly reduced in the presence of combination having IL with shorter alkyl chain whether having an aromatic ring (Fig. 4.4 A and D) or alicyclic ring (Fig. 4.4 C and F), except in the presence of 0.25:1 mixture of BPyroBr+MIC which showed only marginal reduction in the fibrillation rate (Fig. 4.4 F). On the other hand, MIC and HMIC combination showed a different pattern of rates. When MIC's concentration was increased (Fig. 4.4 B), the rate was marginally affected up to 1:1 ratio of both ILs and at higher concentrations of HMIC, the rate was drastically reduced. It was observed that in 0.5:1 ratio of MIC+HMIC (Fig 4.4 B) the fibril formation of Lyz was faster than its fibrillation in buffer alone. When MIC concentration was kept constant at 100 mM, with the increasing concentration of HMIC (Fig 4.4 E) the fibrillation rate was gradually

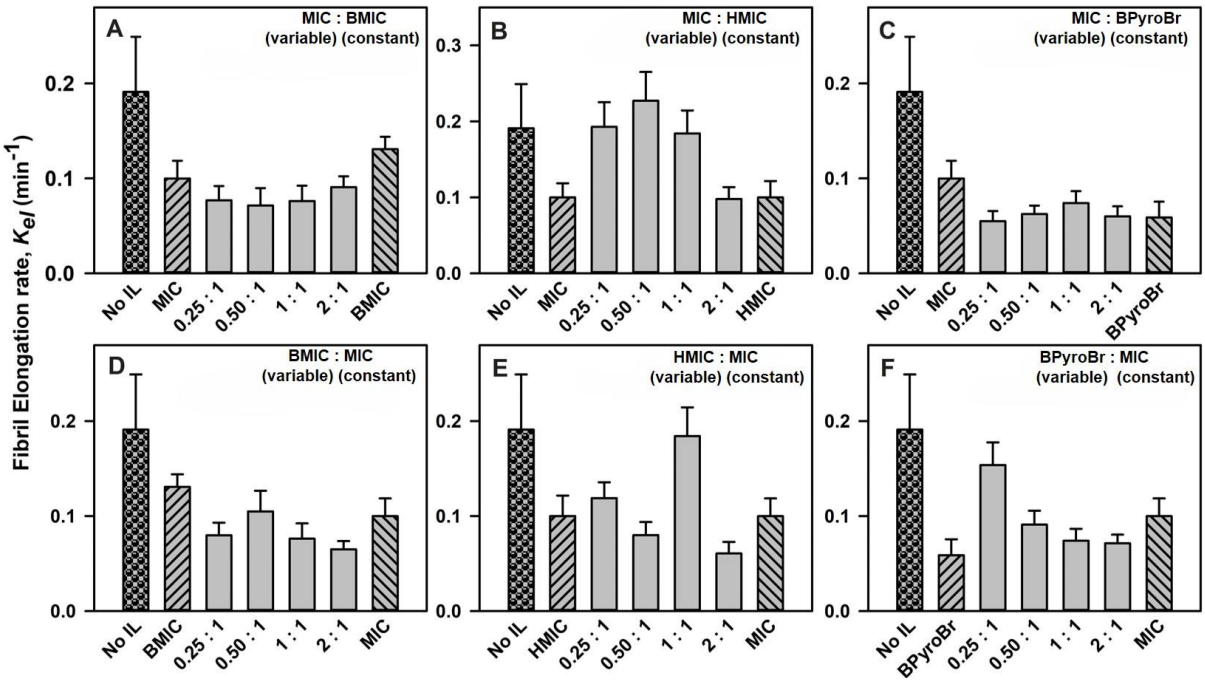

Fig. 4.4. Fibril elongation rates in the presence of MIC in different combinations with BMIC, HMIC and BPyroBr. In the legends, 'constant' represents the concentration of corresponding IL as 100 mM whereas 'variable' represents the different concentrations according to the molar ratios mentioned in the abscissa.

reduced. Exceptionally, at 1:1 concentration of MIC+ HMIC, the fibrillation rate was comparable with the rate in buffer alone.

Lag time was increased in the presence of all combinations of ILs as compared to Lyz fibril formation in buffer. A marginal increase in lag time was observed in the presence of BMIC and BPyroBr. A biphasic trend in the fibrillation lag time was observed with varying concentration MIC when HMIC was constant at 100 mM (Fig. 4.5 B). Lag time gradually increased with increasing concentration of MIC up to 100 mM which drastically reduced at 200 mM concentration. Lag time monotonously increased with increasing concentration of HMIC as MIC concentration was kept constant at 100 mM (Fig. 4.5. E).

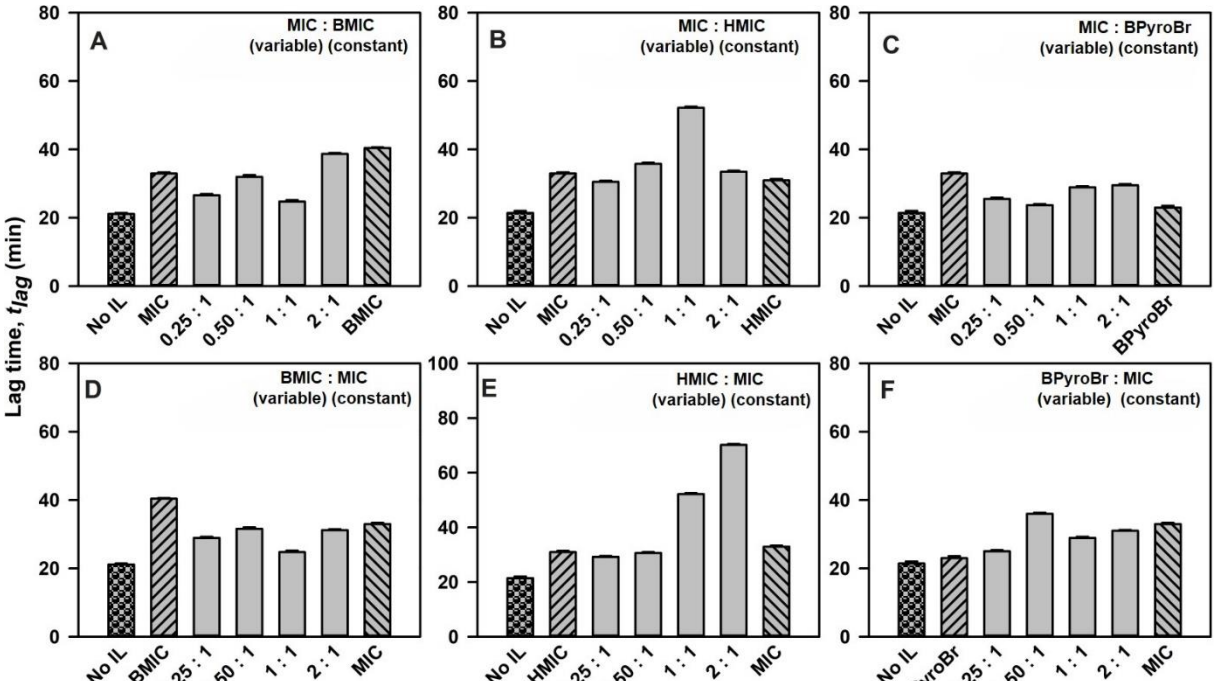

Fig. 4.5. Lag time in the presence of mixtures of MIC with (A & D) BMIC, (B & E) HMIC and (C & F) BPyroBr in varying molar ratios.

Since fibrillation rate and lag time were not related linearly with increasing concentration of ILs, interpreting the effect of mixtures of ILs on the fibrillation of Lyz only based on elongation rate or lag time might be inconclusive. Hence, apparent fibrillation time was calculated. Fig. 4.6 shows the apparent fibrillation time in the presence of combinations of MIC. Apparent fibrillation time (T_{app}) increased with the addition of all the ILs mixtures. Fibrillation was delayed maximum in the presence of HMIC+MIC combination in the ratio 2:1

with apparent fibrillation time of more than two hours. In all other cases, apparent fibrillation time was observed to be slightly more than an hour.

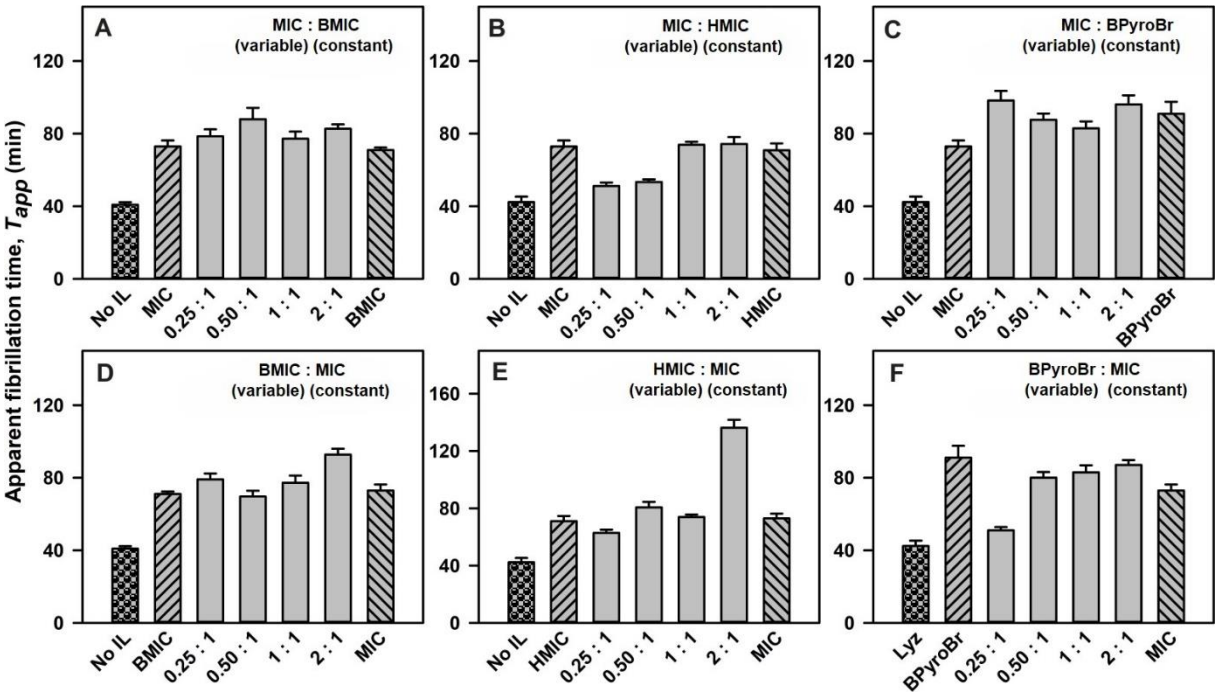

Fig. 4.6. Apparent fibrillation time in the presence of mixtures of MIC with (A & D) BMIC, (B & E) HMIC and (C & F) BPyroBr in varying molar ratios.

4.3.1.b. Combinations of BMIC

Fibrillation rate was reduced in the presence of all the combinations of BMIC (Fig 4.7). When HMIC was kept constant at 100 mM, the rate was marginally decreased with no specific trend as the concentration of BMIC increased (Fig. 4.7 A), but when BMIC concentration was kept at 100 mM, and HMIC was increased there was a monotonous decrease in fibril elongation rates (Fig 4.7 C). When BMIC was mixed with BPyroBr, it showed a drastic reduction in fibrillation rate with only slight differences in fibrillation rates at all the ratio of ILs (Fig. 4.7 B & D). Lag time was marginally decreased in the combinations of BMIC with HMIC except at 2:1 ratio of both ILs which showed longer lag time as compared to the lag time in the absence of any ILs. In the presence of BMIC with BPyroBr mixtures, lag time was more than the time taken only in the buffer (Fig. 4.8). Further, apparent fibrillation time revealed that mixtures of ILs having HMIC were only marginally delaying the fibrillation time except when HMIC+BMIC molar ratio was 2:1(Fig. 4.9 A & C). But, combinations of BMIC with BPyroBr were able to retard the fibrillation process consistently in all the molar ratios as shown in Fig 4.9 B and D.

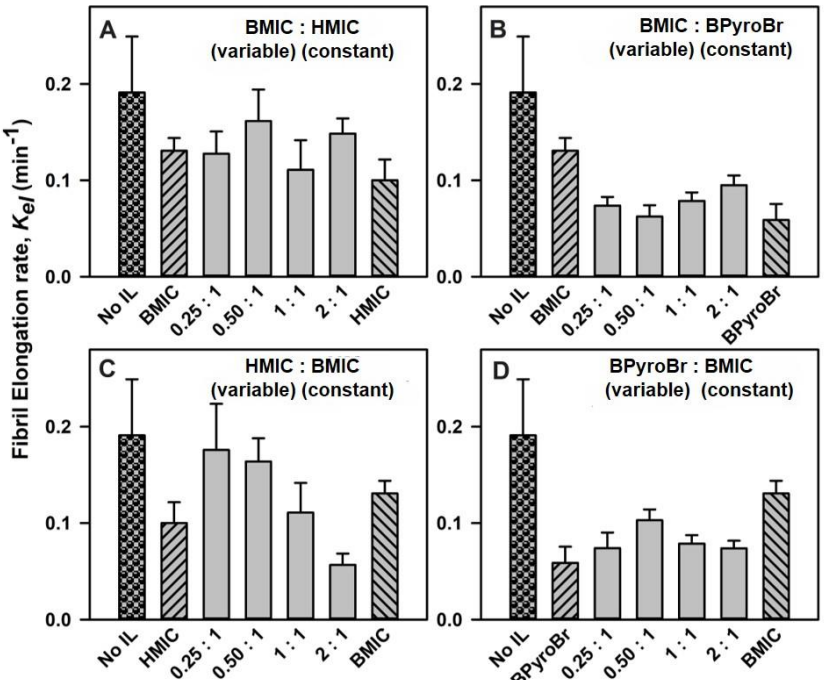

Fig. 4.7. Fibril elongation rates in the presence of BMIC in different combinations with HMIC and BPyroBr. In the legends, 'constant' represents the concentration of corresponding IL as 100 mM whereas 'variable' represents the different concentrations according to the molar ratios mentioned in the abscissa.

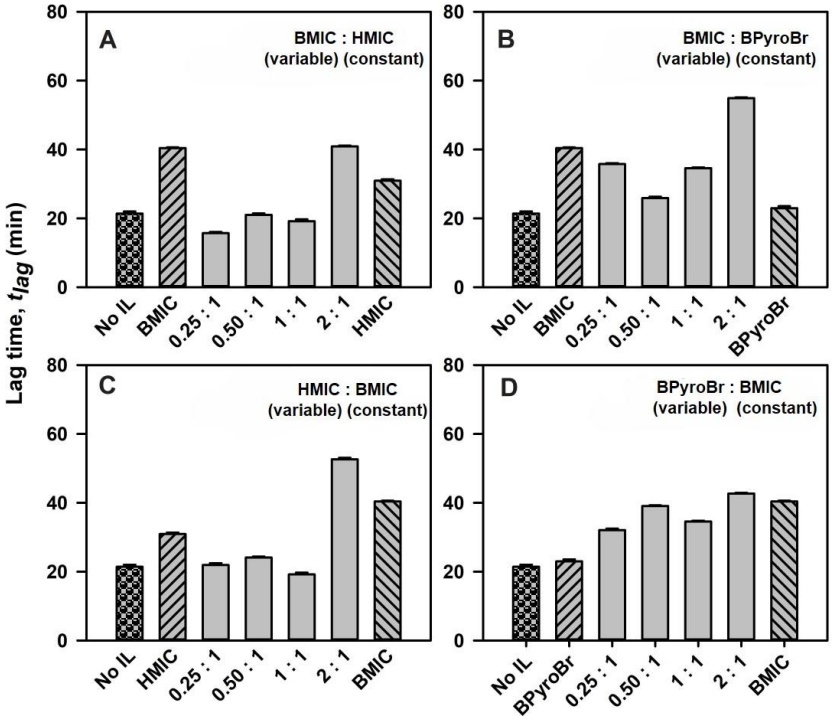

Fig. 4.8. Lag time in the presence of mixtures of BMIC with (A & C) HMIC and (C & D) BPyroBr in varying molar ratios.

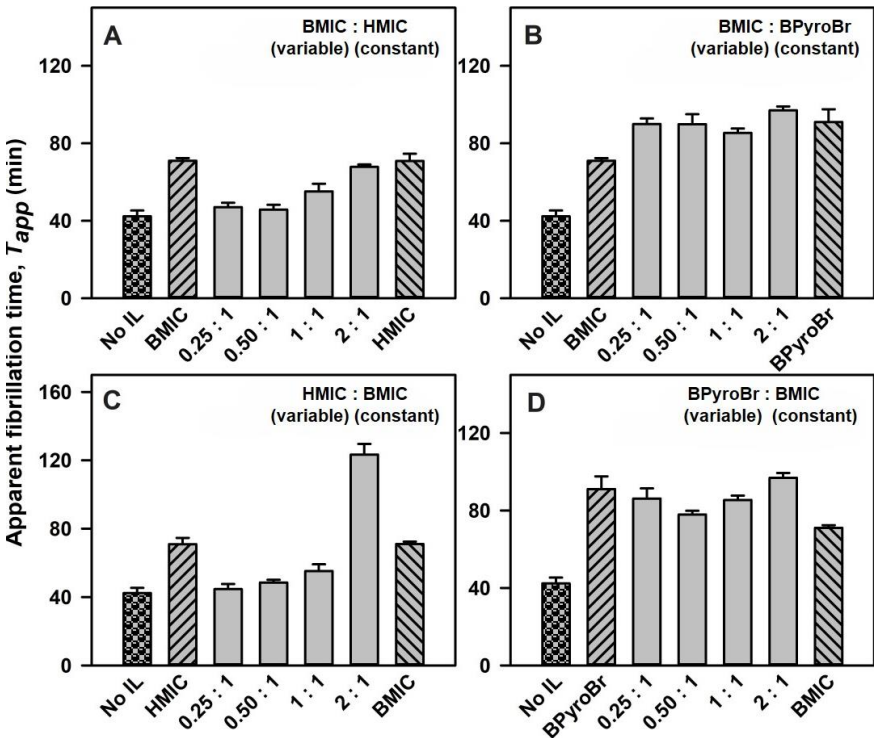

Fig. 4.9. Apparent fibrillation time in the presence of mixtures of BMIC with (A & C) HMIC and (C & D) BPyroBr in varying molar ratios.

The Fibril samples were imaged using transmission electron microscope. Representative fibril images, in the presence of equimolar concentration of MIC+ BMIC, BMIC +HMIC, and BMIC+ BPyroBr, are shown Fig 4.10. In all the cases, a long, unbranched and flexible morphology was obtained in fibrils. Different morphology of fibrils was observed in the presence of BMIC+BPyroBr. Several long fibrils were aligned in parallel and close to each other providing a sheet-like appearance.

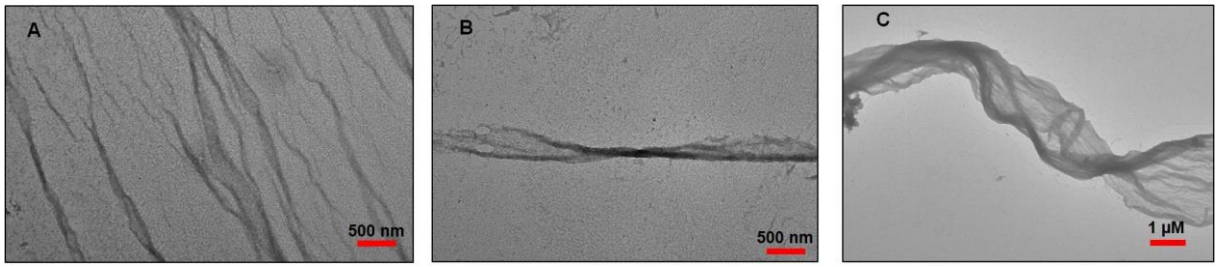

Fig. 4.10. TEM images of the fibrils formed in the presence of 1:1 molar concentration of (A) MIC+BMIC, (B) BMIC+HMIC, and (C) BMIC+BPyroBr.

4.3.2. Thermal stability of Lyz in the presence of IL mixtures

The stability of Lyz against temperature was monitored by the change in absorbance at 301 nm with every 1℃ raise per minute. An increase or decrease in the melting temperature (T_m) of a protein in the presence of cosolvent compared to its melting tempearture in buffer would indicate the stabilization or destabilization induced by the cosolvent, respectively. Unfolding of a protein without any detectable intermediate state shows a sigmoidal thermal denaturation curve also known as two-state transition. In other cases, a double- sigmoidal (or higher order) transition phase might be observed signifying the formation of an intermediate conformation during the unfolding. Such mechanisms of unfolding are termed as three-state (or higher-order states) transitions.

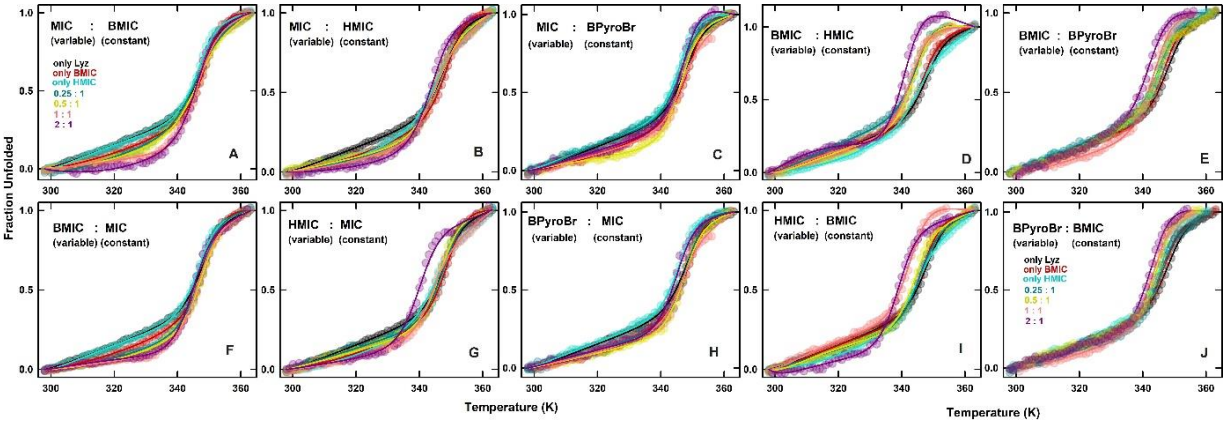

Fig. 4.11 Thermal denaturation of Lyz in the presence of combinations of MIC+BMIC (A & F), MIC+HMIC (B & G) and MIC+BPyroBr (C & H), BMIC+HMIC (D & I) and HMIC+BPyroBr (E & J). In the legends, 'constant' represents the concentration of corresponding IL as 100 mM whereas 'variable' represents different concentrations according to the molar ratios presented in each panel. The solid lines represent the data-fit using equation 5 (section 2.2.4) given in chapter 2.

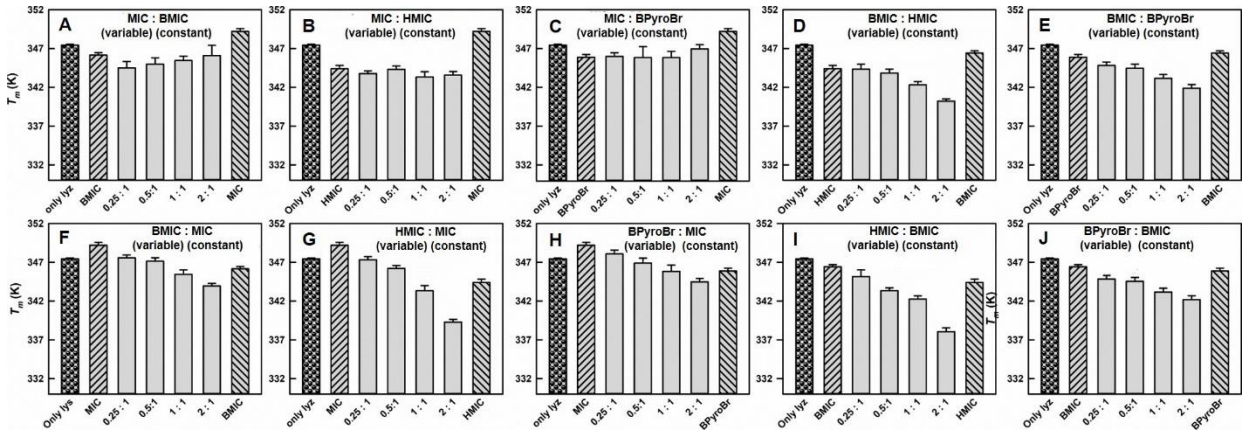

Fig. 4.12. Thermal transition mid points (T_m) in the presence of combinations of MIC+BMIC (A & F), MIC+HMIC (B & G) and MIC+BPyroBr (C & H), BMIC+HMIC (D & I) and HMIC+BPyroBr (E & J). In the legends, 'constant' represents the concentration of corresponding IL as 100 mM whereas 'variable' represents the different concentrations according to the molar ratios mentioned in the abscissa.

Unfolding of Lyz in the presence of all IL mixtures was found to be two state-transitions as shown in Fig. 4.11. All the thermal transitions were fitted to equation 2.5 described in chapter 2, and transition midpoints (T_m) and enthalpy of unfolding (ΔH_m) were evaluated. T_m values of Lyz in the presence of varying concentrations of MIC with 100 mM of BMIC, HMIC and BPyroBr (Fig. 4.12 A-C) showed only marginal destabilization. While in all other cases, T_m values were reduced with increasing concentration of ILs showing significant destabilization of Lyz. The highest destabilization was observed in the presence of 2:1 molar ratio of the mixed ILs. Enthalpy of unfolding (ΔH_m) evaluted for all the thermal transitions are shown in Fig. 4.13.

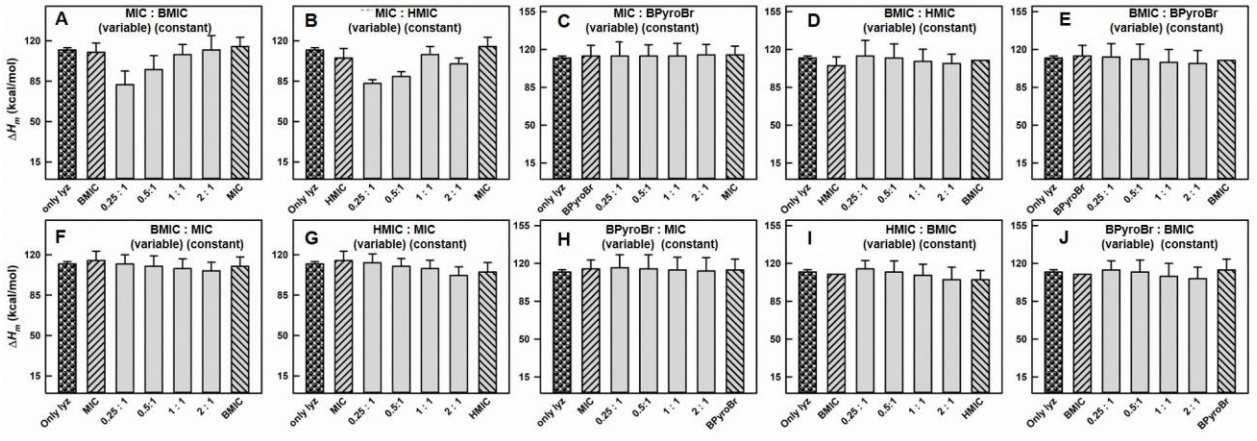

Fig. 4.13. Enthalpy of unfolding (ΔH_m) in the presence of MIC+BMIC (A & F), MIC+HMIC (B & G) and MIC+BPyroBr (C & H), BMIC+HMIC (D & I) and HMIC+BPyroBr (E & J) in varying molar ratios.

ΔH_m values were marginally altered in the presence of all the combinations of ILs. ΔH_m value was significantly reduced when the mixture of MIC and BMIC were added in the ratio of 0.25:1. With further increasing concentration of MIC (BMIC was 100 mM), ΔH_m value was increased and at the highest concentration of MIC, ΔH_m was equal to Lyz in buffer or any of the corresponding individual ILs at 100 mM concentration. Biphasic trend was observed in the presence of combination of varying concentrations of MIC with 100 mM of HMIC. ΔH_m value was reduced at lowest concentration of MIC and increased with increasing concentration of MIC upto the 1:1 ratio of ILs. Further, at higher concentrations of MIC, such that the molar ratio of MIC+ HMIC was 2:1, ΔH_m was again reduced slightly.

4.3.3. Structural studies of Lyz in the presence of IL mixtures

4.3.3.a Absorbance spectra

Lyz spectra were recorded in the presence of mixtures of ILs with varying molar concentrations as shown in Fig 4.14. Only marginal changes were observed in the presence of all the studied IL combinations, except in the presence of the mixture of BMIC and BPyroBr (Fig 4.14 E).

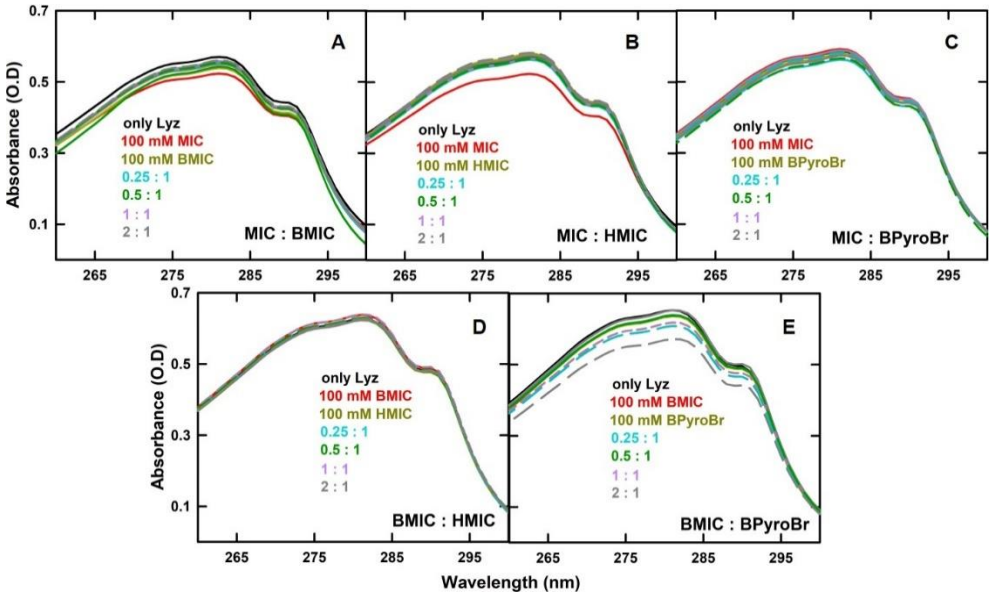

Fig. 4.14. Absorption spectra of Lyz in the presence of varying molar ratio of ILs, (A) MIC+BMIC, (B) MIC+HMIC, (C) MIC+BPyroBr, (D) BMIC+HMIC, and (E) BMIC+BPyroBr. The spectra of Lyz in buffer is shown in black line in each panel.

4.3.3.b Tertiary structural changes by near-UV CD spectra

The tertiary interactions of Lyz in the presence of mixtures of ILs were studied through near-UV CD spectra as shown in Fig. 4.15. Lyz has six Trp residues that have positive peaks in the region of 280-295 nm[199,200]. The protein also has three Tyr residues[201] that show negative peak in the region of 260-280 nm[175]. Thus, changes in ellipticity at different two wavelengths, 273 nm and 294 nm could illustrate the changes in the environment around Tyr and Trp

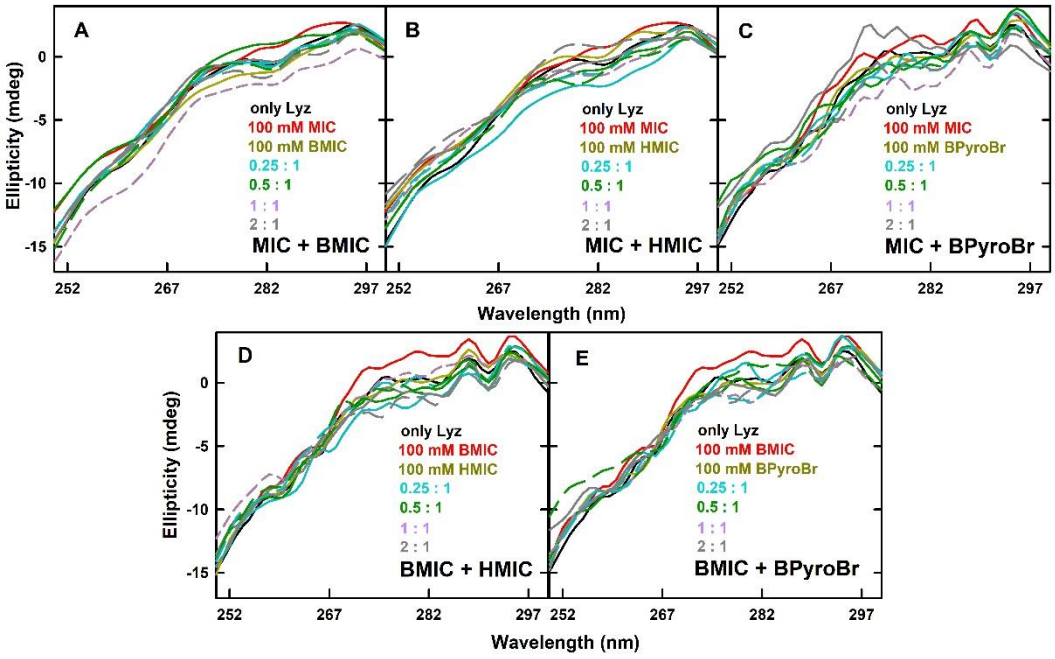

Fig. 4.15. Near-UV CD spectra of Lyz in the presence of varying molar ratio of ILs (A) MIC+BMIC, (B) MIC+HMIC, (C) MIC+BPyroBr, (D) BMIC+HMIC, and (E) BMIC+BPyroBr. The spectra of Lyz in buffer is shown in black line in each panel.

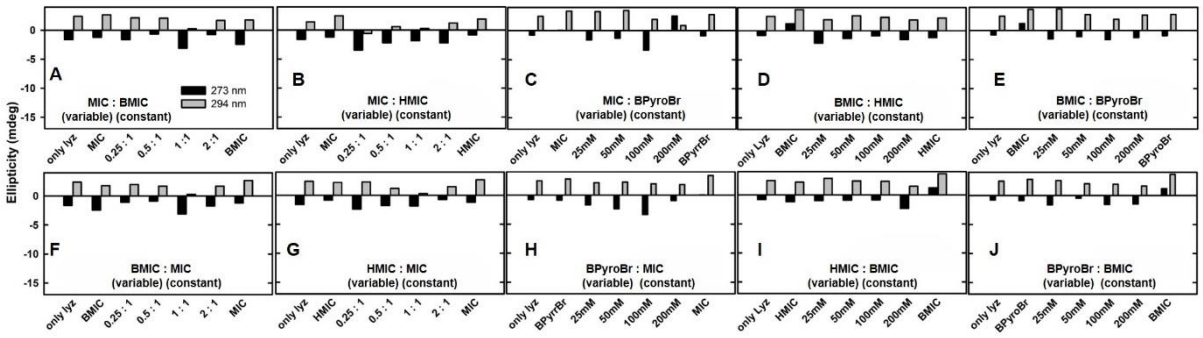

Fig. 4.16. Ellipticity changes in Lyz, at wavelength 273 nm (for Tyr - residues shown in black bars) and 294 nm (for Trp – residues shown in white bars) in the presence of mixtures of MIC with (A & F) BMIC and (B & G) HMIC , (C & H) BPyroBr, and BMIC with (D & I) HMIC and (E & J) BPyroBr in varying molar ratios.

residues, respectively. When the mixtures of ILs were added to Lyz, marginal changes in conformation were observed in all the cases as shown in Fig. 4.16.

4.3.3.c Intrinsic fluorescence changes in Lyz

Intrinsic fluorescence of Lyz was measured in the presence of mixtures of ILs in varying molar ratios by exciting the protein at 280 nm. Also, the fluorescence spectra in the presence of constituent individual ILs were recorded for comparison. Fluorescence maxima of Lyz was observed at 340 nm with little or no shift in the wavelength of maxima in the presence of ILs. Fluorescence intensity at 340 nm was reduced in the presence of all the combinations of ILs (Fig. 4.17). The highest loss of fluorescence was noted when the mixture had imidazolium-ILs. In the presence of MIC+BPyroBr mixtures, Lyz showed only a marginal reduction in fluorescence (Fig. 4.17 C and H). In case of BMIC+ BPyroBr mixtures the fluorescence intensity reduction was more when the BMIC concentration was more than BPyroBr.

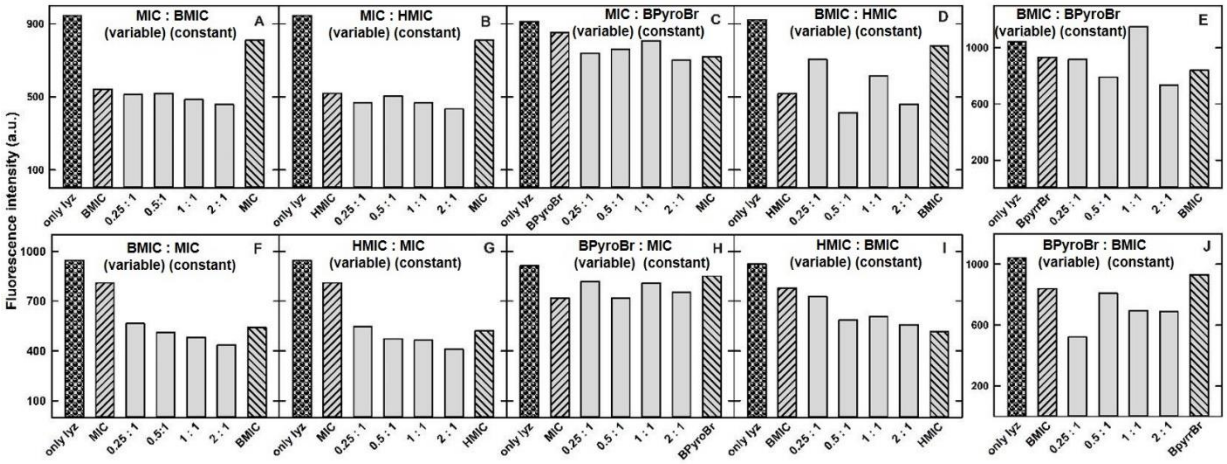

Fig. 4.17. Changes in the fluorescence intensity of Lyz at 340 nm having been excited at 280 nm in the presence of MIC+BMIC (A & F), MIC+HMIC (B & G), MIC+BPyroBr (C & H), BMIC+HMIC (D & I) and HMIC+BPyroBr (E & J) in varying molar ratios.

4.3.4. Molecular dynamic simulation (MD) studies

In order to identify molecular-level interactions between the mixed ILs and the protein, MD simulation of the protein was carried out in the presence of all five different combinations of ILs, MIC+BMIC, MIC+HMIC, MIC+BPyroBr, BMIC+HMIC and BMIC+BPyroBr in the molar ratio of 1:1. The MD simulations were performed in the presence of 100 mM of indiviaul

ILs as well for comparison. All the simulations were run for 200 ns and the trajectories were analyzed to understand the global structural changes and the reside-wise interactions.

4.3.4.a Global analysis

Root mean square deviation (RMSD) of Cα-atoms of all the residues in Lyz was evaluated in the absence and presence of individual and mixed ILs (Fig. 4.18 A1 & A2). There were no significant structural changes observed with the addition of ILs whether individually or in combinations. The average RMSD value for Lyz in water was found to be 0.121±0.03 nm. With the addition of individual ILs, RMSD values were slightly increased in all the cases such that 0.138±0.02 nm in BPyroBr to 0.166±0.02 nm in BMIC. When ILs were added in combination, the average values of RMSD were close to that of Lyz in water such that 0.137±0.02 nm in MIC+BMIC, 0.165±0.02 nm MIC+HMIC, 0.129±0.01 nm in MIC+BPyroBr, 0.158 ±0.01 nm in BMIC+BPyroBr and 0.109±0.02 nm in BMIC+HMIC.

Root mean square fluctuations (RMSF) calculated for individual residues (Fig 4.18 B1 & B2) showed more fluctuations in the regions covering the residues 44-50, 65-76 and 99-105, and moderate fluctuations in the regions from 14-23 and 105-118 of Lyz. Radius of gyration (Rg) and solvent accessible surface area (SASA) were also evaluated and their values showed only marginal differences as compared to Rg and SASA of Lyz in water.

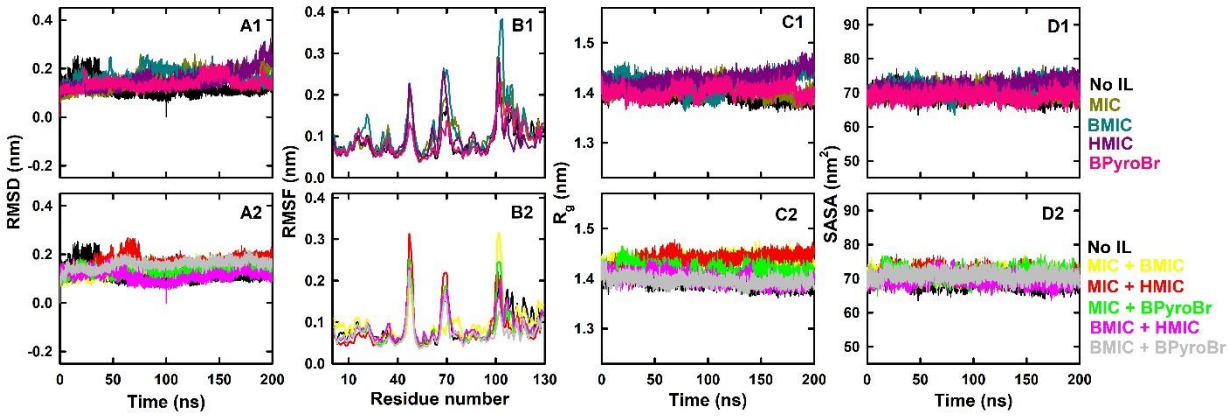

Fig. 4.18 The changes in (A1 & A2) RMSD, (B1 & B2) RMSF, (C1 & C2) R_g, and (D1 & D2) SASA of Lyz in the absence and presence of individual ILs (upper panels) and mixtures of ILs (lower panels). Colors in each panel corresponding to the presence of cosolvents is indicated in the legend.

4.3.4.b Radial distribution function (RDF)

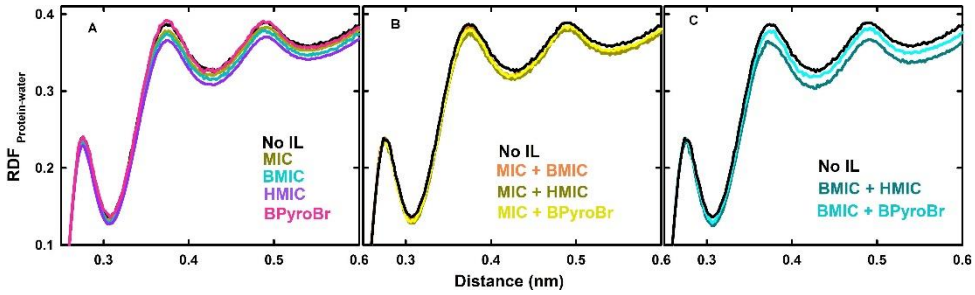

Fig. 4.19 Radial distribution function of water around Lyz in the absence (black) and presence of (A) individual ILs, (B) combinations of MIC and (C) combinations of BMIC.

RDFs of water around the protein are shown in Fig. 4.19. RDF values were reduced with the addition of individual as well as mixtures of ILs. The reduction was observed to be only marginal in the first hydration shell in all the cases whereas significant reduction was noted in the second and third hydration shells. The maximum reduction in the distribution of water molecules around Lyz was observed when the mixture of BMIC and HMIC were added to the protein (Fig. 4.19 C).

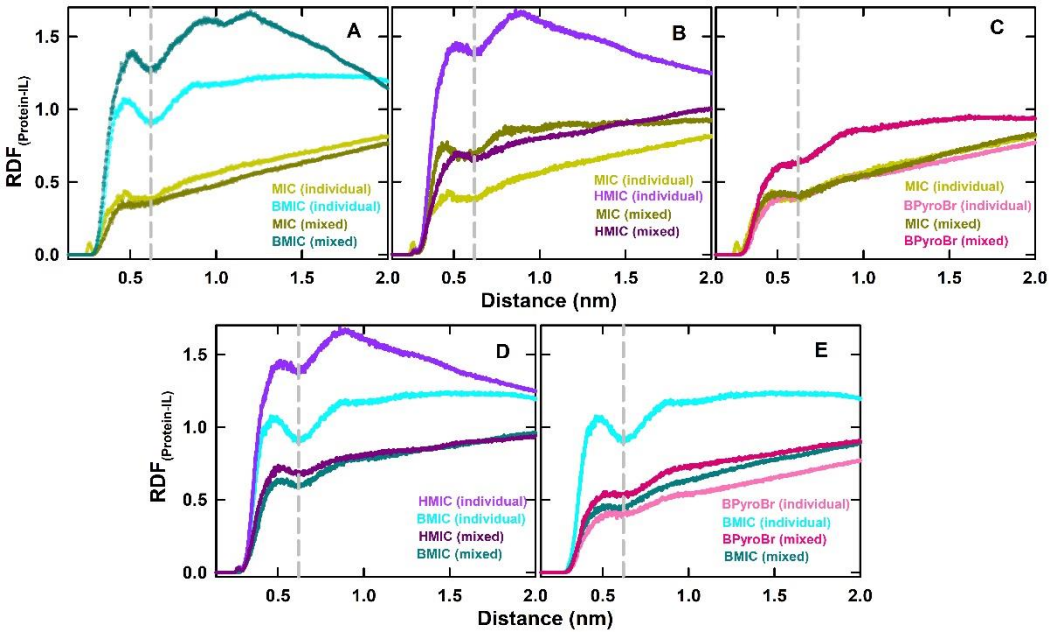

Fig. 4.20 RDFs of ILs around Lyz in the combinations of MIC with (A) BMIC, (B) HMIC and (C) BPyroBr and BMIC with (D) HMIC and (E) BPyroBr. The colors in the panels are explained in the legend such that individual and mixed labels represent, the RDFs calculated from the simulation trajectories of that IL alone and of that IL in the mixed system, respectively

RDFs of ILs around the protein were also evaluated (Fig. 4.20). It was observed that RDF values of the mixtures of Im-ILs are significantly higher than the mixtures containing BPyroBr. In case of MIC+BMIC (Fig. 4.20 A), RDF of BMIC in the mixed simulation was maximum as compared to that in its individual simulation and more than MIC in the mixed as well as individual simulations. RDF of MIC and HMIC was increased and reduced respectively, as compared to their RDFs in individual simulations. However, the distribution of both ILs was similar in the mixed simulation as shown in Fig. 4.20 (B). When BMIC and HMIC were added together to Lyz, the distribution of both ILs was observed to be similar and lower than their individual presence (Fig 4.20 D). In the combinations of ILs having BPyroBr, the distribution was more than MIC in the same simulation system (Fig 4.20 C) and almost similar to BMIC (Fig. 4.20 E).

4.3.4.c Number of water and IL molecules around the protein

The average number of water and IL molecules at three different distance cut-offs from the surface of Lyz were calculated in the presence of individuals and combinations of ILs (Fig. 4.21). Among all the four ILs, the number of water molecules around the protein were reduced to the maximum extend by HMIC. In the combinations of ILs, MIC+HMIC showed larger reduction of water around the Lyz followed by MIC+HMIC. Combinations of BMIC showed

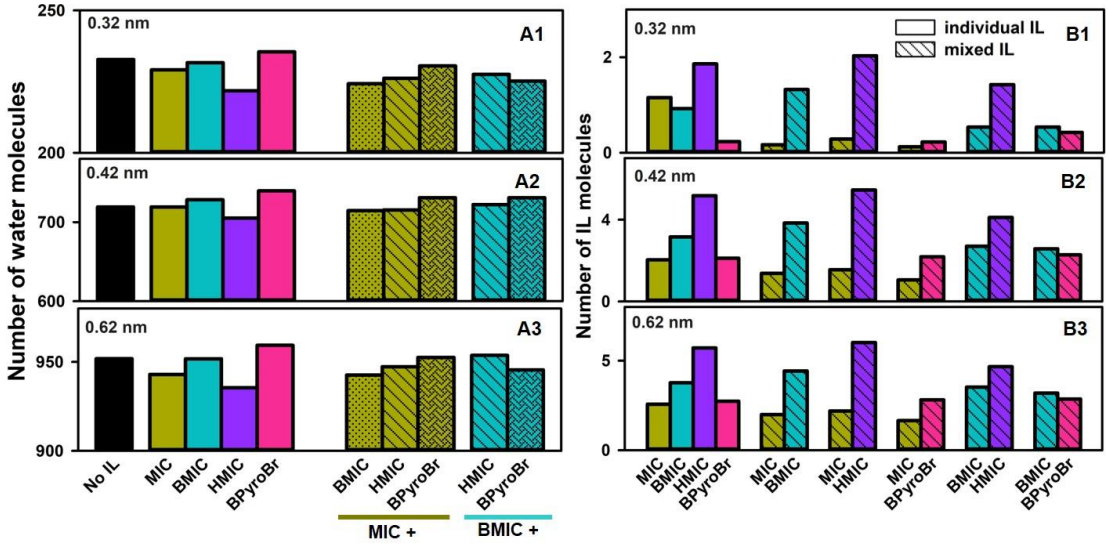

Fig. 4.21 Average number of water molecules (A1-A3) and IL molecules (B1-B3) at the distance cut-off of 0.32 nm, 0.42 nm and 0.62 nm from the surface of the protein. The solid-colored and shaded bars indicate the number of molecules from individual IL and mixed IL simulations. respectively.

only marginal differences in the number of water molecules at all cut-offs. Interestingly, upon evaluation of the number of IL molecules around the protein, it was found that the number of HMIC molecules were always higher whether in individual or mixed IL simulations. Following this, the number of BMIC was more around the protein in the mixed IL simulations with either MIC or BPyroBr. In all the mixed combinations, the number of MIC around the protein remained less. Overall, among all the mixed ILs, HMIC tends to stay more in the vicinity of the protein followed by BMIC and BPyroBr, and MIC had the least occurrence in all the cases.

4.3.4.d Average number of water and IL molecules around each residue

To have a deeper insight into the interactions of each IL with Lyz in a mixed IL simulation system, the number of water and ILs around each amino acid residue was analyzed. The number of water and ILs were calculated for three distance cut-offs, 0.32 nm, 0.42 nm and 0.62 nm from the surface of the protein. Here, the evaluated numbers for only two cut-offs, 0.42 nm and 0.62 nm, are shown. The number of ILs were either very less or negligible at the distance cut-off 0.32 nm, and thus were inconclusive to understand any interactions. The results are discussed below under the head of each combination studied.

(i) MIC+BMIC

The number of water molecules around each amino acid were marginally reduced when MIC or BMIC was individually added into the system. However, in the mixed IL systems, a significant reduction of water was found around hydrophilic amino acids, particularly His and Glu. (Fig. 4.22 A1 & A2). This was complemented with presence of more BMIC molecules around these amino acids Fig 4.22 (B1 & B2). The number of BMIC molecules were always more than MIC in the mixed IL system at both the distance cut-offs.

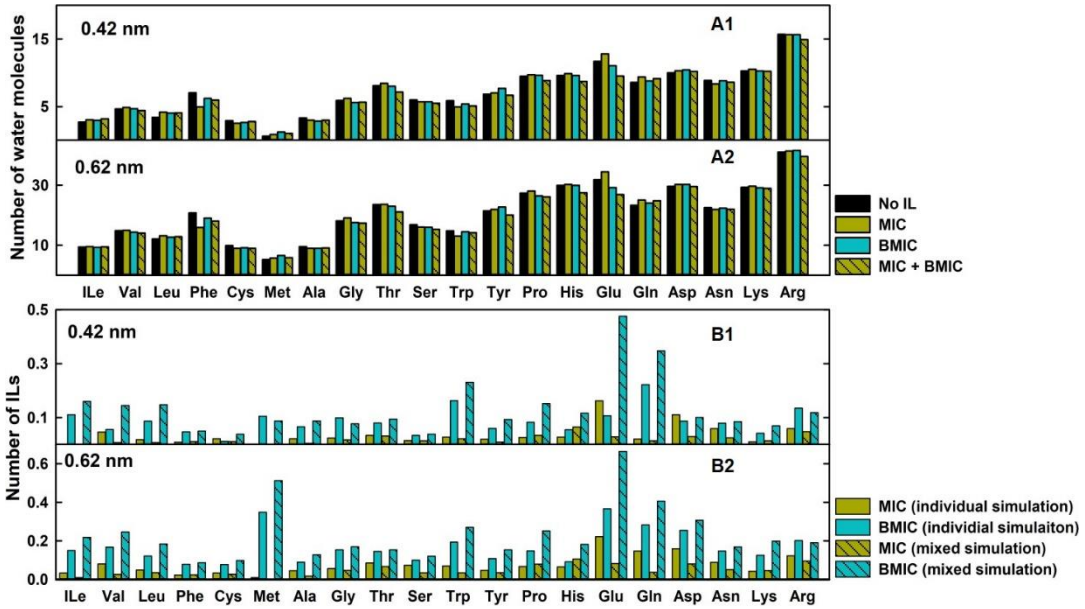

Fig. 4.22 Average number of water molecules around each residue of Lyz in the absence (black bars) and presence of individual ILs (solid-color bars) and mixed ILs (shaded bars) within cut-off of (A1) 0.42 nm & (A2) 0.62 nm from the protein's surface. Average number of ILs around each residue at a distance cut-off (B1) 0.42 nm & (B2) 0.62 nm.

(ii) MIC+HMIC

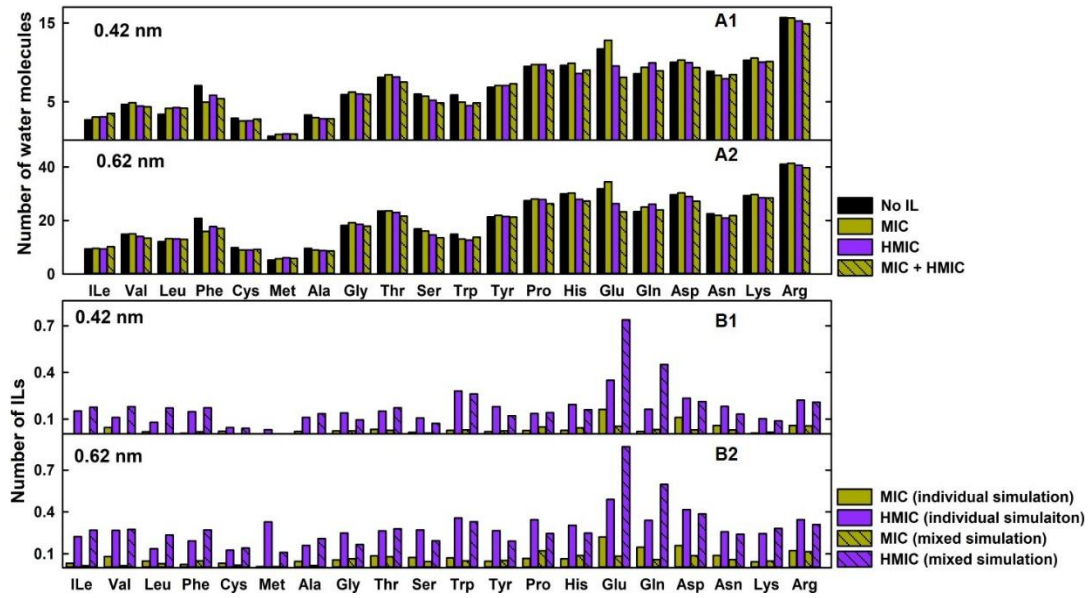

Fig. 4.23 Average number of water molecules around each residue of Lyz in the absence (black bars) and presence of individual ILs (solid-color bars) and mixed ILs (shaded bars) within cut-off of (A1) 0.42 nm & (A2) 0.62 nm from the protein's surface. Average number of ILs around each residue at a distance cut-off (B1) 0.42 nm & (B2) 0.62 nm.

The number of water molecules were marginally reduced with the addition of ILs around most of the amino acids. A significant reduction in numbers was observed around Val, Phe, Thr, Ser, His, Glu, Asp and Arg as shown in Fig 4.22 A1 and A2. Further, the number of HMIC molecules around the protein was always more than MIC whether present individually or in the mixed IL systems (Fig 4.22 B1 & B2) indicating that ILs with longer alkyl sidechain tend to interact more with the protein.

(iii) MIC+BPyroBr

Similar results for the number of water and ILs were observed in the presence of MIC and BPyroBr as well (Fig. 4.24). There were a greater number of BPyroBr molecules around the protein as compared to MIC in their mixed IL simulation (Fig 4.24 B1 & B2). In the presence of BPyroBr the number of MIC around the protein was significantly reduced compared to its presence in individual simulation, particularly around the residues, Glu, Gln Asp and Arg.

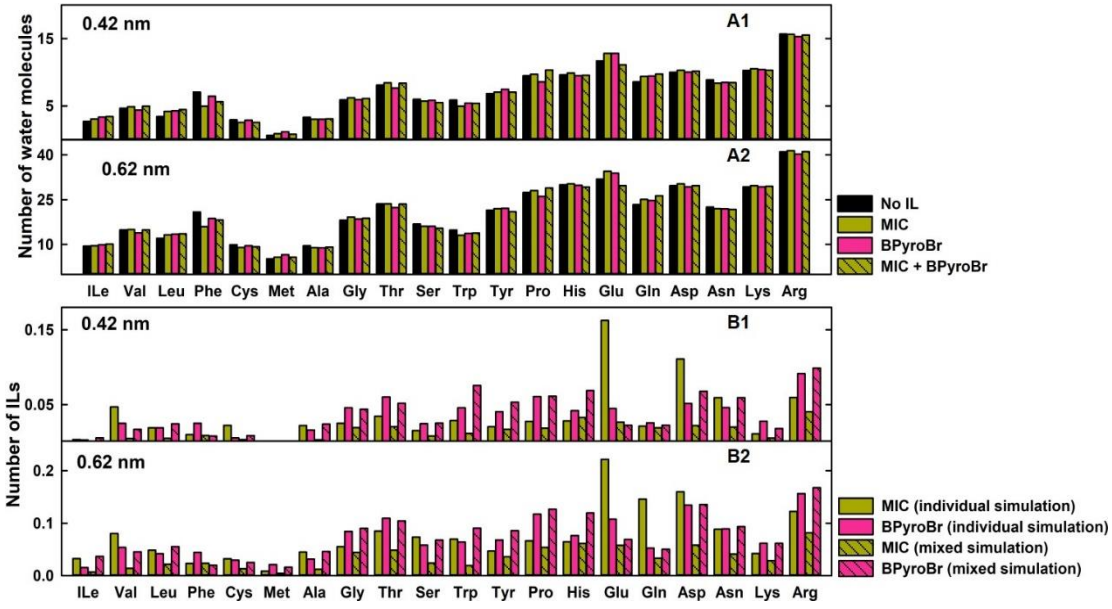

Fig. 4.24 Average number of water molecules around each residue of Lyz in the absence (black bars) and presence of individual ILs (solid-color bars) and mixed ILs (shaded bars) within cut-off of (A1) 0.42 nm & (A2) 0.62 nm from the protein's surface. Average number of ILs around each residue at a distance cut-off (B1) 0.42 nm & (B2) 0.62 nm.

(iv) BMIC+HMIC

As already mentioned in other cases, the number of water molecules around amino acids reduced when BMIC and HMIC were added individually and a pronounced reduction was observed when both ILs were present together (Fig. 4.25 A1 & A2). On the other hand, the number of HMIC around the protein was more than BMIC in the individual simulation systems. Also, when both were present together in the system, the number of HMIC still remained more than BMIC (Fig. 4.25 B1 & B2). These results indicate that both BMIC and HMIC molecules tend to interact competitively with the residues of Lyz to occupy the same sites. In such a scenario, the IL with longer alkyl chain was able to interact more efficiently with the protein.

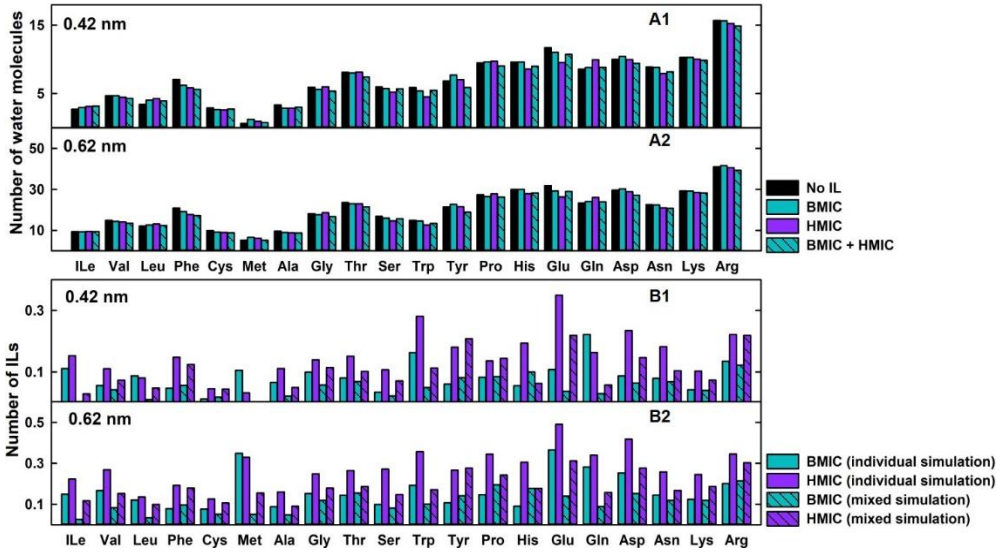

Fig. 4.25 Average number of water molecules around each residue of Lyz in the absence (black bars) and presence of individual ILs (solid-color bars) and mixed ILs (shaded bars) within cut-off of (A1) 0.42 nm & (A2) 0.62 nm from the protein's surface. Average number of ILs around each residue at a distance cut-off (B1) 0.42 nm & (B2) 0.62 nm.

(v) BMIC+BPyroBr

It is understandable so far that longer alkyl chain derivatives of Im-ILs were preferentially interacting with the protein when the other IL in the mixture had a shorter alkyl sidechain. Hence, there raises a question, what happens if the alkyl sidechains of ILs are same, but the ILs differ in their ring moiety? When BMIC (aromatic ring) and BPyroBr (alicyclic ring) were added individually to the protein, the number of BMIC molecules were more as compared to BPyroBr (Fig. 4.26 B1 & B2). In the mixture of BMIC and BPyroBr, the presence both ILs in the vicinity of Lyz was similar in numbers and were less than their numbers in the corresponding individual simulation systems.

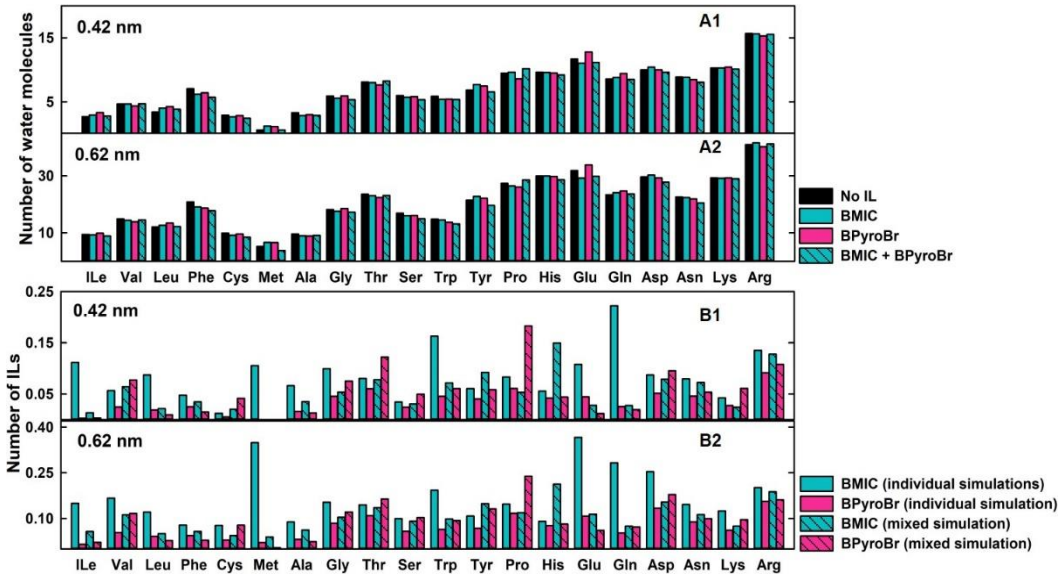

Fig. 4.26 Average number of water molecules around each residue of Lyz in the absence (black bars) and presence of individual ILs (solid-color bars) and mixed ILs (shaded bars) within cut-off of (A1) 0.42 nm & (A2) 0.62 nm from the protein's surface. Average number of ILs around each residue at a distance cut-off (B1) 0.42 nm & (B2) 0.62 nm.

4.3.4.e Solvation properties

Hydration fractions were determined with respect to each IL in the mixed ILs system and compared with their fractions obtained when present individually in the system (Fig. 4.27). For individual IL simulations, the hydration fraction was reduced with increasing alkyl side of Im-ILs, but found to be more in the presence of BPyroBr. The hydration fraction followed the order, MIC ≈ BPyroBr >BMIC > HMIC. In the mixed ILs simulations, it was observed that the hydration fraction in the presence of ILs with longer alkyl chains always remained less than the shorter alkyl chain ILs. For instance, in MIC+BMIC simulation, MIC had more hydration fraction as compared to BMIC. Similarly, in other combinations, MIC+HMIC, BMIC+HMIC and MIC+BPyroBr, the hydration fraction for HMIC and BPyroBr were less, respectively, indicating that ILs with longer alkyl chain tend to replace more water molecules from the vicinity of protein. In BMIC+BPyroBr system, the hydration fraction of BPyroBr was slightly more than that of BMIC suggesting more occupancy of BMIC in the vicinity of protein as compared to BPyroBr.

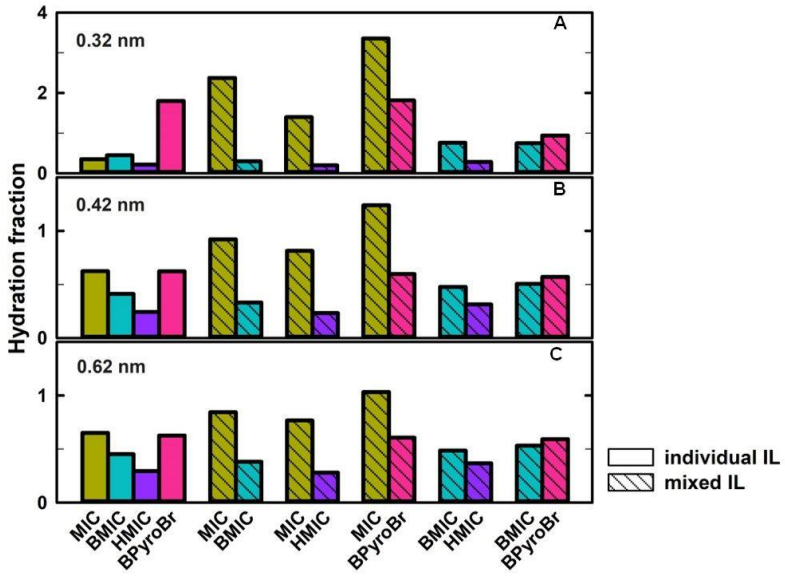

Fig. 4.27 Hydrations fractions calculated at the cut-off of (A) 0.32 nm, (B) 0.42 nm, and (C) 0.62 nm around Lyz in the presence of individual ILs (solid-colored bars) and mixed ILs (shaded bars).

4.3.4.f Preferential interaction coefficient (PIC) and transfer free energy (TFE)

Preferential interaction coefficients were calculated from all the simulations having individual and mixtures of ILs (Fig. 4.28 A1-E1). In all the cases, PIC values were positive indicating that ILs preferentially binding on the surface of the protein. In the combinations of MIC with BMIC, HMIC and BPyroBr (Fig. 4.28A1-C1), the PIC of MIC was reduced in the

mixtures compared to its value when present individually. In the same set of simulations, the PIC of BMIC and HMIC was only marginally altered whereas a significant increase was noted for BPyroBr compared to its values in the individual simulation. In the mixture of BMIC with HMIC (Fig. 4.28D) PIC was reduced for both the ILs. In BMIC+BPyroBr mixture, the PIC value of BMIC was reduced drastically whereas the PIC of BPyroBr increased as compared to their individual presence in the simulation systems. The negative values of transfer free energies (Fig. 4.28A2-E2) for all the ILs individually or in the mixture indicated favorable interaction of the ILs with the protein surface. The energy changes complemented the changes observed in PIC.

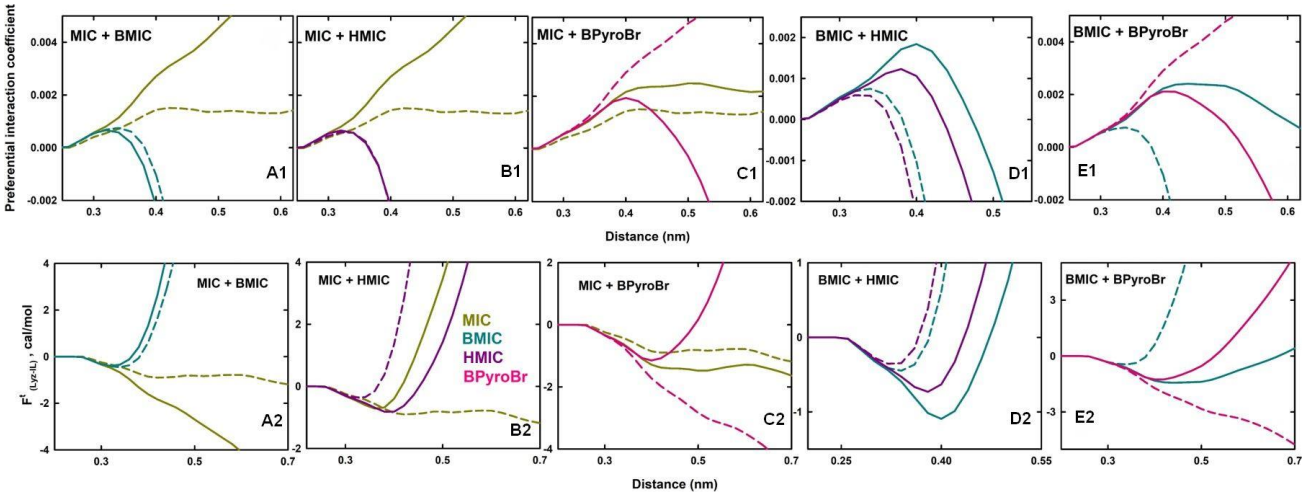

Fig. 4.28 Preferential interaction coefficients calculated using Kirkwood-Buff integral (upper panel) and the transfer free energies (lower panel) calculated for the ILs from the mixture of IL simulations (A1 & A2) MIC+BMIC, (B1 & B2) MIC+HMIC, (C1 & C2) MIC+BPyroBr, (D1 & D2) BMIC+HMIC, and (E1 & E2) BMIC+BPyroBr. The solid lines represent the values calculated from individual IL simulations, whereas the dashed lines represent the values calculated from mixed IL simulations.

4.3.4.g Residue-wise interaction between Lyz and ILs

Further to understand the details about the interaction of ILs with Lyz, the interaction of ILs with individual residues of the protein was analyzed (Fig. 4.29). The color depiction, green, pink and white was used to mark the regions on the protein to represent the more favorable, moderate and less/no interaction of IL on the protein, respectively. MIC showed more regions of binding on Lyz when in combination with BMIC, whereas the binding regions for BMIC in the same simulation system was lesser compared to the systems with their individual presence. It was observed that HMIC had more favourable binding to the protein

when in combination with MIC. As a result, fewer MIC molecules were found on the protein. The interaction profile of MIC and BPyroBr were marginally altered. It was noticed that binding regions and strength of binding of both ILs were almost similar when present in combination as well as individually. Interestingly, when BMIC and HMIC were present together, they compete almost equally with each other for the binding sites on the protein. It is evident from the binding regions on the protein for both ILs which were similar to the regions

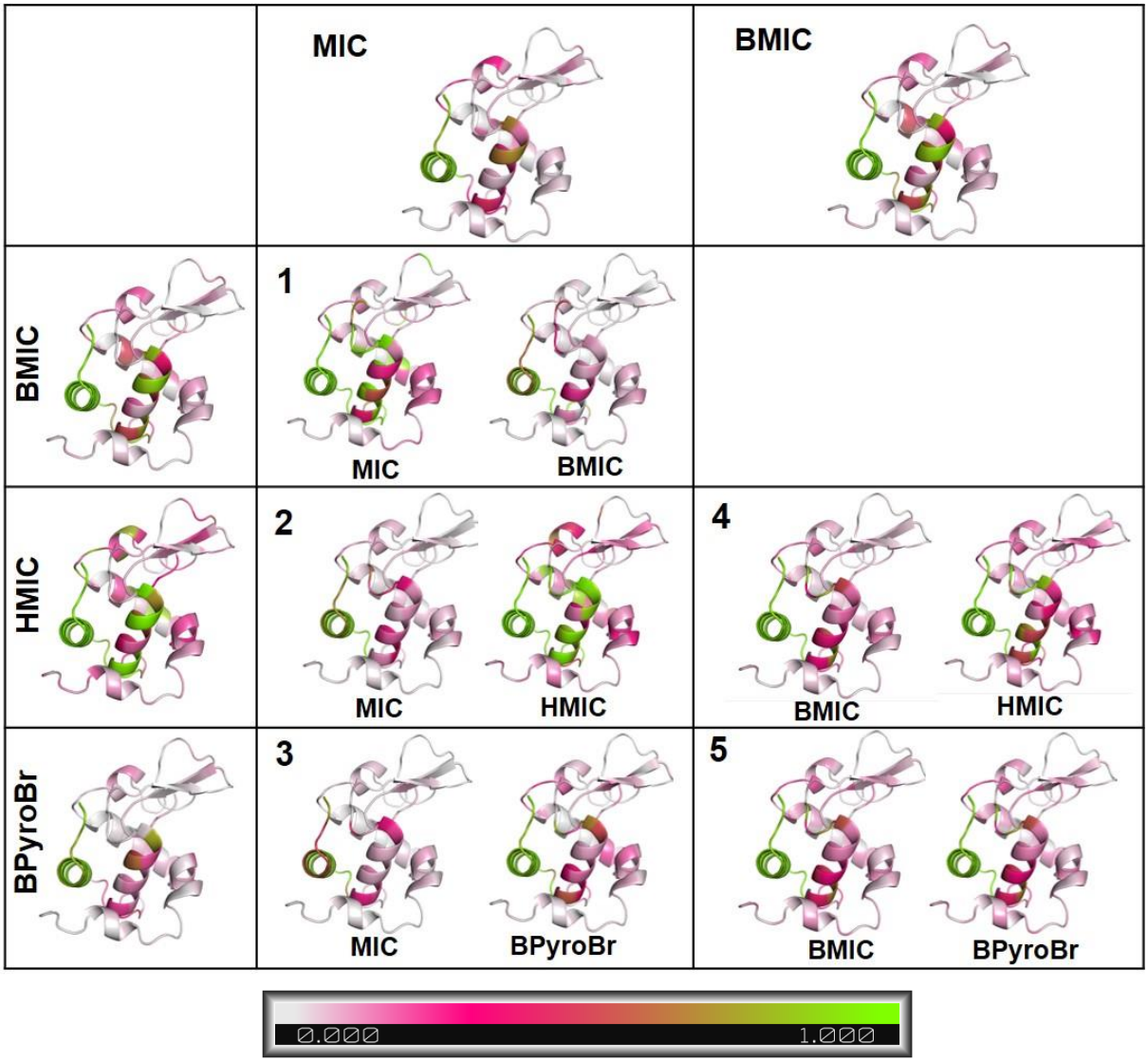

Fig. 4.29 Cartoon diagram depicting the regions of interactions of ILs on Lyz. The interaction regions from individual IL simulations are shown in the top row (for MIC and BMIC) and the first column (for BMIC, HMIC and BPyroBr). Regions of interaction for each IL present in the mixed simulation systems are shown for (1) MIC+BMIC, (2) MIC+HMIC, (3) MIC+BPyroBr, (4) BMIC+HMIC, and (5) BMIC+BPyroBr. The bar shows the color indication used in the cartoons where from white to green represent the non-interactive region to most favorably interacting region.

found when each IL presents individually. The combination of BMIC with BPyroBr also showed similar behaviour.

4.4 Discussion

Effect of mixtures of two cosolvents can be additive[202], non-additive, synergistic[203] or counteracting[190] on the stability of a protein. Similarly, the effects of mixed cosolvents can be evaluated on the fibrillation propensity and the structure of a protein as well. The present study analyzes the combinatorial effect of four different ILs with varying hydrophobic properties on the fibrillation, stability of Lyz. The interaction of mixtures of ILs with the protein was also examined using MD simulation.

4.4.1 Delayed fibrillation time in mixtures of ILs

Fibrillation of Lyz was performed at 40 ℃ in DTT-reduced condition which was completed in an hour by following a nucleation-dependent kinetics (Fig. 4.2). It has been noted that the addition of individual ILs and their mixtures does not alter the fibrillation mechanism (Fig. 4.3). However, the rate of fibrillation is reduced in all cases, except in few combinations having HMIC (Fig. 4.4 & 4.7). Lange et al.[204] commented that Im-ILs behave as refolding agents for partially or fully unfolded proteins while testing the effect of ethyl-, butyl-, hexyl-imidazolium ILs on the unfolded Lyz. Interestingly, all the ILs could refold the fully denatured Lyz and thus preventing aggregation. Another study suggests that more the length of alkyl sidechain, more the refolding activity of IL[205]. It is intriguing that two ILs when added to protein simultaneously whether it suppresses the fibrillation in a more pronounced manner. It is observed that MIC with BMIC slightly increases the overall fibrillation time (Fig. 4.6.) whereas MIC+HMIC delays the fibrillation only when their ratio is 1:2. Similarly, BMIC with HMIC also delays the fibrillation only when the ratio is 1:2. The other combination of ILs either shorten or do not show notable differences in the apparent fibrillation time. These results suggest that only the excessive presence of long alkyl sidechain ILs could delay the fibril formation.

4.4.2 Thermal stability and structural changes in Lyz

Thermal denaturation in the presence of IL mixtures show that except in the excessive presence of MIC in the mixture, all other combinations of IL destabilise the protein. The

destabilization effect is significant as the concentration of BMIC, BPyroBr or HMIC is more in any of the combinations. This has been observed earlier as well by Takekiyo et al.[206] that the structure of Lyz is altered in a concentration-dependent manner and completely distorted at higher concentrations of Im-ILs. Loss of structural integrity of Lyz leads to destabilization which is more pronounced when HMIC is present in the mixture. It is evident from the results that as the alkyl chain length increases, the tendency of IL to interact with the protein also increases, thus destabilization effect is more. This effect persists even when the mixture has another IL with a shorter alkyl chain as the longer alkyl chain of HMIC strongly competes with MIC or BMIC. This also corroborates with the earlier finding from Lange's work[204] which mentions the concept of decreased stability of Lyz with increasing alkyl chain i.e., increased hydrophobicity of IL. The increased hydrophobicity, thus, making the IL more suitable to interact with the hydrophobic core of Lyz.

Structural changes in Lyz were only marginal in all the cases as evident from absorbance and near-UV CD spectra. RMSD, radius of gyration and SASA values obtained from the MD simulation of Lyz in the presence of IL mixtures also show only marginal differences implying that structural changes are quite minimal supporting the results from the spectroscopic experiments. The regions showing residue fluctuations are reduced in the mixture of ILs (Fig. 4.18 B) as compared to the fluctuations in the presence of individual ILs (Fig. 4.18 B1 & B2). This shows that when ILs are present in combination, they tend to occupy more regions on Lyz leaving only a few residues to show fluctuations.

4.4.3 Hydration properties and occupancy of ILs in the vicinity of Lyz

Reduced RDFs of water (Fig. 4.19 A, B & C) and the number of water molecules (Fig. 4.21 A1-A3) with the addition of individual and mixed ILs indicate the preferential occupancy of ILs in the vicinity of Lyz by replacing the water molecules. However, in each combination, the probability of each IL to be found near the protein is different as compared to their individual presence. The distribution of MIC is less which is not altered in the mixture of ILs as well, whereas the distribution of BMIC or HMIC around the protein increased in the mixture of ILs, MIC+BMIC and MIC+HMIC (Fig. 4.20). This is further confirmed by the number of each IL when present individually and in combination (Fig. 4.21). Also, there is a greater reduction of hydration fraction with respect to BMIC as compared the hydration of fraction of MIC in the same mixture (Fig. 4.27).

Similarly, the combinations with largely dissimilar alkyl chain lengths showed a stark differences in their distribution around the protein and associated hydration fraction. In MIC+HMIC and MIC+BPyroBr mixtures, the number of HMIC and BPyroBr are more as compared to MIC, respectively (Fig. 4.21 B1-B3). This strongly favours the argument that more the hydrophobicity of IL, more competitively it would bind to the protein. However, when the length of alkyl chain in the mixture of ILs is comparable or similar, as in BMIC+HMIC and BMIC+BPyroBr combinations, the number of each IL and hydration fraction are similar (Fig. 4.27). This is again well supported by the distribution of ILs around the protein as evident from the RDF plots of ILs from each simulation (Fig. 4.20 D & E). All these results indicate that more the difference in alkyl chain length of ILs in combination (difference in hydrophobicity), more is the difference in their tendency to interact with the protein. Though in a combination of BMIC and BPyroBr, alkyl chain length is same, but they differ in their ring moiety that BMIC is aromatic and BPyroBr is alicyclic. This makes BMIC slightly more hydrophobic as compared to BPyroBr. In this case, the number of water and ILs calculated around each amino acid shows similar results (Fig. 4.22-4.26).

4.4.4 Binding profile of ILs and its impact on fibrillation of Lyz

The regions occupied by ILs individually and in combinations are shown in Fig. 4.29. MIC occupies more regions on Lyz when in combination, while BMIC has a reduced interaction in the same regions. However, BMIC shows favourable binding when present individually. When HMIC is in combination with MIC, the binding profile of HMIC remains unchanged with a slight reduction in the occupancy of MIC on the protein. This indicated that HMIC being more hydrophobic interacts with the protein favourably which is unaffected by the presence of another IL which is less hydrophobic. But the binding regions for both BMIC and HMIC are slightly reduced when added together compared to their individual presence, explaining their competition to bind on the same regions of the protein. Since, both ILs possess high hydrophobicity, they exhibit similar tendency to bind with protein. Combination of MIC with BPyroBr displayed similar binding profile as they are present individually. Both are weekly hydrophobic due to different reasons, MIC without any alkyl side chain and BPyroBr with alicyclic ring system. In case of BMIC and BPyroBr, both ILs possess butyl side chain, but differ in their overall hydrophobicity due to ring moiety. Both ILs make an almost equal competition to occupy the binding sites on Lyz.

All the combinations, show two binding sites in common, *N*-terminal and the cleft formed between α- and β- domain of the protein. As it is already known, the long-range interactions established between hydrophobic cluster 3 (part of β-domain) and cluster 5 (part of α-domain) initiate the fibril formation[45], any cosolvent molecule binding to these regions may interfere with the fibrillation assembly. We could clearly observe from the fibrillation in the presence of MIC-BMIC that the fibrillation rate is reduced by them. Whereas in other cases, the binding may not linearly correlate with the rate of fibrillation. It could be attributed to the fact that the fibrillation is initiated from a partially-unfolded state where the binding of mixture of ILs on the exposed residues of Lyz could be different from their binding on surface-exposed residues in the native state.

4.5 Conclusion

The mixtures of various ILs have been studied to modulate the solvent properties such that protein is stabilized for longer duration. In some cases, the destabilizing effects of IL is counteracted by the addition of other ILs (stabilizer or destabilizer) and proved as excellent stabilizers for the prolonged storage of proteins. But studies on overcoming the fibrillation/aggregation of protein by using mixtures of two or more ionic liquid is still scanty. Here, we have studied the imidazolium ILs in combinations to understand how they affect the fibrillation parameters. As imidazolium ILs are proven inhibitor of fibrillation (earlier chapters) by interacting with Lyz, we are intrigued that the combination of ILs might either inhibit fibrillation in additive or synergistic manner. We found that all the ILs individually or in combination delayed fibrillation. Destabilization of Lyz in the presence of IL combination with more hydrophobicity was observed. It is also noted that ILs with longer alkyl chain reduce more water molecules in the vicinity of the protein. The results suggest that IL with longer alkyl chain competes with lower alkyl chain IL to interact with the protein. Compared to individual effect, longer alkyl chain ILs delays fibril formation more effectively in combination with other ILs.

Overall Summary of the thesis

Folded state of a protein is dictated by various non-covalent interactions such as coulombic, hydrogen bonding and hydrophobic. Disruption of any of these interactions may direct the protein to a misfolded state which might proceed to a deleterious self-aggregation or fibril formation pathway. The effects specifically induced by hydrophobic interactions of different functional groups namely, aliphatic, aromatic and alicyclic, on the stability and fibrillation propensity of a protein were investigated using lysozyme as a model protein and different ionic liquids with varying hydrophobic moieties as cosolvents.

When imidazolium-based ILs with varying alkyl sidechains were added to Lyz, the ILs with the longest alkyl chains, HMIC and OMIC, imparted the highest destabilization to the protein. Also, HMIC and OMIC delayed the fibrillation by 55-fold at higher concentrations and OMIC completely inhibited the fibrillation at 500 mM. The ILs with longer alkyl chains were found to replace more water molecules around Lyz and had stronger interactions with the protein compared to the ILs with shorter alkyl chains.

Compared to the ILs with aromatic moieties, the extent of destability-induced by alicyclic ILs was lesser. However, they could be slightly more effective in slowing down the fibril formation of Lyz. The destabilization effect by all the ILs was enthalpy-driven, except for BPyrdBr which showed entropy-driven destabilization at concentrations above 200 mM. The molecular-level interaction analyses showed that the aromatic-ILs had slightly stronger interactions with the protein compared to alicyclic-ILs.

When the ILs with varying hydrophobicity were added together, the ILs with longer alkyl chains and aromatic rings competed with alicyclic and lower alkyl chain ILs to interact with the protein. The ability of longer alkyl chain ILs to inhibit fibril formation was enhanced in the presence of shorter alkyl chain ILs. Therefore, it is proposed that the mixture of ILs could be more effective in preventing protein fibrillation.

References

1. Dobson, C. M. Principles of protein folding, misfolding and aggregation. *Semin Cell Dev Biol* **15**, 3–16 (2004).

2. Dobson, C. M., Swoboda, B. E. P., Joniau, M. & Weissman, C. The structural basis of protein folding and its links with human disease. *Philos Trans R Soc Lond B Biol Sci* **356**, 133–145 (2001).

3. Anson, M. L. Protein Denaturation and the Properties of Protein Groups. *Adv Protein Chem* **2**, 361–386 (1945).

4. Lumry, R. & Eyring, H. Conformation changes of proteins. *Journal of Physical Chemistry* **58**, 110–120 (1954).

5. Sela, M., White, F. H. & Anfinsen, C. B. Reductive Cleavage of Disulfide Bridges in Ribonuclease. *Science (1979)* **125**, 691–692 (1957).

6. Gutte, B. & Merrifield, R. B. The synthesis of ribonuclease A. *Journal of Biological Chemistry* **246**, 1922–1941 (1971).

7. Anfinsen, C. B. Principles that govern the folding of protein chains. *Science (1979)* **181**, 223–230 (1973).

8. Levinthal, C. Are there pathways for protein folding? *Journal de Chimie Physique* **65**, 44–45 (1968).

9. Dill, K. A. & Chan, H. S. From Levinthal to pathways to funnels. *Nature Structural Biology 1997 4:1* **4**, 10–19 (1997).

10. Wolynes, P. G. Folding funnels and energy landscapes of larger proteins within the capillarity approximation. *Proc Natl Acad Sci U S A* **94**, 6170–6175 (1997).

11. Nelson, D. L. (David L. & Cox, M. M. *Lehninger: principles of biochemistry*. (W. H. Freeman & Co., 2005). doi:10.1002/cbf.1216.

12. Kauzmann, W. Some Factors in the Interpretation of Protein Denaturation. *Adv Protein Chem* **14**, 1–63 (1959).

13. Kauzmann, W. Thermodynamics of unfolding. *Nature 1987 325:6107* **325**, 763–764 (1987).

14. Chandler, D. Interfaces and the driving force of hydrophobic assembly. *Nature 2005 437:7059* **437**, 640–647 (2005).

15. Dinner, A. R., Šalib, A., Smitha, L. J., Dobsona, C. M. & Karplus, M. Understanding protein folding via free-energy surfaces from theory and experiment. *Trends Biochem Sci* **25**, 331–339 (2000).

16. Adamcik, J. & Mezzenga, R. Amyloid Polymorphism in the Protein Folding and Aggregation Energy Landscape. *Angewandte Chemie International Edition* **57**, 8370–8382 (2018).

17. Fändrich, M. & Dobson, C. M. The behaviour of polyamino acids reveals an inverse side chain effect in amyloid structure formation. *EMBO J* **21**, 5682–5690 (2002).

18. Perutz, M. F., Johnson, T., Suzuki, M. & Finch, J. T. Glutamine repeats as polar zippers: their possible role in inherited neurodegenerative diseases. *Proceedings of the National Academy of Sciences* **91**, 5355–5358 (1994).

19. DePace, A. H., Santoso, A., Hillner, P. & Weissman, J. S. A Critical Role for Amino-Terminal Glutamine/Asparagine Repeats in the Formation and Propagation of a Yeast Prion. *Cell* **93**, 1241–1252 (1998).

20. West, M. W. *et al.* De novo amyloid proteins from designed combinatorial libraries. *Proc Natl Acad Sci U S A* **96**, 11211–11216 (1999).

21. Dobson, C. M. Protein misfolding, evolution and disease. *Trends Biochem Sci* **24**, 329–332 (1999).

22. Vivekanandan, S., Brender, J. R., Lee, S. Y. & Ramamoorthy, A. A partially folded structure of amyloid-beta(1–40) in an aqueous environment. *Biochem Biophys Res Commun* **411**, 312–316 (2011).

23. Yonemoto, I. T., Kroon, G. J. A., Dyson, H. J., Balch, W. E. & Kelly, J. W. Amylin proprotein processing generates progressively more amyloidogenic peptides that initially sample the helical state. *Biochemistry* **47**, 9900–9910 (2008).

24. Iadanza, M. G., Jackson, M. P., Hewitt, E. W., Ranson, N. A. & Radford, S. E. A new era for understanding amyloid structures and disease. *Nature Reviews Molecular Cell Biology 2018 19:12* **19**, 755–773 (2018).

25. Canchi, D. R. & García, A. E. Cosolvent Effects on Protein Stability. *https://doi.org/10.1146/annurev-physchem-040412-110156* **64**, 273–293 (2013).

26. Dobson, C. M. The Amyloid Phenomenon and Its Links with Human Disease. *Cold Spring Harb Perspect Biol* **9**, a023648 (2017).

27. Baldwin, A. J. *et al.* Metastability of Native Proteins and the Phenomenon of Amyloid Formation. (2011) doi:10.1021/JA2017703.

28. Cherny, I. & Gazit, E. Amyloids: Not Only Pathological Agents but Also Ordered Nanomaterials. *Angewandte Chemie International Edition* **47**, 4062–4069 (2008).

29. Tipping, K. W., van Oosten-Hawle, P., Hewitt, E. W. & Radford, S. E. Amyloid Fibres: Inert End-Stage Aggregates or Key Players in Disease? *Trends Biochem Sci* **40**, 719–727 (2015).

30. Williams, A. D., Shivaprasad, S. & Wetzel, R. Alanine Scanning Mutagenesis of Aβ(1-40) Amyloid Fibril Stability. *J Mol Biol* **357**, 1283–1294 (2006).

31. Stefani, M. & Dobson, C. M. Protein aggregation and aggregate toxicity: new insights into protein folding, misfolding diseases and biological evolution. *Journal of Molecular Medicine 2003 81:11* **81**, 678–699 (2003).

32. Haass, C. & Selkoe, D. J. Soluble protein oligomers in neurodegeneration: lessons from the Alzheimer's amyloid β-peptide. *Nature Reviews Molecular Cell Biology 2007 8:2* **8**, 101–112 (2007).

33. Chiti, F. & Dobson, C. M. Protein misfolding, functional amyloid, and human disease. *Annual Review of Biochemistry* vol. 75 333–366 Preprint at https://doi.org/10.1146/annurev.biochem.75.101304.123901 (2006).

34. Sawaya, M. R. *et al.* Atomic structures of amyloid cross-β spines reveal varied steric zippers. *Nature 2006 447:7143* **447**, 453–457 (2007).

35. Nelson, R. *et al.* Structure of the cross-β spine of amyloid-like fibrils. *Nature 2005 435:7043* **435**, 773–778 (2005).

36. Eisenberg, D. & Jucker, M. The Amyloid State of Proteins in Human Diseases. *Cell* **148**, 1188–1203 (2012).

37. Adamcik, J. & Mezzenga, R. Proteins Fibrils from a Polymer Physics Perspective. *Macromolecules* **45**, 1137–1150 (2011).

38. Dogra, P., Bhattacharya, M. & Mukhopadhyay, S. pH-Responsive Mechanistic Switch Regulates the Formation of Dendritic and Fibrillar Nanostructures of a Functional Amyloid. *Journal of Physical Chemistry B* **121**, 412–419 (2017).

39. Kushwaha, P. & Prabhu, N. P. Imidazolium-based ionic liquids with increasing alkyl chain length of cations decrease the stability and fibrillation propensity of lysozyme. *New Journal of Chemistry* (2022) doi:10.1039/D2NJ00559J.

40. Ghosh, S., Saurabh, A. & Prabhu, N. P. Spectroscopic studies on the stability and nucleation-independent fibrillation of partially-unfolded proteins in crowded environment. *Spectrochim Acta A Mol Biomol Spectrosc* **264**, 120307 (2022).

41. Bishop, M. F. & Ferrone, F. A. Kinetics of nucleation-controlled polymerization. A perturbation treatment for use with a secondary pathway. *Biophys J* **46**, 631–644 (1984).

42. Knowles, T. P. J. *et al.* An analytical solution to the kinetics of breakable filament assembly. *Science (1979)* **326**, 1533–1537 (2009).

43. Frieden, C. Protein aggregation processes: In search of the mechanism. *Protein Science* **16**, 2334–2344 (2007).

44. Kumar, S. & Udgaonkar, J. B. Mechanisms of amyloid fibril formation by proteins on JSTOR. *Current Science* 639–656 https://www.jstor.org/stable/24111817#metadata_info_tab_contents (2010).

45. Klein-Seetharaman, J. *et al.* Long-range interactions within a nonnative protein. *Science (1979)* **295**, 1719–1722 (2002).

46. Frare, E., Polverino De Laureto, P., Zurdo, J., Dobson, C. M. & Fontana, A. A Highly Amyloidogenic Region of Hen Lysozyme. *J Mol Biol* **340**, 1153–1165 (2004).

47. Takano, K., Funahashi, J. & Yutani, K. The stability and folding process of amyloidogenic mutant human lysozymes. *Eur J Biochem* **268**, 155–159 (2001).

48. Booth, D. R. *et al.* Instability, unfolding and aggregation of human lysozyme variants underlying amyloid fibrillogenesis. *Nature 1997 385:6619* **385**, 787–793 (1997).

49. Canet, D. *et al.* Mechanistic studies of the folding of human lysozyme and the origin of amyloidogenic behavior in its disease-related variants. *Biochemistry* **38**, 6419–6427 (1999).

50. Canet, D. *et al.* Local cooperativity in the unfolding of an amyloidogenic variant of human lysozyme. *Nature Structural Biology 2002 9:4* **9**, 308–315 (2002).

51. Dumoulin, M. *et al.* A camelid antibody fragment inhibits the formation of amyloid fibrils by human lysozyme. *Nature* **424**, 783–788 (2003).

52. Morozova-Roche, L. A. *et al.* Amyloid Fibril Formation and Seeding by Wild-Type Human Lysozyme and Its Disease-Related Mutational Variants. *J Struct Biol* **130**, 339–351 (2000).

53. Krebs, M. R. H. *et al.* Formation and seeding of amyloid fibrils from wild-type hen lysozyme and a peptide fragment from the β-domain. *J Mol Biol* **300**, 541–549 (2000).

54. Blake, C. C. F. *et al.* Structure of Hen Egg-White Lysozyme: A Three-dimensional Fourier Synthesis at 2 Å Resolution. *Nature 1965 206:4986* **206**, 757–761 (1965).

55. Schwalbe, H. *et al.* A refined solution structure of hen lysozyme determined using residual dipolar coupling data. *Protein Science* **10**, 677–688 (2001).

56. Evans, P. A., Topping, K. D., Woolfson, D. N. & Dobson, C. M. Hydrophobic clustering in nonnative states of a protein: Interpretation of chemical shifts in NMR spectra of denatured states of lysozyme. *Proteins: Structure, Function, and Bioinformatics* **9**, 248–266 (1991).

57. Radford, S. E., Dobson, C. M. & Evans, P. A. The folding of hen lysozyme involves partially structured intermediates and multiple pathways. *Nature 1992 358:6384* **358**, 302–307 (1992).

58. Buck, M., Radford, S. E. & Dobson, C. M. A Partially Folded State of Hen Egg White Lysozyme in Trifluoroethanol: Structural Characterization and Implications for Protein Folding. *Biochemistry* **32**, 669–678 (1993).

59. Chen, L., Hodgson, K. O. & Doniach, S. A Lysozyme Folding Intermediate Revealed by Solution X-ray Scattering. *J Mol Biol* **261**, 658–671 (1996).

60. Mittermaier, A., Kay, L. E. & Forman-Kay, J. D. Analysis of deuterium relaxation-derived methyl axis order parameters and correlation with local structure. *Journal of Biomolecular NMR 1999 13:2* **13**, 181–185 (1999).

61. Khurana, R., Hate, A. T., Nath, U. & Udgaonkar, J. B. pH dependence of the stability of barstar to chemical and thermal denaturation. *Protein Science* **4**, 1133–1144 (1995).

62. Neri, D., Billeter, M., Wider, G. & Wüthrichf, K. NMR Determination of Residual Structure in a Urea-Denatured Protein, the 434-Repressor. *Science (1979)* **257**, 1559–1563 (1992).

63. Hodsdon, M. E. & Frieden, C. Intestinal fatty acid binding protein: The folding mechanism as determined by NMR studies. *Biochemistry* **40**, 732–742 (2001).

64. Schwalbe, H. *et al.* Structural and dynamical properties of a denatured protein. Heteronuclear 3D NMR experiments and theoretical simulations of lysozyme in 8 M urea. *Biochemistry* **36**, 8977–8991 (1997).

65. Mishima, T., Ohkuri, T., Monji, A., Imoto, T. & Ueda, T. A particular hydrophobic cluster in the residual structure of reduced lysozyme drastically affects the amyloid fibrils formation. *Biochem Biophys Res Commun* **356**, 769–772 (2007).

66. Khan, J. M. *et al.* Sodium louroyl sarcosinate (sarkosyl) modulate amyloid fibril formation in hen egg white lysozyme (HEWL) at alkaline pH: a molecular insight study. *J Biomol Struct Dyn* **36**, 1550–1565 (2017).

67. Chaturvedi, S. K., Khan, J. M., Siddiqi, M. K., Alam, P. & Khan, R. H. Comparative insight into surfactants mediated amyloidogenesis of lysozyme. *Int J Biol Macromol* **83**, 315–325 (2016).

68. Kumar, E. K. & Prabhu, N. P. Differential effects of ionic and non-ionic surfactants on lysozyme fibrillation. *Physical Chemistry Chemical Physics* **16**, 24076–24088 (2014).

69. Choudhary, S., Save, S. N., Kishore, N. & Hosur, R. v. Synergistic Inhibition of Protein Fibrillation by Proline and Sorbitol: Biophysical Investigations. *PLoS One* **11**, e0166487 (2016).

70. Ghosh, S., Pandey, N. K. & Dasgupta, S. (−)-Epicatechin gallate prevents alkali-salt mediated fibrillogenesis of hen egg white lysozyme. *Int J Biol Macromol* **54**, 90–98 (2013).

71. Kumari, A., Ahmad, B. & Ahmad, B. The physical basis of fabrication of amyloid-based hydrogels by lysozyme. *RSC Adv* **9**, 37424–37435 (2019).

72. Arnaudov, L. N. & de Vries, R. Thermally induced fibrilar aggregation of hen egg white lysozyme. *Biophys J* **88**, 515–526 (2005).

73. Vernaglia, B. A., Huang, J. & Clark, E. D. Guanidine hydrochloride can induce amyloid fibril formation from hen egg-white lysozyme. *Biomacromolecules* **5**, 1362–1370 (2004).

74. Kumar, S., Ravi, V. K. & Swaminathan, R. How do surfactants and DTT affect the size, dynamics, activity and growth of soluble lysozyme aggregates? *Biochemical Journal* **415**, 275–288 (2008).

75. Moosavi-Movahedi, A. A. *et al.* Fibril formation of lysozyme upon interaction with sodium dodecyl sulfate at pH 9.2. *Colloids Surf B Biointerfaces* **60**, 55–61 (2007).

76. Stenstam, A., Montalvo, G., Grillo, I. & Gradzielski, M. Small angle neutron scattering study of lysozyme-sodium dodecyl sulfate aggregates. *The Journal of Physical Chemistry Part B* **107**, 12331–12338 (2003).

77. Morén, A. K. & Khan, A. Phase Equilibria of an Anionic Surfactant (Sodium Dodecyl Sulfate) and an Oppositely Charged Protein (Lysozyme) in Water. *Langmuir* **11**, 3636–3643 (1995).

78. Schröder, C. Proteins in Ionic Liquids: Current Status of Experiments and Simulations. *Topics in Current Chemistry* vol. 375 Preprint at https://doi.org/10.1007/s41061-017-0110-2 (2017).

79. Reslan, M. & Kayser, V. Ionic liquids as biocompatible stabilizers of proteins. *Biophys Rev* **10**, 781–793 (2018).

80. Wilkes, J. S. & Zaworotko, M. J. Air and water stable 1-ethyl-3-methylimidazolium based ionic liquids. *J Chem Soc Chem Commun* 965–967 (1992) doi:10.1039/C39920000965.

81. Welton, T. Room-Temperature Ionic Liquids. Solvents for Synthesis and Catalysis. *Chem Rev* **99**, 2071–2083 (1999).

82. Sheldon, R. Catalytic reactions in ionic liquids. *Chemical Communications* **1**, 2399–2407 (2001).

83. Egorova, K. S., Gordeev, E. G. & Ananikov, V. P. Biological Activity of Ionic Liquids and Their Application in Pharmaceutics and Medicine. *Chem Rev* **117**, 7132–7189 (2017).

84. Weber, C. C., Kulkarni, S. A., Kunov-Kruse, A. J., Rogers, R. D. & Myerson, A. S. The Use of Cooling Crystallization in an Ionic Liquid System for the Purification of Pharmaceuticals. *Cryst Growth Des* **15**, 4946–4951 (2015).

85. An, J. H., Kim, J. M., Chang, S. M. & Kim, W. S. Application of ionic liquid to polymorphic design of pharmaceutical ingredients. *Cryst Growth Des* **10**, 3044–3050 (2010).

86. Dang, D. T., Ha, S. H., Lee, S. M., Chang, W. J. & Koo, Y. M. Enhanced activity and stability of ionic liquid-pretreated lipase. *J Mol Catal B Enzym* **3–4**, 118–121 (2007).

87. Lee, S. H., Doan, T. T. N., Ha, S. H., Chang, W. J. & Koo, Y. M. Influence of ionic liquids as additives on sol–gel immobilized lipase. *J Mol Catal B Enzym* **47**, 129–134 (2007).

88. Attri, P. & Venkatesu, P. Thermodynamic characterization of the biocompatible ionic liquid effects on protein model compounds and their functional groups. *Physical Chemistry Chemical Physics* **13**, 6566–6575 (2011).

89. Byrne, N., Wang, L.-M., Belieres, J.-P. & Angell, C. A. Reversible folding-unfolding, aggregation protection, and multi-year stabilization, in high concentration protein solutions, using ionic liquids. (2007) doi:10.1039/b618943a.

90. Tietze, A. A. *et al.* On the Nature of Interactions between Ionic Liquids and Small Amino-Acid-Based Biomolecules. *ChemPhysChem* **14**, 4044–4064 (2013).

91. Page, T. A., Kraut, N. D., Page, P. M., Baker, G. A. & Bright, F. v. Dynamics of loop 1 of domain I in human serum albumin when dissolved in ionic liquids. *Journal of Physical Chemistry B* **113**, 12825–12830 (2009).

92. Mell, A. & Kragl, U. Ionic Liquids. *Comprehensive Biotechnology, Second Edition* **2**, 999–1006 (2011).

93. Egorova, K. S., Gordeev, E. G. & Ananikov, V. P. Biological Activity of Ionic Liquids and Their Application in Pharmaceutics and Medicine. *Chem Rev* **117**, 7132–7189 (2017).

94. Sivapragasam, M., Moniruzzaman, M. & Goto, M. Recent advances in exploiting ionic liquids for biomolecules: Solubility, stability and applications. *Biotechnol J* **11**, 1000–1013 (2016).

95. van Rantwijk, F. & Sheldon, R. A. Biocatalysis in Ionic Liquids. *Chem Rev* **107**, 2757–2785 (2007).

96. Summers, C. A. & Flowers, R. A. Protein renaturation by the liquid organic salt ethylammonium nitrate. *Protein Science* **9**, 2001–2008 (2000).

97. Kumar, A., Bisht, M. & Venkatesu, P. Biocompatibility of ionic liquids towards protein stability: A comprehensive overview on the current understanding and their implications. *Int J Biol Macromol* **96**, 611–651 (2017).

98. Naushad, M., ALOthman, Z. A., Khan, A. B. & Ali, M. Effect of ionic liquid on activity, stability, and structure of enzymes: A review. *Int J Biol Macromol* **51**, 555–560 (2012).

99. Shukla, S. K. & Mikkola, J.-P. Use of Ionic Liquids in Protein and DNA Chemistry. *Front Chem* **0**, 1219 (2020).

100. Brogan, A. P. S. & Hallett, J. P. Solubilizing and Stabilizing Proteins in Anhydrous Ionic Liquids through Formation of Protein–Polymer Surfactant Nanoconstructs. *J Am Chem Soc* **138**, 4494–4501 (2016).

101. Moniruzzaman, M., Kamiya, N. & Goto, M. Activation and stabilization of enzymes in ionic liquids. *Org Biomol Chem* **8**, 2887–2899 (2010).

102. Attri, P., Jha, I., Choi, E. H. & Venkatesu, P. Variation in the structural changes of myoglobin in the presence of several protic ionic liquid. *Int J Biol Macromol* **69**, 114–123 (2014).

103. Kumar, A., Rani, A. & Venkatesu, P. A comparative study of the effects of the Hofmeister series anions of the ionic salts and ionic liquids on the stability of α-chymotrypsin. *New Journal of Chemistry* **39**, 938–952 (2015).

104. Kumar, A. & Venkatesu, P. A comparative study of myoglobin stability in the presence of Hofmeister anions of ionic liquids and ionic salts. *Process Biochemistry* **49**, 2158–2169 (2014).

105. Takekiyo, T., Koyama, Y., Yamazaki, K., Abe, H. & Yoshimura, Y. Ionic Liquid-Induced Formation of the α-Helical Structure of β-Lactoglobulin. *Journal of Physical Chemistry B* **117**, 10142–10148 (2013).

106. Wei, W. & Danielson, N. D. Fluorescence and Circular Dichroism Spectroscopy of Cytochrome c in Alkylammonium Formate Ionic Liquids. *Biomacromolecules* **12**, 290–297 (2011).

107. Baker, G. A. & Heller, W. T. Small-angle neutron scattering studies of model protein denaturation in aqueous solutions of the ionic liquid 1-butyl-3-methylimidazolium chloride. *Chemical Engineering Journal* **147**, 6–12 (2009).

108. Constatinescu, D., Herrmann, C. & Weingärtner, H. Patterns of protein unfolding and protein aggregation in ionic liquids. *Physical Chemistry Chemical Physics* **12**, 1756–1763 (2010).

109. Gao, W. W., Zhang, F. X., Zhang, G. X. & Zhou, C. H. Key factors affecting the activity and stability of enzymes in ionic liquids and novel applications in biocatalysis. *Biochem Eng J* **99**, 67–84 (2015).

110. Constantinescu, D., Weingärtner, H. & Herrmann, C. Protein Denaturation by Ionic Liquids and the Hofmeister Series: A Case Study of Aqueous Solutions of Ribonuclease A. *Angewandte Chemie International Edition* **46**, 8887–8889 (2007).

111. Sarkar, N. & Dubey, V. K. Exploring critical determinants of protein amyloidogenesis: a review. *Journal of Peptide Science* **19**, 529–536 (2013).

112. Doig, A. J. & Derreumaux, P. Inhibition of protein aggregation and amyloid formation by small molecules. *Curr Opin Struct Biol* **30**, 50–56 (2015).

113. Stefani, M. & Rigacci, S. Protein Folding and Aggregation into Amyloid: The Interference by Natural Phenolic Compounds. *International Journal of Molecular Sciences 2013, Vol. 14, Pages 12411-12457* **14**, 12411–12457 (2013).

114. Iadanza, M. G., Jackson, M. P., Hewitt, E. W., Ranson, N. A. & Radford, S. E. A new era for understanding amyloid structures and disease. *Nature Reviews Molecular Cell Biology 2018 19:12* **19**, 755–773 (2018).

115. Saha, S. & Deep, S. Switch in the Aggregation Pathway of Bovine Serum Albumin Mediated by Electrostatic Interactions. *Journal of Physical Chemistry B* **118**, 9155–9166 (2014).

116. Dogra, P., Bhattacharya, M. & Mukhopadhyay, S. pH-Responsive Mechanistic Switch Regulates the Formation of Dendritic and Fibrillar Nanostructures of a Functional Amyloid. *Journal of Physical Chemistry B* **121**, 412–419 (2017).

117. Mastrella, L. *et al.* Taurine Stabilizing Effect on Lysozyme. *Life 2022, Vol. 12, Page 133* **12**, 133 (2022).

118. Ashrafian, H. *et al.* Discovery of a tetracyclic indole alkaloid that postpones fibrillation of hen egg white lysozyme protein. *Int J Biol Macromol* **183**, 1939–1947 (2021).

119. Khan, J. M. *et al.* Sodium louroyl sarcosinate (sarkosyl) modulate amyloid fibril formation in hen egg white lysozyme (HEWL) at alkaline pH: a molecular insight study. *J Biomol Struct Dyn* **36**, 1550–1565 (2017).

120. Chaturvedi, S. K., Khan, J. M., Siddiqi, M. K., Alam, P. & Khan, R. H. Comparative insight into surfactants mediated amyloidogenesis of lysozyme. *Int J Biol Macromol* **83**, 315–325 (2016).

121. Tokunaga, Y., Sakakibara, Y., Kamada, Y., Watanabe, K. I. & Sugimoto, Y. Analysis of core region from egg white lysozyme forming amyloid fibrils. *Int J Biol Sci* **9**, 219–227 (2013).

122. Kumar, E. K. & Prabhu, N. P. Differential effects of ionic and non-ionic surfactants on lysozyme fibrillation. *Physical Chemistry Chemical Physics* **16**, 24076–24088 (2014).

123. Frare, E., Polverino De Laureto, P., Zurdo, J., Dobson, C. M. & Fontana, A. A Highly Amyloidogenic Region of Hen Lysozyme. *J Mol Biol* **340**, 1153–1165 (2004).

124. Choudhary, S., Save, S. N., Kishore, N. & Hosur, R. v. Synergistic Inhibition of Protein Fibrillation by Proline and Sorbitol: Biophysical Investigations. *PLoS One* **11**, e0166487 (2016).

125. Ghosh, S., Pandey, N. K. & Dasgupta, S. (−)-Epicatechin gallate prevents alkali-salt mediated fibrillogenesis of hen egg white lysozyme. *Int J Biol Macromol* **54**, 90–98 (2013).

126. Borana, M. S., Mishra, P., Pissurlenkar, R. R. S., Hosur, R. v. & Ahmad, B. Curcumin and kaempferol prevent lysozyme fibril formation by modulating aggregation kinetic parameters. *Biochimica et Biophysica Acta (BBA) - Proteins and Proteomics* **1844**, 670–680 (2014).

127. Chen, X. *et al.* Inhibition of Lysozyme Amyloid Fibrillation by Silybin Diastereoisomers: The Effects of Stereochemistry. *ACS Omega* **6**, 3307–3318 (2021).

128. Gao, W. *et al.* Inhibition behavior of Sennoside A and Sennoside C on amyloid fibrillation of human lysozyme and its possible mechanism. *Int J Biol Macromol* **178**, 424–433 (2021).

129. Basu, A., Mahammad, A. & Das, A. Inhibition of the formation of lysozyme fibrillar assemblies by the isoquinoline alkaloid coralyne. *New Journal of Chemistry* **46**, 3258–3269 (2022).

130. Meena, P. & Kishore, N. Potential of tetradecyltrimethylammonium bromide in preventing fibrillation/aggregation of lysozyme: biophysical studies.

https://doi.org/10.1080/07391102.2021.1987989 (2021) doi:10.1080/07391102.2021.1987989.

131. Ermakova, E. A., Makshakova, O. N., Zuev, Y. F. & Sedov, I. A. Fibril fragments from the amyloid core of lysozyme: An accelerated molecular dynamics study. *J Mol Graph Model* **106**, 107917 (2021).

132. Ghosh, S., Saurabh, A. & Prabhu, N. P. Spectroscopic studies on the stability and nucleation-independent fibrillation of partially-unfolded proteins in crowded environment. *Spectrochim Acta A Mol Biomol Spectrosc* **264**, 120307 (2022).

133. Uversky, V. N., Li, J. & Fink, A. L. Evidence for a Partially Folded Intermediate in α-Synuclein Fibril Formation *. *Journal of Biological Chemistry* **276**, 10737–10744 (2001).

134. Kumar, E. K., Haque, N. & Prabhu, N. P. Kinetics of protein fibril formation: Methods and mechanisms. *Int J Biol Macromol* **100**, 3–10 (2017).

135. Wei, W. & Danielson, N. D. Fluorescence and Circular Dichroism Spectroscopy of Cytochrome c in Alkylammonium Formate Ionic Liquids. *Biomacromolecules* **12**, 290 (2011).

136. Pabbathi, A., Ghosh, S. & Samanta, A. FCS Study of the Structural Stability of Lysozyme in the Presence of Morpholinium Salts. *Journal of Physical Chemistry B* **117**, 16587–16593 (2013).

137. Bui-Le, L. *et al.* Revealing the complexity of ionic liquid–protein interactions through a multi-technique investigation. *Communications Chemistry 2020 3:1* **3**, 1–9 (2020).

138. Khurana, R., Hate, A. T., Nath, U. & Udgaonkar, J. B. pH dependence of the stability of barstar to chemical and thermal denaturation. *Protein Science* **4**, 1133–1144 (1995).

139. Jorgensen, W. L. & Tirado-Rives, J. Potential energy functions for atomic-level simulations of water and organic and biomolecular systems. *Proc Natl Acad Sci U S A* **102**, 6665–6670 (2005).

140. Dodda, L. S., de Vaca, I. C., Tirado-Rives, J. & Jorgensen, W. L. LigParGen web server: an automatic OPLS-AA parameter generator for organic ligands. *Nucleic Acids Res* **45**, W331–W336 (2017).

141. Dodda, L. S., Vilseck, J. Z., Tirado-Rives, J. & Jorgensen, W. L. 1.14∗CM1A-LBCC: Localized Bond-Charge Corrected CM1A Charges for Condensed-Phase Simulations. *Journal of Physical Chemistry B* **121**, 3864–3870 (2017).

142. Kirkwood, J. G. & Buff, F. P. The Statistical Mechanical Theory of Solutions. I. *J Chem Phys* **19**, 774 (2004).

143. Anumalla, B. & Prabhu, N. P. Surface hydration and preferential interaction directs the charged amino acids-induced changes in protein stability. *J Mol Graph Model* **98**, 107602 (2020).

144. Smiatek, J. Osmolyte effects: Impact on the aqueous solution around charged and neutral spheres. *Journal of Physical Chemistry B* **118**, 771–782 (2014).

145. Mann, J. P., McCluskey, A. & Atkin, R. Activity and thermal stability of lysozyme in alkylammonium formate ionic liquids—influence of cation modification. *Green Chemistry* **11**, 785–792 (2009).

146. Royer, C. A. Fluorescence Spectroscopy. *Methods Mol Biol* **40**, 65–89 (1995).

147. Joseph R. Lakowicz. *Principles of Fluorescence Spectroscopy*. (Springer US, 2006). doi:10.1007/978-0-387-46312-4.

148. Pieraccini, S., Burgi, L., Genoni, A., Benedusi, A. & Sironi, M. Atomic level description of the protecting effect of osmolytes against thermal denaturation of proteins. *Chem Phys Lett* **438**, 298–303 (2007).

149. Ghanta, K. P., Mondal, S. & Bandyopadhyay, S. Exploring the Dynamic Heterogeneity at the Interface of a Protein in Aqueous Ionic Liquid Solutions. *Journal of Physical Chemistry B* **126**, 7271–7285 (2022).

150. Kiran Kumar, E., Prasad, D. K. & Prakash Prabhu, N. Concentration dependent switch in the kinetic pathway of lysozyme fibrillation: Spectroscopic and microscopic analysis. *Spectrochim Acta A Mol Biomol Spectrosc* **183**, 187–194 (2017).

151. Juárez, J., López, S. G., Cambón, A., Taboada, P. & Mosquera, V. Influence of Electrostatic Interactions on the Fibrillation Process of Human Serum Albumin. *Journal of Physical Chemistry B* **113**, 10521–10529 (2009).

152. Powers, E. T. & Powers, D. L. The Kinetics of Nucleated Polymerizations at High Concentrations: Amyloid Fibril Formation Near and Above the "Supercritical Concentration". *Biophys J* **91**, 122–132 (2006).

153. Sukenik, S., Sapir, L. & Harries, D. Balance of enthalpy and entropy in depletion forces. *Curr Opin Colloid Interface Sci* **18**, 495–501 (2013).

154. Naidu, K. T., Rao, D. K. & Prabhu, N. P. Cryo vs Thermo: Duality of Ethylene Glycol on the Stability of Proteins. *Journal of Physical Chemistry B* **124**, 10077–10088 (2020).

155. Sukenik, S., Sapir, L. & Harries, D. Balance of enthalpy and entropy in depletion forces. *Curr Opin Colloid Interface Sci* **18**, 495–501 (2013).

156. Garajová, K., Sedláková, D., Berta, M., Gazova, Z. & Sedlák, E. Destabilization effect of imidazolium cation-Hofmeister anion salts on cytochrome c. *Int J Biol Macromol* **164**, 3808–3813 (2020).

157. Jha, I., Kumar, A. & Venkatesu, P. The Overriding Roles of Concentration and Hydrophobic Effect on Structure and Stability of Heme Protein Induced by Imidazolium-Based Ionic Liquids. *Journal of Physical Chemistry B* **119**, 8357–8368 (2015).

158. Acharyya, A., DiGiuseppi, D., Stinger, B. L., Schweitzer-Stenner, R. & Vaden, T. D. Structural Destabilization of Azurin by Imidazolium Chloride Ionic Liquids in Aqueous Solution. *J Phys Chem B* **123**, 6933–6945 (2019).

159. Ghosh, S., Parui, S., Jana, B. & Bhattacharyya, K. Ionic liquid induced dehydration and domain closure in lysozyme: FCS and MD simulation. *J Chem Phys* **143**, 125103 (2015).

160. Salahuddin, P., Fatima, M. T., Abdelhameed, A. S., Nusrat, S. & Khan, R. H. Structure of amyloid oligomers and their mechanisms of toxicities: Targeting amyloid oligomers using novel therapeutic approaches. *Eur J Med Chem* **114**, 41–58 (2016).

161. Sgarbossa, A. Natural Biomolecules and Protein Aggregation: Emerging Strategies against Amyloidogenesis. *International Journal of Molecular Sciences 2012, Vol. 13, Pages 17121-17137* **13**, 17121–17137 (2012).

162. HARADA, A., AZAKAMI, H. & KATO, A. Amyloid Fibril Formation of Hen Lysozyme Depends on the Instability of the C-Helix (88-99). *Biosci Biotechnol Biochem* **72**, 1523–1530 (2008).

163. Sivapragasam, M., Moniruzzaman, M. & Goto, M. Recent advances in exploiting ionic liquids for biomolecules: Solubility, stability and applications. *Biotechnol J* **11**, 1000–1013 (2016).

164. Rodrigues, R. F., Freitas, A. A., Canongia Lopes, J. N. & Shimizu, K. Ionic Liquids and Water: Hydrophobicity vs. Hydrophilicity. *Molecules 2021, Vol. 26, Page 7159* **26**, 7159 (2021).

165. Kurnia, K. A. *et al.* The effect of the cation alkyl chain branching on mutual solubilities with water and toxicities. *Physical Chemistry Chemical Physics* **16**, 19952–19963 (2014).

166. Freire, M. G. *et al.* Mutual solubility of water and structural/positional isomers of N-alkylpyridinium-based ionic liquids. *Journal of Physical Chemistry B* **114**, 15925–15934 (2010).

167. Freire, M. G. *et al.* Solubility of non-aromatic ionic liquids in water and correlation using a QSPR approach. *Fluid Phase Equilib* **294**, 234–240 (2010).

168. Khan, I., Taha, M., Pinho, S. P. & Coutinho, J. A. P. Interactions of pyridinium, pyrrolidinium or piperidinium based ionic liquids with water: Measurements and COSMO-RS modelling. *Fluid Phase Equilib* **414**, 93–100 (2016).

169. Tomé, L. I. N., Jorge, M., Gomes, J. R. B. & Coutinho, J. A. P. Molecular dynamics simulation studies of the interactions between ionic liquids and amino acids in aqueous solution. *Journal of Physical Chemistry B* **116**, 1831–1842 (2012).

170. Tomé, L. I. N. *et al.* On the interactions between amino acids and ionic liquids in aqueous media. *Journal of Physical Chemistry B* **113**, 13971–13979 (2009).

171. Yamamoto, E., Yamaguchi, S. & Nagamune, T. Protein refolding by N-alkylpyridinium and n-alkyl-n-methylpyrrolidinium ionic liquids. *Appl Biochem Biotechnol* **164**, 957–967 (2011).

172. Constantinescu, D., Weingärtner, H. & Herrmann, C. Protein Denaturation by Ionic Liquids and the Hofmeister Series: A Case Study of Aqueous Solutions of Ribonuclease A. *Angewandte Chemie International Edition* **46**, 8887–8889 (2007).

173. Takekiyo, T., Koyama, Y., Yamazaki, K., Abe, H. & Yoshimura, Y. Ionic Liquid-Induced Formation of the α-Helical Structure of β-Lactoglobulin. *Journal of Physical Chemistry B* **117**, 10142–10148 (2013).

174. Takekiyo, T., Yamaguchi, E., Abe, H. & Yoshimura, Y. Suppression Effect on the Formation of Insulin Amyloid by the Use of Ionic Liquids. *ACS Sustain Chem Eng* **4**, 422–428 (2016).

175. Teichberg, V. I., Kay, C. M. & Sharon, N. Separation of Contributions of Tryptophans and Tyrosines to the Ultraviolet Circular Dichroism Spectrum of Hen Egg-White Lysozyme. *Eur J Biochem* **16**, 55–59 (1970).

176. Kelly, S. M., Jess, T. J. & Price, N. C. How to study proteins by circular dichroism. *Biochimica et Biophysica Acta (BBA) - Proteins and Proteomics* **1751**, 119–139 (2005).

177. Ajmal, M. R. *et al.* Biophysical insights into the interaction of hen egg white lysozyme with therapeutic dye clofazimine: modulation of activity and SDS induced aggregation of model protein. *https://doi.org/10.1080/07391102.2016.1211552* **35**, 2197–2210 (2016).

178. Ali, S. *et al.* Identification and Evaluation of Inhibitors of Lipase from Malassezia restricta using Virtual High-Throughput Screening and Molecular Dynamics Studies. *International Journal of Molecular Sciences 2019, Vol. 20, Page 884* **20**, 884 (2019).

179. Akbarian, M. & Chen, S.-H. Instability Challenges and Stabilization Strategies of Pharmaceutical Proteins. *Pharmaceutics 2022, Vol. 14, Page 2533* **14**, 2533 (2022).

180. Colaço, C., Sen, S., Thangavelu, M., Pinder, S. & Roser, B. Extraordinary Stability of Enzymes Dried in Trehalose: Simplified Molecular Biology. *Bio/Technology 1992 10:9* **10**, 1007–1011 (1992).

181. Devi, Y. S., Nair, U. B. & Bhat, R. Effect of a mixed stabilizer-denaturant system on the stability of enzyme activity at high temperatures : lysozyme as a model. *Progress in Biotechnology* **15**, 263–268 (1998).

182. Ghosh, R. & Kishore, N. Physicochemical Insights into the Stabilization of Stressed Lysozyme and Glycine Homopeptides by Sorbitol. *Journal of Physical Chemistry B* **122**, 7839–7854 (2018).

183. van der Vegt, N. F. A. & Nayar, D. The Hydrophobic Effect and the Role of Cosolvents. *Journal of Physical Chemistry B* **121**, 9986–9998 (2017).

184. Lee, J. C. & Timasheff, S. N. The stabilization of proteins by sucrose. *Journal of Biological Chemistry* **256**, 7193–7201 (1981).

185. de Cordt, S., Hendrickx, M., Maesmans, G. & Tobback, P. The influence of polyalcohols and carbohydrates on the thermostability of α-amylase. *Biotechnol Bioeng* **43**, 107–114 (1994).

186. Santoro, M. M., Liu, Y., Khan, S. M. A., Hou, L. X. & Bolen, D. W. Increased Thermal Stability of Proteins in the Presence of Naturally Occurring Osmolytes. *Biochemistry* **31**, 5278–5283 (1992).

187. Arakawa, T. & Timasheff, S. N. Preferential Interactions of Proteins with Salts in Concentrated Solutions. *Biochemistry* **21**, 6545–6552 (1982).

188. Summers, C. A. & Flowers, R. A. Protein renaturation by the liquid organic salt ethylammonium nitrate. *Protein Science* **9**, 2001–2008 (2000).

189. Veríssimo, N. v., Saponi, C. F., Ryan, T. M., Greaves, T. L. & Pereira, J. F. B. Imidazolium-based ionic liquids as additives to preserve the Enhanced Green Fluorescent Protein fluorescent activity. *Green Chemical Engineering* **2**, 412–422 (2021).

190. Kumar, A. & Venkatesu, P. Innovative aspects of protein stability in ionic liquid mixtures. *Biophys Rev* **10**, 841–846 (2018).

191. Kumar, A., Rani, A. & Venkatesu, P. A comparative study of the effects of the Hofmeister series anions of the ionic salts and ionic liquids on the stability of α-chymotrypsin. *New Journal of Chemistry* **39**, 938–952 (2015).

192. Kumar, A. & Venkatesu, P. A comparative study of myoglobin stability in the presence of Hofmeister anions of ionic liquids and ionic salts. *Process Biochemistry* **49**, 2158–2169 (2014).

193. Constatinescu, D., Herrmann, C. & Weingärtner, H. Patterns of protein unfolding and protein aggregation in ionic liquids. *Physical Chemistry Chemical Physics* **12**, 1756–1763 (2010).

194. Lozano, P., Bernal, B., Bernal, J. M., Pucheault, M. & Vaultier, M. Stabilizing immobilized cellulase by ionic liquids for saccharification of cellulose solutions in 1-butyl-3-methylimidazolium chloride. *Green Chemistry* **13**, 1406–1410 (2011).

195. Reddy, P. M., Umapathi, R. & Venkatesu, P. A green approach to offset the perturbation action of 1-butyl-3-methylimidazolium iodide on α-chymotrypsin. *Physical Chemistry Chemical Physics* **17**, 184–190 (2014).

196. Sasmal, D. K. *et al.* An FCS Study of Unfolding and Refolding of CPM-Labeled Human Serum Albumin: Role of Ionic Liquid. *Journal of Physical Chemistry B* **115**, 13075–13083 (2011).

197. Mojumdar, S. sen, Chowdhury, R., Chattoraj, S. & Bhattacharyya, K. Role of ionic liquid on the conformational dynamics in the native, molten globule, and unfolded

states of cytochrome c: a fluorescence correlation spectroscopy study. *J Phys Chem B* **116**, 12189–12198 (2012).

198. Kumar, A. & Venkatesu, P. Overview of the stability of α-chymotrypsin in different solvent media. *Chem Rev* **112**, 4283–4307 (2012).

199. Xu, M. *et al.* The first step of hen egg white lysozyme fibrillation, irreversible partial unfolding, is a two-state transition. *Protein Science* **16**, 815–832 (2007).

200. Mann, J. P., McCluskey, A. & Atkin, R. Activity and thermal stability of lysozyme in alkylammonium formate ionic liquids—influence of cation modification. *Green Chemistry* **11**, 785–792 (2009).

201. Latovitzki, N., Halper, J. P. & Beychok, S. Spectrophotometric Titration of Tyrosine Residues in Human Lysozyme. *Journal of Biological Chemistry* **246**, 1457–1460 (1971).

202. Poddar, N. K., Ansari, Z. A., Singh, R. K. B., Moosavi-Movahedi, A. A. & Ahmad, F. Effect of monomeric and oligomeric sugar osmolytes on ΔGD, the Gibbs energy of stabilization of the protein at different pH values: Is the sum effect of monosaccharide individually additive in a mixture? *Biophys Chem* **138**, 120–129 (2008).

203. Shukla, D. & Trout, B. L. Understanding the synergistic effect of arginine and glutamic acid mixtures on protein solubility. *Journal of Physical Chemistry B* **115**, 11831–11839 (2011).

204. Lange, C., Patil, G. & Rudolph, R. Ionic liquids as refolding additives: N′-alkyl and N′-(ω-hydroxyalkyl) N-methylimidazolium chlorides. *Protein Science* **14**, 2693–2701 (2005).

205. Singh, U. K. & Patel, R. Dynamics of Ionic Liquid-Assisted Refolding of Denatured Cytochrome c: A Study of Preferential Interactions toward Renaturation. *Mol Pharm* (2018) doi:10.1021/ACS.MOLPHARMACEUT.8B00212.

206. Takekiyo, T., Yamazaki, K., Yamaguchi, E., Abe, H. & Yoshimura, Y. High ionic liquid concentration-induced structural change of protein in aqueous solution: A case study of lysozyme. *Journal of Physical Chemistry B* **116**, 11092–11097 (2012).

Protein stability and fibrillation in ionic liquids: a special reference to hydrophobic interactions.

by Pratibha Kushwaha

Submission date: 29-Dec-2022 10:25AM (UTC+0530)
Submission ID: 1987217926
File name: Thesis_Copy_Plag_Check_01.pdf (10.18M)
Word count: 29731
Character count: 152044

Protein stability and fibrillation in ionic liquids: a special reference to hydrophobic interactions.

ORIGINALITY REPORT

25%	4%	25%	1%
SIMILARITY INDEX	INTERNET SOURCES	PUBLICATIONS	STUDENT PAPERS

PRIMARY SOURCES

1	Pratibha Kushwaha, N. Prakash Prabhu. "Imidazolium-based ionic liquids with increasing alkyl chain length of cation decrease the stability and fibrillation propensity of lysozyme", New Journal of Chemistry, 2022 Publication	17%
2	Pratibha Kushwaha, N. Prakash Prabhu. "Imidazolium-based ionic liquids with increasing alkyl chain length of cations decrease the stability and fibrillation propensity of lysozyme", New Journal of Chemistry, 2022 Publication	3%
3	Bramhini Anumalla, N. Prakash Prabhu. "Surface hydration and preferential interaction directs the charged amino acids-induced changes in protein stability", Journal of Molecular Graphics and Modelling, 2020 Publication	1%

N. PRAKASH PRABHU PhD
Associate Professor,
Dept. Biotechnology & Bioinformatics
School of Life Sciences
University of Hyderabad
Hyderabad-500 046

N. PRAKASH PRABHU PhD
Associate Professor,
Dept. Biotechnology & Bioinformatic
School of Life Sciences
University of Hyderabad
Hyderabad-500 046

4	Subhasree Ghosh, Archi Saurabh, N. Prakash Prabhu. "Spectroscopic studies on the stability and nucleation-independent fibrillation of partially-unfolded proteins in crowded environment", Spectrochimica Acta Part A: Molecular and Biomolecular Spectroscopy, 2022 Publication	<1 %
5	Bramhini Anumalla, N. Prakash Prabhu. "Glutamate Induced Thermal Equilibrium Intermediate and Counteracting Effect on Chemical Denaturation of Proteins", The Journal of Physical Chemistry B, 2018 Publication	<1 %
6	K. Tejaswi Naidu, D. Krishna Rao, N. Prakash Prabhu. "Cryo vs Thermo: Duality of Ethylene Glycol on the Stability of Proteins", The Journal of Physical Chemistry B, 2020 Publication	<1 %
7	tudr.thapar.edu:8080 Internet Source	<1 %
8	Ksenia S. Egorova, Evgeniy G. Gordeev, Valentine P. Ananikov. "Biological Activity of Ionic Liquids and Their Application in Pharmaceutics and Medicine", Chemical Reviews, 2017 Publication	<1 %

9	Submitted to University of Hyderabad, Hyderabad Student Paper	<1 %
10	Diwakar Shukla, Chetan Shinde, Bernhardt L. Trout. "Molecular Computations of Preferential Interaction Coefficients of Proteins", The Journal of Physical Chemistry B, 2009 Publication	<1 %
11	Erica Frare, Patrizia Polverino de Laureto, Jesús Zurdo, Christopher M Dobson, Angelo Fontana. "A Highly Amyloidogenic Region of Hen Lysozyme", Journal of Molecular Biology, 2004 Publication	<1 %
12	"Instrumental Analysis of Intrinsically Disordered Proteins", Wiley, 2010 Publication	<1 %
13	www.ias.ac.in Internet Source	<1 %
14	www.frontiersin.org Internet Source	<1 %
15	scholarship.shu.edu Internet Source	<1 %
16	www.repository.unipr.it Internet Source	<1 %

17	link.springer.com Internet Source	<1 %
18	www.science.org Internet Source	<1 %
19	R. H. Khan. "The Minimal Structural Requirement of Concanavalin A that Retains Its Functional Aspects", Journal of Biochemistry, 06/13/2007 Publication	<1 %
20	publications.aston.ac.uk Internet Source	<1 %
21	dyuthi.cusat.ac.in Internet Source	<1 %
22	ebin.pub Internet Source	<1 %
23	Tina Akhavan, Mehdi Ebrahimi, Azadeh Hekmat. "Structural evidence for kinetic and thermal stability changes of α-amylase due to exposure to [emim][lactate] ionic liquid", Turkish Journal of Biochemistry, 2020 Publication	<1 %
24	uvidok.rcub.bg.ac.rs Internet Source	<1 %
25	Hamada, H.. "l-Argininamide improves the refolding more effectively than l-arginine", Journal of Biotechnology, 20070615	<1 %

Publication

26	Gary W. Daughdrill. "Natively Disordered Proteins", Protein Folding Handbook, 01/01/2005 Publication	<1 %
27	Paridhi Sanchora, Deepak Kumar Pandey, Hardik L Kagdada, Arnulf Materny, Dheeraj Kumar Singh. "Impact of Alkyl Chain Length and Water on the Structure and Properties of 1-alkyl-3-methylimidazolium Chloride Ionic Liquids", Physical Chemistry Chemical Physics, 2020 Publication	<1 %
28	Zurdo, J., Carlos González, Jesús M. Sanz, Manuel Rico, M. Remacha, and J. P. G. Ballesta. "Structural Differences between *Saccharomyces cerevisiae* Ribosomal Stalk Proteins P1 and P2 Support Their Functional Diversity†", Biochemistry, 2000. Publication	<1 %
29	discovery.ucl.ac.uk Internet Source	<1 %
30	Sanjay Gairola. "A 36-Pulse AC-DC Converter for Line Current Harmonic Reduction", 2006 International Conference on Power Electronic Drives and Energy Systems, 12/2006 Publication	<1 %

31	archives.njit.edu Internet Source	<1 %
32	epub.uni-regensburg.de Internet Source	<1 %
33	L. Ye, Z. Wu, M. Eleftheriou, R. Zhou. "Single-mutation-induced stability loss in protein lysozyme", Biochemical Society Transactions, 2007 Publication	<1 %
34	coek.info Internet Source	<1 %
35	eprints.lincoln.ac.uk Internet Source	<1 %
36	Bramhini Anumalla, N. Prakash Prabhu. "Counteracting Effect of Charged Amino Acids Against the Destabilization of Proteins by Arginine", Applied Biochemistry and Biotechnology, 2019 Publication	<1 %
37	Zahra Nikfarjam, Omid Bavi, Saeed K. Amini. "Potential effective inhibitory compounds against Prostate Specific Membrane Antigen (PSMA): A molecular docking and molecular dynamics study", Archives of Biochemistry and Biophysics, 2021 Publication	<1 %

38	dspace.nm-aist.ac.tz Internet Source	<1%
39	Parashar, R.. "Excess molar volumes of some partially miscible liquid mixtures", The Journal of Chemical Thermodynamics, 200006 Publication	<1%
40	U. G. Deshpande, J. R. Shah. "Preparation and Characterization of Some New Coordination Polymers", Synthesis and Reactivity in Inorganic and Metal-Organic Chemistry, 2006 Publication	<1%

Exclude quotes	On	Exclude matches	< 14 words
Exclude bibliography	On		